Partitioning And Transmuter Research Initiative in a Collaborative Innovation Action

PATRICIA

Grant Agreement Number 945077

Research and Innovation Action

Activity: NFRP-2019-2020

Topic: NFRP-2019-2020-07 Safety Research and Innovation for Partitioning and/or Transmutation

Start date: 01/09/2020 – Duration: 60 months

DELIVERABLE

D5.3 Results of the fuel performance code benchmark assessment

Authors: M. Lainet (CEA), M. Di Gennaro, A. Magni, D. Pizzocri, L. Luzzi (POLIMI), A. Schubert, P. Van Uffelen, E. D'Agata (JRC), V. Romanello (CVR), A. Rineiski, K. Sturm (KIT)

This project has received funding from the Euratom Research and Training programme 2019-2020 under grant agreement No 945077.

DOCUMENT CONTROL SHEET

DOCUMENT INFORMATION	
Document title	Results of the fuel performance code benchmark assessment
Authors, (organisation)	M. Lainet (CEA), M. Di Gennaro, A. Magni, D. Pizzocri, L. Luzzi (POLIMI), A. Schubert, P. Van Uffelen, E. D'Agata (JRC), V. Romanello (CVR), A. Rineiski, K. Sturm (KIT)
Document type	Deliverable
Document ID	D5.3
Work package n°	WP5 (Domain: Transmutation)
Work package title	WP5 Improvement of modelling and fuel performance codes
Lead beneficiary	CEA
Dissemination level	Public
Date of issue	17/02/2026
Archive ID reference	SCK CEN/86563692

DOCUMENT SUMMARY
The main objective of the work carried out in the Task 5.3 of PATRICIA project is to assess the capability of different Fuel Performance Codes (FPCs) to simulate the behaviour under irradiation of Am-bearing fuels. The assessment of the modelling involved in the simulation tools is obtained by benchmarking the computation results against experimental data. Two complementary irradiation experiments are considered in this work, both performed in the past years in the High Flux Reactor (HFR) at Petten: SPHERE experiment with Minor Actinide Bearing Driver Fuel $(U,Pu,Am)O_{2-x}$, and MARINE experiment with Minor Actinide Bearing Blanket material $(U,Am)O_{2-x}$. The report describes the methodology implemented in this benchmark activity, based on the chaining of neutronic simulations with Fuel Performance Codes computations. This chaining was necessary for investigating further the conditions of the experiments. The outcome of this work is thus not only an assessment of the capabilities of the codes to simulate the irradiation of Am-bearing fuels, especially with regards to the inert gases behaviour – xenon, krypton and helium, but also a contribution to improve the interpretation of SPHERE and MARINE experiments.

DOCUMENT HISTORY		
Version	**Status**	**Date**
v0	Final	30/09/2024

DOCUMENT APPROVAL	
Date	**Author(s), WP leader – Domain leader, organisation**
26/09/2024	Author: Marc Lainet (CEA)
30/09/2024	WP leader: Lelio Luzzi (POLIMI)
30/09/2024	Domain leader: Lelio Luzzi (POLIMI)

Date	Coordinator
12/02/2026	Paul Schuurmans (SCK CEN) 

DISTRIBUTION LIST		
Project Officer Renata Bachorczyk-Nagy	EC	Copy on PATRICIA SharePoint
PATRICIA Beneficiaries	PATRICIA Consortium	

Table of contents

1 Introduction

The main objective of the work carried out in the Task 5.3 of PATRICIA project is to assess the capability of different Fuel Performance Codes (FPCs) to simulate the behaviour under irradiation of Am-bearing fuels. The assessment of the modelling involved in the simulation tools is obtained by benchmarking the computation results against experimental data. Two complementary irradiation experiments are considered in this work:

- the SPHERE experiment (D'Agata 2014, Gallais-During 2018) performed with Minor Actinide Bearing Driver Fuel $(U,Pu,Am)O_{2-x}$, with a Pu content of 20% and an Am content of ~3%. The present study focuses on the pin #1 of SPHERE with pelletized fuel. SPHERE is a transmutation experiment in homogeneous mode, introducing a small amount of minor actinide – namely, americium – in the composition of a driver fuel;
- the MARINE experiment (D'Agata 2017) performed with Minor Actinide Bearing Blanket material $(U,Am)O_{2-x}$, with an Am content of 13%. Again, the study focuses on the pelletized fuel loaded in the pin #1 of MARINE. It is a transmutation experiment in heterogeneous mode, introducing a higher amount of minor actinide – again, americium – in the composition of a blanket fuel material, with a low fissile content.

Both SPHERE and MARINE experiments were performed in the High Flux Reactor (HFR) at Petten.

The benchmark activity started with the simulation of SPHERE experiment, and the first computation results immediately showed important discrepancies in the predictions of the inert gases production and release (fission gases, xenon and krypton, and helium). This highlighted the need to investigate the neutronic conditions of the experiment, which may have been very peculiar due to the presence of a neutron shield surrounding the device, aiming at hardening the neutron flux and creating conditions close to those in a fast spectrum reactor. Practically speaking, the spectrum conditions may have evolved throughout the experiment, likely due to the gradual depletion of the neutron shield. This would result in a shift from an initially hardened neutron flux to a more thermalized one over time. It was thus necessary to adapt the methodology for simulating the SPHERE experiment, by implementing preliminary neutronics analyses with the goal to derive adequate basic nuclear data to be used on input by the FPCs calculations.
The same process was adopted further for the simulation of MARINE experiment.
Finally, the outcome of this work is not only an assessment of the capabilities of the codes to simulate the behaviour of Am-bearing fuels, but also a contribution to improve the interpretation of SPHERE and MARINE experiments.

The next Section 2 describes the methodology adopted for the simulation of both SPHERE and MARINE experiments: the neutronics tools used for the studies are introduced, then the principles of the chaining of these neutronics tools with the Fuel Performance Codes, and finally the FPCs and their upgrades. Then the Section 3 presents a new interpretation of the SPHERE experiment. The main characteristics of SPHERE irradiation are firstly recalled. Then the modelling of the experiment by the neutronics tools and the FPCs are described and the computation results are analysed, in comparison with the experimental data. Some sensitivity studies performed with the different FPCs are also presented. The content of the Section 4 is similar and pertains to the MARINE experiment. . The main outcomes of this work and the perspectives are given finally in the conclusion.

2 Methodology adopted for simulating SPHERE and MARINE experiments

2.1 Neutronics tools used for the study

Most benchmark participants used data provided by SERPENT-2, a three-dimensional continuous energy Monte Carlo burn-up calculation code mainly for reactor physics applications, developed at the VTT Technical Research Centre of Finland since 2004. The current version 2.2.0 of SERPENT-2 (Leppänen 2015) was used for the study. The neutron transport resolution is based on a combination of conventional surface-to-surface ray-tracing and the Woodcock delta-tracking method. Burn-up depletion equations are solved using the matrix exponential method CRAM (*Chebyshev Rational Approximation Method*), providing a robust and accurate solution with a very short computation time and is entirely based on built-in calculation routines, without coupling the code to any external solver. A comparison between CRAM, ORIGEN solver and other TTA (*Truncated Taylor Approximation*) methods proved the advantages of the CRAM method in terms of accuracy and running time, thanks to its mathematical approach. Continuous-energy cross-sections read from the library files are reconstructed on a unionized energy grid, used for all reaction modes: the use of a single energy grid results in a significant speed-up in calculation times. Macroscopic cross-sections for each material are pre-generated before the transport simulation: instead of calculating the cross-sections by summing over the constituent nuclides during tracking, the values are read from pre-generated tables, which is another effective strategy useful in order to improve the code overall performance. The pre-generated macroscopic cross-sections are updated at different burn-up steps, properly chosen with regards to the irradiation progression. The effect of a neutron spectrum change along irradiation is thus duly taken into account in this way. SERPENT-2 was validated against various criticality benchmarks, experiments, research reactors tests, burn-up and full core calculations, duly reported and documented in the manuals of the code.

At KIT a neutronics code and data system, C^4P-TRAIN (Rineiski 2018), was employed for generation of self-shielded 560-group cross-sections and for burn-up calculations, using JEFF 3.1.1 data (Santamarina, 2009). Neutron transport calculations at several times were performed with a Sn deterministic transport code, DANTSYS (Alcouffe 1995). These updates in the neutron transport computations – the number of which is adapted with regards to the duration of the experiment – are performed with the goal to take into account variations in the test fuel isotopic composition under irradiation. At every updating time, the microscopic and macroscopic cross-sections in the test fuel region are recalculated, then the neutron flux and radial power profile are recomputed. Two 1D models with white (similar to reflective) radial boundary conditions were employed with DANTSYS: (1) a core model with irradiated pin surrounded by sodium container and other core elements, including driver fuel, and (2) a cell model with irradiated pin surrounded by sodium. As the approximate core model includes part of the reactor core, especially the driver fuel with the cooling water around, the neutron spectrum in this model is quite thermalized due to the moderation by the water: in case of the SPHERE fuel, about 95% of Pu-239 fissions occurs below 0.1 MeV. Whereas the spectrum in the cell model is rather fast, as no moderator is considered: again with SPHERE fuel, about 55% of Pu-239 fissions occurs above 0.1 MeV. Therefore, thermal fission product yields (FPYs) for Pu-239 were used for the core model, while fast FPYs were used for the cell one. In addition to C^4P-TRAIN-DANTSYS, also a Monte-Carlo (MC) code, OpenMC (Romano 2015), was used for cross-checking at KIT at the beginning of irradiation.

2.2 Chaining neutronics tools with fuel performance codes

The present work includes neutronics simulations of the experimental device, that are chained with simulations of the irradiation with FPCs. The results obtained with SERPENT-2 are used for simulations with TRANSURANUS and GERMINAL fuel performance codes.

In case of the SPHERE experiment, preliminary computations with the FPCs exhibited a clear trend to underestimate both the production and release of fission gases (Xe, Kr) and He. This was due to assumptions about the neutron spectrum. Indeed, the assumption of fast spectrum conditions, given the neutron shield surrounding the device, do not reflect accurately the real conditions of the experiment. These may have evolved progressively from those of a hardened neutron flux, targeted by the Hf shield, to more thermalized conditions as irradiation proceeds. Two main consequences are to be considered: firstly, the creation rates of the different isotopes are evolving during the experiment; secondly, the neutron flux and consequently the power created in the fuel are radially heterogeneous, and also varying during the experiment.
It was thus decided to investigate the neutronic conditions of the SPHERE experiment, through dedicated neutronics modelling and simulations of the device. The goal was to derive adequate basic nuclear data to be used as input for the computations with the FPCs: namely, one-energy group averaged cross-sections (fission and capture) and fission yields, being the basic parameters of the point kinetic neutronics modules embedded in FPCs. The radial (and time-dependent) depletion shape of the power in the fuel is also an output of neutronics simulations, and can be provided as an input to the FPCs.
The same process was further adopted for the simulation of MARINE experiment, with the goal to derive in the same way a tailored set of nuclear data for MARINE. In this experiment, as a main difference with regards to SPHERE, there was no neutron shield on the device aiming at hardening the neutron flux. Thus the spectrum conditions for MARINE are clearly thermal conditions – namely the conditions in the HFR. However, adequate nuclear data are still needed to simulate MARINE experiment with FPCs, tailored for $(U,Am)O_{2-x}$ material irradiated in thermal spectrum conditions.
Thus the chaining of neutronics simulations with FPCs computations was an important and necessary methodological progression implemented in this work, with the goal to improve the reliability of the predictions for such experiments like SPHERE and MARINE performed in a material testing reactor.

In order to use the nuclear data for the TRANSURANUS computations, two dedicated source codes of TRANSURANUS were modified and updated according to the outcome of the SERPENT-2 neutronics simulation, for introducing first the tailored cross-sections and then the fission yields related to the Kr, Xe, Nd and Cs isotopes originated form the fission of U-235, Pu-239 and Pu-241.
In case of GERMINAL, the basic nuclear data used by the point kinetic neutronics model are provided in a dedicated input file. New pre-processing tools have been implemented, enabling the possibility of a parameterization of this input file. The tailored data related to both the SPHERE and MARINE experiments, issued from the SERPENT-2 simulations, have been introduced in that way for the GERMINAL computations. Additionally, the possibility to account for a time-dependent radial depletion of the power in fuel was also introduced in the code, as a complementary loading part of the irradiation history.

As the outcome of the neutronics simulation was issued by the SERPENT-2 code in form of a table of numbers (*detector card*), it was necessary to post-process it with a dedicated code written on purpose in Octave language (Eaton 2016), named OVERPROTECT (*OctaVe readEr irRadiation exPeriments cROss-secTions & yiElds CalculaTor*). The code checks all the burn-up steps available from the neutronics calculation and asks the user to choose one irradiation time point: then it reads and displays the neutron flux (including fast and thermal components) and the radial profile of the fission power; the code provides also the uranium, plutonium and americium radial distributions. A table of cross-sections is then extracted from the SERPENT's output and organized in tabular format (details are provided in the Sections 3.2.2 and 4.2.2 presenting the results from the neutronics simulations). Finally, fission yields for SERPENT are calculated considering the averaged neutron spectrum and the fission cross-sections of the nuclides.

At KIT, the results obtained with C^{4}P-TRAIN-DANTSYS, including the radial power profiles in the pellet and fuel isotopic compositions at different times, for the core (thermal) and cell (fast) models are used for simulations with the fuel performance code FEMAXI (Okawa 2015). The neutronics results at the beginning of irradiation obtained with different simulation tools at KIT are in general agreement, as shown on the Figure 1 presenting the in-pin power profiles obtained with different options for the core model, in case of the SPHERE experiment.

Figure 1: Radial power profiles in the test pin at the beginning of irradiation computed with C^{4}P-TRAIN-DANTSYS and OpenMC

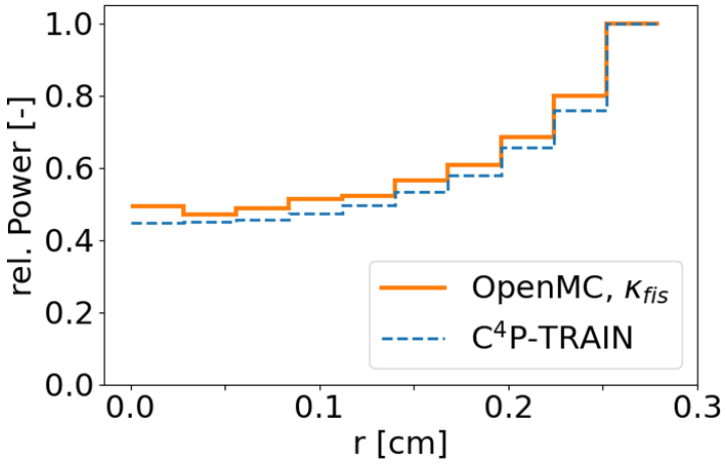

In the C^{4}P-TRAIN models elaborated for SPHERE, the test fuel pellet and gap are considered as one region with a radius of 28 mm. This region is subdivided into 10 radial meshes. The OpenMC and C^{4}P-TRAIN results given in Figure 1 show the relative power density at the beginning of irradiation in the radial meshes, including the last one with the boundaries of 25 and 28 mm vs the pellet center. The variations of the isotopic composition and radial power profile under irradiation are computed in C^{4}P-TRAIN at several times during irradiation, as already explained in the previous Section 2.1. These variations are further taken into account in the FEMAXI simulations.

2.3 Fuel performance codes and their upgrades

The FPCs applied in the present analysis of SPHERE are: FEMAXI (Okawa 2015), used by KIT; GERMINAL (Lainet 2019), used by CEA; TRANSURANUS version v1m4j22 (Magni 2021-1), used by JRC and CVR; the coupled suite TRANSURANUS v1m4j22 // SCIANTIX 2.0 (Pizzocri 2022), developed and used by POLIMI. Advanced versions of the FPCs are herein applied. This is relevant considering the peculiarities of the irradiation experiments, i.e., the set-up of the capsules and the “hybrid” thermal / fast neutron spectrum conditions in case of SPHERE, with the presence of a neutron shield surrounding the device. GERMINAL and TRANSURANUS benefit from the nuclear data derived from the specific neutronics models, implemented in the respective code burn-up modules. The chaining process and the related evolutions introduced for the neutronics modules embedded in the FPCs have been previously described in the Section 2.2. For what concerns physics-based models, the application of SCIANTIX 2.0 (Pizzocri 2022) allows a mechanistic evaluation of the fuel swelling and gas release by following the intra- and inter-granular dynamics of Xe, Kr and He. Moreover, advanced laws for Am-bearing fuel properties, based on both experimental and lower-length data and enhancing the physical ground of FPCs, are applied. These include in particular (i) a heat capacity model for MOX fuels in GERMINAL, recently extended to account for the fuel Am content (Labonne 2023), (ii) thermal conductivity and melting temperature models for minor actinide-bearing fuels (Magni 2021-2), (iii) models for MOX fuel mechanical properties recently inserted in GERMINAL and TRANSURANUS, including a more mechanistic model for oxide fuel creep.

3 Interpretation of the SPHERE experiment

3.1 Main characteristics of the SPHERE experiment

The SPHERE experiment (D'Agata 2014, Gallais-During 2018) aimed at studying the behaviour of Minor Actinide-bearing Driver Fuel (MADF) by comparing sphere-packed and pelletized fuels. It consists of two pins with $(U,Pu,Am)O_{2-x}$ fuel (~ 3 wt.% Am) irradiated in the HFR (High Flux Reactor, Petten). The pins were stored for seven months before post-irradiation examinations (PIEs). We focus here on the pin #1 that contains 10 fuel pellets in a stack. The SPHERE program (fabrication, irradiation and experimental investigations) was part of the former European Projects FAIRFUELS (European Commission 2015) and PELGRIMM (European Commission 2017). The post-irradiation examinations were performed during the PELGRIMM Project along with a first assessment of the experiment with fuel performance codes (FPCs). In the frame of the PATRICIA Project (European Union 2020), which focuses on advancements on partitioning and transmutation of Am-bearing fuels, the SPHERE experiment is re-analysed since it is considered as a reference experimental case for the advancement and assessment of fuel performance codes.

The SPHERE irradiation was carried out in the HFR from 28/8/2013 till 30/12/2014 always maintaining a constant irradiation temperature of the fuel, as illustrated on the following Figure 2 showing the monitoring of the middle-height cladding temperatures of both fuel pins. In Figure 2, pin #1, containing pelletized fuel, is referred to as the 'bottom pin,' while pin #2, containing sphere-packed fuel, is referred to as the 'top pin,' based on their respective positions in the sample holder.

Figure 2: Monitoring of the middle-height cladding temperatures during the SPHERE experiment in the HFR

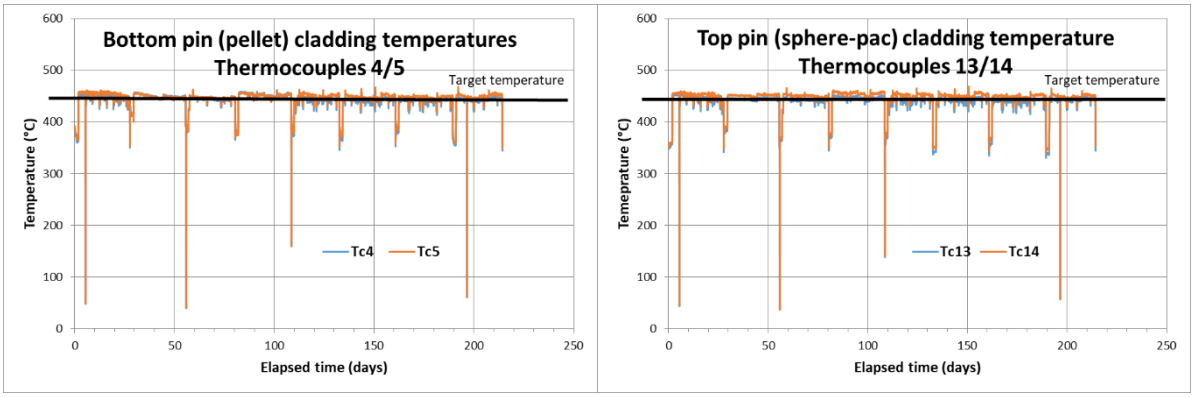

A detailed description of the experiment is provided in (D'Agata 2014). The fuel irradiated was a Minor Actinide-bearing Driver Fuel containing about 3% americium and 20 % Plutonium. The main characteristics and composition of SPHERE fuel are given in the following Table 1.

Table 1: SPHERE fuel characteristics

Pin Nr.	Composition	Isotopic composition	Fuel Density [g cm^{-3}]	^{241}Am contents [g]	^{238}U contents [g]	^{239}Pu contents [g]
#1 Pellets	$U_{0.76}Pu_{0.2}Am_{0.03}$ O_{2-x}	MOX + ^{241}Am	10.393 ≈ 93.8 % TD	0.388	10.192	2.442
#2 Spheres	$U_{0.75}Pu_{0.22}Am_{0.034}$ O_{2-x}	MOX + ^{241}Am	8.33*	0.320	7.167	1.869

* This overall density takes into account both the density of the sphere and the packing density.

The fuel irradiated was in the form of:

- pellets of an average diameter of 5.38 mm stacked one on top of the other for a total length of 58 mm, held in place with a spring. Two Hf pellets have been positioned at the top and bottom of the fuel stack to reduce power peaking at the edges. A diagram of the SPHERE pin #1 with pelletized fuel is shown in Figure 3;
- sphere-pac fuel, composed of small spherical pebbles of two sizes, 0.8 and 0.05 mm, to enhance the packing density. Also the sphere-pac fuel stack had two Hf pellets at either end to keep the sphere-pac in place and to minimize power peaking.

The two pins made of 15-15 Ti steel and containing pellets and sphere-pac fuel in an inert environment (helium) were contained into an assembly which comprises two sample holders made of stainless steel one inside the other:

- the internal sample holder was containing the two pins immersed in a bath of sodium and equipped with thermocouples, fluence detectors and pressure transducers;
- the external sample holder, which housed the internal sample holder and its contents, was encased in a liner of 0.8 mm thick Hafnium foils to harden the neutron spectrum. It is thus important to underline here that the device was designed with the goal to create inside the HFR experimental conditions representative of those in a fast spectrum reactor. Finally, the external sample holder was cooled down with the water of the primary cooling system of the HFR.

The gap between the sample holders were filled with gas, either helium or neon or a mix of the two, in order to adjust the temperature of the experiment.

Figure 3: Cross-sectional diagram of the SPHERE pellet pin, showing Hafnium pellets, MOX+Am fuel pellets and structural components

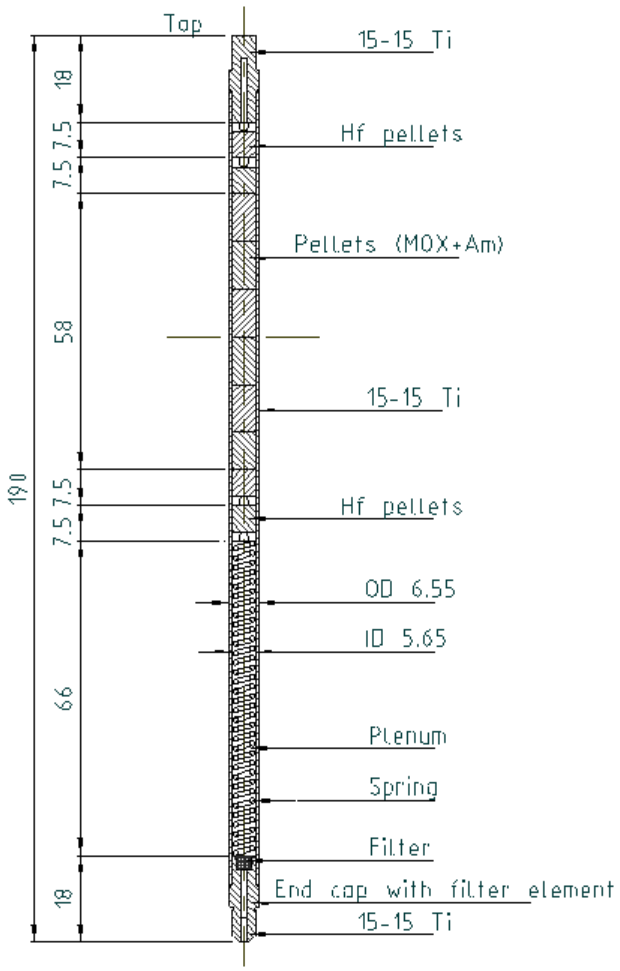

3.2 Interpretation of the SPHERE experiment with the neutronics tools

3.2.1 Modelling of the SPHERE experiment with the neutronics tools

SERPENT-2 modelling is obtained by simulating only the irradiated pin (as shown on Figure 4), by imposing as a boundary condition an external flux provided by the SPHERE test experimenters – this flux is calculated with MCNP (Kulesza 2022) by simulating the entire core. The simulated pin dimensions are summarized in Table 2, while the neutron flux obtained in the voided pellet position is shown in Figure 5. The flux in the voided pellet position is that computed for a fuel rod emptied from any active (i.e., fissile-containing) fuel material. It is issued from the simulation at the scale of the core, performed by the reactor operator. The pin is divided into 10 radial zones in order to track the nuclides distribution evolution during irradiation (although it is not representative of the actual distribution as the neutronics calculation does not take into account thermal gradient re-distribution). The fuel material used for the simulation was a MOX with a 3% (*weight fraction*) content of Am-241, according to irradiation's report specification (isotopic composition is defined in Table 3); at the bottom and top of the fuel column two HfO_2 (with 2.5% Y_2O_3) pellets are present and included in the neutronics model. The gap is filled with a gas mixture of He (99%) and Ne (1%) at a pressure at room temperature of 0.1 MPa, coherently with the SPHERE experiment specifications.

Figure 4: SERPENT-2 model of the SPHERE irradiated pin

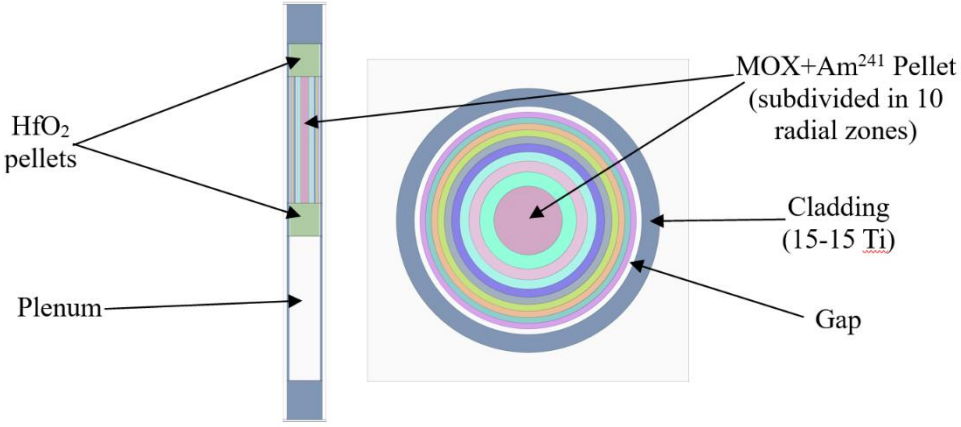

Table 2: Main characteristics of the SPHERE pellet pin

Pellet diameter (mm)	5.38
Gap size (µm)	136
Cladding diameter (mm)	6.55
Cladding material	15-15 Ti
Cladding thickness (mm)	0.45
Fuel weight (g)	13.89
Fuel stack length (mm)	58.92
Free plenum (cm^3)	1.48

Figure 5: Neutron spectra calculated in the voided pellet position for the first 8 irradiation cycles (black continuous line), from cycle 9 to 10 (red dotted line) and 11 (blue dashed line)

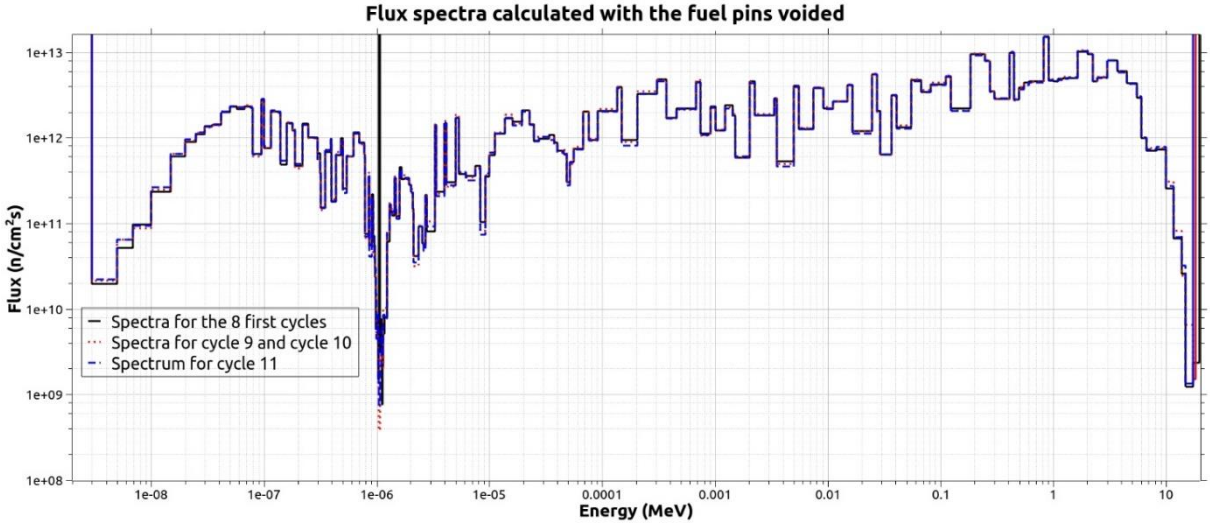

Table 3: Mass composition of the SPHERE pelletized fuel

Nuclide	wt(%)
U-234	0.0209
U-235	0.1949
U-236	0.0122
U-238	67.5060
Pu-238	0.0031
Pu-239	16.2502
Pu-240	1.6418
Pu-241	0.0222
Pu-242	0.0132
Am-241	2.6040
O-16	11.7313

The adopted cross-sections library is JEFF-3.1.1 (Santamarina 2009) and the pin power associated to the irradiation cycles is imposed according to the experimental records provided till 606.19 effective full power days. The power and temperature histories of the simulated pin are shown on the Figure 6 – the plotted temperature corresponding to the maximum clad outer temperature over the pin height, for each irradiation cycle. Fission and capture cross-sections were obtained with SERPENT-2 in the fuel material with 'detectors' using ENDF (*Evaluated Nuclear Data File*) reaction numbers 18 and 102 for total fission and radiative capture, respectively. The simulation is run as a subcritical pin (as the model of the whole core was not available), just defining the neutron flux as the boundary condition (and the power recorded along the experiment). The number of particles simulated in external source mode was 10^7 with an Intel processor i7 (2.67 GHz). The isotopic compositions after irradiation obtained with C^4P-TRAIN-DANTSYS for the core model are qualitatively similar to those obtained with SERPENT-2.

Figure 6: Power and temperature histories of the SPHERE pellet pin simulated with SERPENT

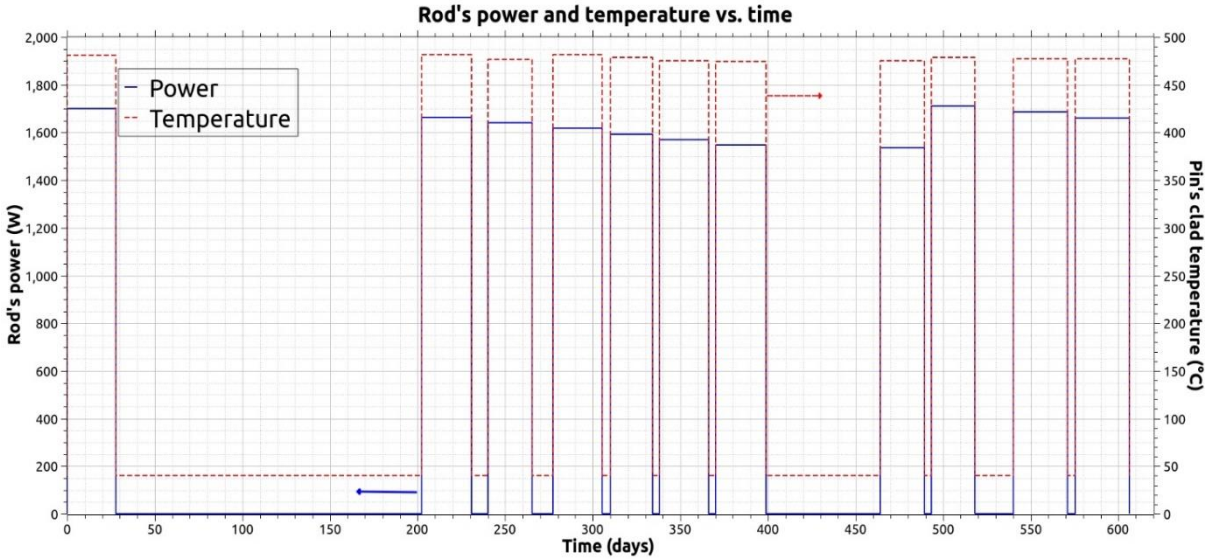

3.2.2 Results from the neutronics simulations of SPHERE

The output of the SERPENT-2 neutronics simulation is the one-group cross-sections table and the neutron spectrum in the pellet at every burn-up step defined in the input. These quantities are read by the Octave dedicated program OVERPROTECT in order to issue the one-group cross-sections and fission yields in tabular format, to be further introduced in the FPCs, as previously explained. The code

provides a plot of the averaged flux in the pellet, the flux radial profile (for every point defined in the SERPENT-2 input – in this case 10 radial points equally spaced) and the radial profiles of the thermal and fast flux.

The whole SERPENT-2 calculation was based on a subcritical calculation with an external, imposed source issued from a simulation at the scale of the core, performed by the operator of the experiment. In order to obtain a reasonable value for radially-averaged cross-sections, a proper ratio between a surface and bulk source term had to be investigated and parametrized.

Based on the SERPENT-generated one-group cross-sections, the values considered by the FPCs are averaged quantities between the beginning of irradiation (BOI) and the end of irradiation (EOI), both for fission and capture reactions. The outcome and the structure are reported in the Table 4, together with the capture/fission values ratio (which was identified as a critical indicator of the reliability of the produced data), in particular concerning Am-241. The neutron capture by Am-241 further leads by chain reaction to the creation of Cm-242, which has a very high alpha-decay frequency and is consequently the main contributor to the helium production by a fuel loaded with minor actinides.

Concerning the fission yields, based on the flux in the pellet issued from the neutronics calculation, the yields were calculated with the following (approximate) formula:

$$FPY_Z^A = \frac{\sum_1^i \left[\Phi_i \cdot \sigma_i^{fiss} \cdot FPY_i^{interp}\right]}{\left(\sum_1^i \Phi_i\right) \cdot \sigma_{1-group}^{fiss}} \quad \textbf{Equation 1}$$

For this purpose, the fission cross-sections of every considered nuclide as a function of energy are stored in an appropriate file to be read by the OVERPROTECT code. The values of the fission yields are interpolated with available data of the JEFF-3.1.1 library. The obtained yields are averaged between beginning and end of irradiation, as it was done for cross-sections. The produced output is reported in the Table 5.

Table 4: Fission and capture cross-sections at the BOI and EOI, their average and ratio computed with SERPENT-2

Nuclide	FissXS_BOI	CaptXS_BOI	FissXS_EOI	CaptXS_EOI	***FissXS_aver.***	***CaptXS_aver.***	*Capt/Fiss*
U-234	0.743972	9.12681	0.735301	10.5624	*0.740*	*9.845*	*13.3*
U-235	12.0319	3.09394	12.706	3.16224	*12.369*	*3.128*	*0.3*
U-236	0.303893	1.9287	0.302516	2.0638	*0.303*	*1.996*	*6.6*
U-238	0.0786835	0.380611	0.0764123	0.404253	*0.078*	*0.392*	*5.1*
U-239	0.730064	1.89387	0.756083	1.90559	*0.743*	*1.900*	*2.6*
Np-237	0.854008	13.7039	0.844389	14.1884	*0.849*	*13.946*	*16.4*
Np-238	37.3667	3.75668	40.1807	4.03901	*38.774*	*3.898*	*0.1*
Np-239	1.00561	7.14152	0.996624	7.31763	*1.001*	*7.230*	*7.2*
Pu-238	2.15938	7.173	2.10413	7.91169	*2.132*	*7.542*	*3.5*
Pu-239	19.9388	8.98851	21.9027	10.0494	*20.921*	*9.519*	*0.5*
Pu-240	0.888979	11.1436	0.882237	11.3837	*0.886*	*11.264*	*12.7*
Pu-241	23.085	7.48475	25.179	8.257	*24.132*	*7.871*	*0.3*
Pu-242	0.793909	6.75086	0.786217	7.8179	*0.790*	*7.284*	*9.2*
Pu-243	9.28288	4.34004	9.49124	4.44079	*9.387*	*4.390*	*0.5*
Am-241	0.906101	24.5003	0.909857	26.4179	*0.908*	*25.459*	***28.0***
Am-242	47.1781	5.82107	50.5868	6.09906	*48.882*	*5.960*	*0.1*
Am-242m	133.536	25.3404	145.495	27.651	*139.516*	*26.496*	*0.2*
Am-243	0.565361	17.4037	0.559781	17.3398	*0.563*	*17.372*	*30.9*
Cm-242	1.60527	5.53658	1.5546	4.89938	*1.580*	*5.218*	*3.3*
Cm-243	22.878	3.46352	24.1851	3.67082	*23.532*	*3.567*	*0.2*
Cm-244	1.20628	2.70474	1.21012	3.38071	*1.208*	*3.043*	*2.5*
Cm-245	33.1655	5.04772	35.5422	5.41745	*34.354*	*5.233*	*0.2*

Table 5: Fractional fission yields calculated with the OVERPROTECT tool, further used on input by the TRANSURANUS and GERMINAL FPCs

	U-234	*U-235*	*U-236*	*U-238*	*Np-237*	*Np-238*	*Pu-238*	*Pu-239*	*Pu-240*	*Pu-241*	*Pu-242*	*Am-241*	*Am-242m*	*Am-243*	*Cm-243*	*Cm-244*	*Cm-245*
Kr-83	0.007765	0.005827	0.005952	0.003436	0.004877	0.003378	0.003002	0.002987	0.002308	0.002037	0.001806	0.002700	0.002168	0.001244	0.001213	0.001366	0.001317
Kr-84	0.012600	0.010622	0.010234	0.006843	0.007964	0.006382	0.004618	0.004951	0.004130	0.003747	0.003604	0.004090	0.002721	0.002005	0.001899	0.002061	0.002045
Kr-85	0.003874	0.002892	0.002954	0.001864	0.002042	0.001781	0.001499	0.001365	0.000957	0.000918	0.000682	0.001272	0.000834	0.000624	0.000651	0.000652	0.000783
Kr-86	0.025528	0.020242	0.019456	0.012182	0.013385	0.010912	0.009745	0.007982	0.006532	0.006287	0.005457	0.007835	0.005553	0.004383	0.004105	0.004270	0.006326
Nd-143	0.051152	0.057218	0.051152	0.046058	0.047128	0.043626	0.044854	0.044103	0.045236	0.044476	0.045815	0.038594	0.043215	0.041439	0.041037	0.043538	0.043884
Nd-144	0.042862	0.052570	0.047204	0.045701	0.041227	0.037457	0.039041	0.036643	0.039798	0.041424	0.042890	0.034095	0.041939	0.039288	0.034558	0.040229	0.040825
Nd-145	0.035247	0.038548	0.042478	0.038023	0.032161	0.038203	0.033577	0.030361	0.031377	0.031822	0.033914	0.035532	0.038174	0.035904	0.033257	0.035216	0.032331
Nd-146	0.027342	0.029460	0.034917	0.034878	0.028111	0.033385	0.027026	0.025074	0.025769	0.026833	0.029195	0.029402	0.030847	0.030054	0.026230	0.031202	0.027544
Nd-148	0.014112	0.016662	0.019527	0.022130	0.017418	0.018091	0.016459	0.016722	0.017979	0.019012	0.020242	0.019305	0.021915	0.020610	0.018241	0.023440	0.025960
Nd-150	0.006160	0.006706	0.010079	0.012812	0.009859	0.009356	0.008460	0.009859	0.010654	0.011686	0.013169	0.012578	0.002799	0.012753	0.006248	0.014600	0.006284
Cs-133	0.073178	0.065829	0.066532	0.066255	0.066912	0.067955	0.069819	0.070062	0.069835	0.066314	0.068301	0.057957	0.053601	0.055086	0.053959	0.050748	0.054004
Cs-134	0.000004	0.000003	0.000000	0.000000	0.000003	0.000000	0.000052	0.000008	0.000002	0.000000	0.000000	0.000025	0.000003	0.000001	0.000079	0.000027	0.000004
Cs-135	0.077665	0.064890	0.061551	0.063473	0.076160	0.075183	0.077772	0.074403	0.075614	0.070985	0.068896	0.071277	0.070127	0.070290	0.065754	0.064018	0.062061
Cs-137	0.061652	0.060584	0.057881	0.059857	0.062663	0.069359	0.064344	0.065020	0.065276	0.063107	0.061486	0.065968	0.061473	0.064278	0.072522	0.065892	0.066710
Cs-139	0.061154	0.062797	0.063322	0.057646	0.055667	0.053955	0.049858	0.055245	0.056628	0.059785	0.059020	0.062030	0.055669	0.055384	0.052407	0.051877	0.062889
Xe-131	0.029039	0.031220	0.029857	0.033477	0.037342	0.030720	0.035474	0.038561	0.035716	0.031034	0.030971	0.039498	0.034944	0.035233	0.032831	0.029980	0.031004
Xe-132	0.053211	0.044812	0.040527	0.047513	0.046880	0.047997	0.054276	0.052390	0.046522	0.045491	0.044860	0.047371	0.043349	0.044785	0.045120	0.039807	0.043274
Xe-134	0.080692	0.077374	0.077107	0.067853	0.073511	0.065622	0.078438	0.071087	0.071879	0.075905	0.073452	0.062340	0.063203	0.063846	0.064466	0.059853	0.058898
Xe-136	0.070440	0.064627	0.068313	0.072184	0.070552	0.080917	0.067685	0.069881	0.067076	0.070381	0.072106	0.066236	0.067165	0.071106	0.066258	0.062155	0.051095
He-4	0.002309	0.001699	0.001899	0.001428	0.002060	0.001860	0.002420	0.002191	0.002781	0.001860	0.002370	0.002370	0.002100	0.001820	0.002580	0.002420	0.002280

3.3 Interpretation of the SPHERE experiment with the upgraded fuel performance codes

3.3.1 Modelling of the SPHERE experiment with the fuel performance codes

Compared to the first assessment of the SPHERE experiment performed during the PELGRIMM Project (D'Agata 2014), the present work relies on refined irradiation and boundary conditions for the fuel performance code simulations. The thermal boundary condition is updated by taking into account the temperature monitoring along the experiment, hence the initial assumption of a uniform and time-invariant temperature on the clad outer bound is replaced by a history of an axially varying temperature (Figure 7 – left showcases the axial clad outer temperature profiles during the first and last SPHERE irradiation cycles). The revision of the linear heat rating history takes into account the measured activities on the fluence monitor sets. As illustrated in Figure 7 – right, the estimations of the maximum linear heat rating during the first eight cycles of irradiation are significantly increased: from 293 W/cm to 327 W/cm during the first cycle. Details about the clad temperature profiles and the linear power during the SPHERE irradiation cycles are provided in the Table 6, which also includes the axial distribution of pin linear power (assumed constant along irradiation). The pin geometry and composition are already described in Section 3.1. The nuclear data derived specifically for SPHERE and adopted for the fuel performance code simulations are given by the Table 4 and Table 5 in the Section 3.2.2.

Figure 7: Revised thermal boundary condition and linear heat rating history

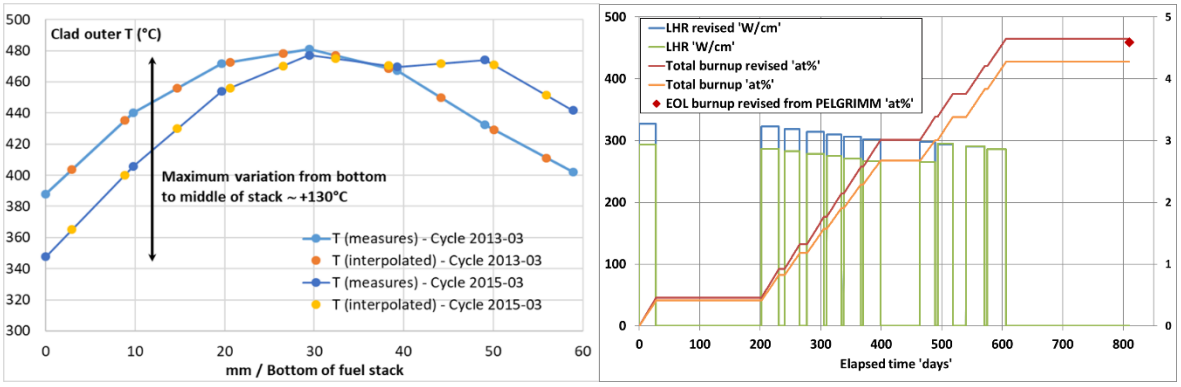

For what concerns the neutron spectrum during the SPHERE experiment, as the exact evolution during irradiation of the spectrum conditions inside the experimental assembly could not be easily retrieved (due to uncertainties about the effectiveness and degradation of the Hf shield for thermal neutrons), two bounding assumptions for the FPC computations are adopted. The first option is fast spectrum conditions, corresponding to a flat radial power profile inside the fuel, and the second one is thermal spectrum associated to a time-dependent radial depletion of power in the fuel. Considering these two assumptions for the neutron spectrum, being so far from each other, also means that the uncertainty on the linear heat rating throughout the irradiation may be high. It is unfortunately not possible to provide at this stage an accurate estimation of the uncertainty on the linear heat rating. As previously described, the neutronic simulation of the experiment implements a succession of computational steps, each one combining the evaluation of the neutron spectrum followed by the fuel depletion calculation, using the updated spectrum. There is consequently a cumulation of uncertainties over all the successive computational steps. The estimation of a statistical uncertainty on the linear heat rating throughout the irradiation would thus require multiple independent simulations of the whole experiment. Even if such process remains technically feasible, it would be very costly in computation time, and one should also consider that the number of independent simulations required to obtain a converged estimation of the uncertainty on the linear heat rating can't be defined a priori. This is why such process has not been implemented up to now. For both options of fast or thermal spectrum, a

tailored set of basic nuclear data is used, resulting from the neutronics modelling of SPHERE (Section 3.2.1). The depletion shape which is considered in thermal spectrum corresponds to the default TRANSURANUS model for LWR cases, illustrated in Figure 8. These profiles are derived from the TRANSURANUS burn-up model (Botazzoli, 2011) and reflect the specific evolution of the SPHERE fuel geometry, microstructure and composition during irradiation, i.e., fuel restructuring with the formation of a central hole, as well as a moderate redistribution of Pu towards the hole. The fast / thermal neutron spectrum of the two bounding simulations of SPHERE impacts on irradiation-driven phenomena, e.g., creep of both fuel and cladding.

Table 6: Details about the revised thermal boundary condition (axial profiles of cladding outer temperature) and linear heat rating history along the cycles of the SPHERE irradiation

	Fuel axial discretization: slice number (mm / bottom of fuel stack)										
Cycle	1 (2.95)	2 (8.84)	3 (14.73)	4 (20.62)	5 (26.51)	6 (32.40)	7 (38.29)	8 (44.19)	9 (50.08)	10 (55.97)	Max Linear Heat Rate * (W/cm)
2013-03	403.8	435.1	456.0	472.6	478.3	476.9	468.5	449.7	429.3	411.1	327.05
2014-02	400.3	430.5	451.3	468.4	477.1	477.3	469.0	461.2	446.0	393.3	322.43
2014-03	394.4	424.6	447.3	466.1	472.8	471.7	462.8	459.4	451.8	417.3	318.15
2014-04	399.0	429.7	451.0	468.7	477.6	477.2	467.7	459.6	445.3	398.6	314.21
2014-05	383.0	414.2	440.6	463.3	472.5	474.0	467.8	464.4	457.5	430.1	309.93
2014-06	394.1	422.8	446.8	466.9	472.8	471.2	462.2	459.6	453.1	420.8	306.16
2014-07	391.6	420.9	445.7	466.6	472.5	470.8	461.3	460.3	455.9	425.9	301.71
2014-08	394.6	422.8	446.9	467.1	472.4	470.3	460.6	459.4	454.8	424.4	297.26
2015-01	380.6	414.3	442.9	467.2	474.9	474.1	464.8	464.9	461.0	426.8	294.01
2015-02	379.9	414.4	442.5	466.3	474.2	473.8	464.9	466.0	463.4	432.3	289.9
2015-03	365.1	400.1	429.9	456.2	470.2	474.9	470.4	471.9	470.9	451.3	285.62
LHR axial peak factors	0.94	0.95	0.95	0.96	0.97	0.97	0.98	0.99	0.99	1	

* The linear heat rate provided in this table corresponds to the maximum value experienced by the fuel during the SPHERE irradiation (i.e., at axial slice 10 where peak factor is 1).

Figure 8: Radial profiles of power depletion adopted by the fuel performance codes for the "LWR simulation" of SPHERE, in terms of local power density at three representative times during the experiment: 5 h = beginning of irradiation (beginning of cycle 2013-03), 8020.7 h = mid-irradiation (end of cycle 2014-05), 14548.7 h = end of irradiation (end of cycle 2015-03)

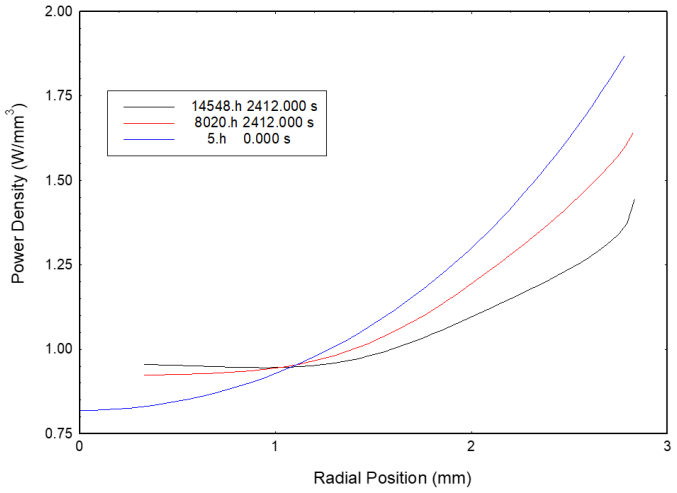

As for the modelling setup adopted by the applied codes, different input choices can be selected, appropriate for the "LWR" or "FBR" interpretation of the SPHERE pin performance. As an example, the TRANSURANUS and TRANSURANUS//SCIANTIX simulations rely on different models for the fuel-cladding gap conductance applied under the thermal / fast spectrum assumptions, i.e., the URGAP model (Lassmann, Hohlefeld 1987) or its version adjusted for FR simulations, based on (Charles, Bruet, 1984). Another example of dedicated model choice employed concerns the fuel relocation behaviour, impacting the gap width evolution especially at beginning of irradiation. Different relocation parameters are used in FEMAXI for "LWR" and "FBR" simulations of SPHERE, and in parallel, parametric computations have been performed with GERMINAL about the pellet relocation modelling. Concerning the mechanistic inert gas behaviour modelling performed with SCIANTIX, it includes the physics-based consideration of the intra- and inter-granular dynamics of inert gases (Xe, Kr, He), the treatment of the micro-cracking of the fuel grain boundaries, and the percolation of gases from the bubbles on the intact grain boundaries (Zullo, 2023). The helium production rate in the SPHERE fuel is reproduced via a surrogate model which is tailored according to the TRANSURANUS calculations, with regards to the evolution with time along the experiment and the final value of helium produced after irradiation and storage. This modelling choice is supported by the fact that the estimated amount of helium produced from the available neutronics calculations (FISPACT) is lower than the measurement of helium released, leading to more than 100% of helium fractional release and questioning the reliability of the FISPACT estimation. The main modelling options adopted by the fuel performance codes for the two bounding simulations of the SPHERE irradiation experiment are collected and referenced in Table 7.

Table 7: Details about the main modelling options adopted by the fuel performance codes for the simulations of the SPHERE irradiation experiment

Option 1 **Fast spectrum** ("FBR simulation")	TRANSURANUS	TRANSURANUS //SCIANTIX	GERMINAL[1]	FEMAXI[2]
Gap conductance	URGAP model modified for FBR conditions (Charles, Bruet, 1984)	URGAP model modified for FBR conditions (Charles, Bruet, 1984)	Arnaud-Roche model	Modified Ross & Stoute model (Suzuki 2005)
Fuel relocation	Model calibrated on liquid-metal FBR	Model calibrated on liquid-metal FBR	Empirical correlation to the temperature gradient	SIEX code correlation (Dutt 1975)
Fuel densification	Pore migration model for FBR conditions	Pore migration model for FBR conditions	Empirical correlation to the temperature	Schlemmer & Ichikawa model
Fuel thermal conductivity	Magni 2021-2	Magni 2021-2	Magni 2021-2	Philipponneau 1992
Fission gas production	Fission yields for Xe and Kr from SPHERE neutronic modelling (Section 3.2.2) **Flat radial power profile**	Fission yields for Xe and Kr from (Motta, Olander 2017) **Flat radial power profile**	Point kinetic neutronics model **Flat radial power profile**	Neutronics by C^{4}P-TRAIN in **fast spectrum**
Helium production	From TUBRNP (TRANSURANUS burn-up module), including fission yields for He from SPHERE neutronic modelling (Section 3.2.2)	Surrogate model tailored for SPHERE	Point kinetic neutronics model	Neutronics by C^{4}P-TRAIN
Helium release	Based on He diffusion according to Fédérici, 2007	Treated by SCIANTIX physics-based module	Temperature threshold for helium release	Power threshold for helium release
Inert gas behaviour	Semi-empirical TRANSURANUS model for FBR conditions	Treated by SCIANTIX physics-based module	Fission gas release model	Mechanistic fission gas release model
Option 2 **Thermal spectrum** ("LWR simulation")	TRANSURANUS	TRANSURANUS //SCIANTIX	GERMINAL[1]	FEMAXI[2]
Gap conductance	URGAP model (Lassmann, Hohlefeld 1987)	URGAP model (Lassmann, Hohlefeld 1987)	Same as option 1	Same as option 1
Fuel relocation	Modified FRAPCON-3 model	Modified FRAPCON-3 model	Same as option 1	Same as option 1
Fuel densification	Empirical model for LWR conditions	Empirical model for LWR conditions	Same as option 1	Same as option 1
Fuel thermal conductivity	Magni 2021-2	Magni 2021-2	Same as option 1	Same as option 1
Fission gas production	Fission yields for Xe and Kr from SPHERE neutronic modelling (Section 3.2.2) **Radial depletion of power in fuel**	Fission yields for Xe and Kr from (Motta, Olander 2017) **Radial depletion of power in fuel**	Point kinetic neutronics model **Radial depletion of power in fuel**	Neutronics by C^{4}P-TRAIN in **thermal spectrum**
Helium production	From TUBRNP (TRANSURANUS burn-up module), including fission yields for He from SPHERE	Surrogate model tailored for SPHERE	Point kinetic neutronics model	Neutronics by C^{4}P-TRAIN

	neutronic modelling (Section 3.2.2)			
Helium release	Based on He diffusion according to Fédérici, 2007	Treated by SCIANTIX physics-based module	Same as option 1	Same as option 1
Inert gas behaviour	Mechanistic TRANSURANUS model for LWR conditions	Treated by SCIANTIX physics-based module	Same as option 1	Same as option 1
Cladding properties/behaviour	TRANSURANUS models for 15-15Ti stainless steel	TRANSURANUS models for 15-15Ti stainless steel	AIM1	Stainless steel 15-15Ti

[1] The models implemented in GERMINAL and used for this study are mainly described in (Lainet 2019), except the law for the fuel thermal conductivity (Magni 2021-2).
[2] The models implemented in FEMAXI and used for this study are mainly described in (Suzuki 2005), except the law for the fuel thermal conductivity (Philipponneau, 1992). The neutronics analysis is performed by C^4P-TRAIN (Rineiski 2018) prior to the FEMAXI computation, providing the fission gas and helium productions on input.

3.3.2 Results from the simulations of SPHERE with the fuel performance codes

The first analysed results focus on the production and release of inert gases: namely, fission gases (Xe, Kr) and helium, which is a major concern for fuels bearing minor actinides. The calculation results obtained under both of the assumptions of fast and thermal spectrum are summarized in Table 8, along with the corresponding puncturing examination results on the SPHERE pelletized fuel pin.

Table 8: FPCs results for inert gas production and release and puncturing examination results

FPCs results Option 1 Fast spectrum	Xe + Kr produced (atoms)	Xe + Kr released (atoms)	Xe + Kr release rate (%)	He produced (atoms)	He released (atoms)	He release rate (%)
TRANSURANUS	4.23E+20	2.00E+20	47.2%	1.77E+20	1.13E+20	63.8%
TRANSURANUS //SCIANTIX	4.08E+20	2.92E+20	71.6%	1.20E+20	8.44E+19	70.3%
GERMINAL	3.65E+20	1.06E+20	29.0%	1.82E+20	1.28E+20	70.3%
FEMAXI //C^4P-TRAIN	3.67E+20	2.08E+20	56.7%	1.20E+20	8.25E+19	68.8%
FPCs results Option 2 Thermal spectrum	Xe + Kr produced (atoms)	Xe + Kr released (atoms)	Xe + Kr release rate (%)	He produced (atoms)	He released (atoms)	He release rate (%)
TRANSURANUS	4.78E+20	3.38E+20	70.6%	1.80E+20	1.17E+20	65.0%
TRANSURANUS //SCIANTIX	4.02E+20	3.67E+20	91.3%	1.19E+20	8.73E+19	73.4%
GERMINAL	3.64E+20	1.07E+20	29.4%	1.82E+20	1.29E+20	70.9%
FEMAXI //C^4P-TRAIN	3.92E+20	1.91E+20	48.7%	1.73E+20	1.23E+20	71.1%
Experimental data from puncturing N.B. Xe, Kr and He productions issued from computations [1]	Xe + Kr produced (atoms)	Xe + Kr released (atoms)	Xe + Kr release rate (%)	He produced (atoms)	He released (atoms)	He release rate (%) [2]
	4.12E+20	3.28E+20	79.6%	1.13E+20	1.56E+20	138% [2]

[1] The productions of xenon, krypton and helium used for estimating the release rates with the puncturing results are issued from a FISPACT (Sublet 2017) computation performed by the reactor operator.
[2] The helium release rate exceeding 100% is a consequence of using of an estimated production issued from computations.

The first results analysed here are those for helium production. They are shown in Figure 9. One can notice that the adoption of a tailored set of basic nuclear data for the SPHERE experiment does not solve all the discrepancies between the computation results. The predictions obtained by GERMINAL and TRANSURANUS do not evolve significantly when moving from fast to thermal spectrum assumption. The SCIANTIX surrogate model for helium production is tailored for retrieving the helium production evolution and final amount according to the TRANSURANUS calculations, thus avoiding the information of more than 100% release resulting from an estimated helium production via FISPACT which is lower than the released quantity of helium retrieved at puncturing (cf. Table 8). As a consequence for the TRANSURANUS//SCIANTIX suite, there is no difference between the two cases in the computation of helium production. On the contrary, the production computed by FEMAXI//C^{4}P-TRAIN is about 44% higher in thermal spectrum, compared to that in fast spectrum. The explanation for this discrepancy is the fact that the C^{4}P-TRAIN computations produce from multi-group data different sets of one-group (n, alpha) cross-sections and different branching ratios in fast and thermal spectrum. This underlines the need for a complete neutronic characterization of such an experiment like SPHERE. Having determined a tailored set of capture, fission cross-sections and fission yields in the frame of this work only represents a first step in this characterization, to be extended to all basic nuclear data and also completed by considering the depletion of the neutron shield along the experiment. The helium production estimated with FISPACT is more in line with the C^{4}P-TRAIN result in fast spectrum. This tends to confirm the assumption that was retained for the FISPACT computation, regarding the neutron spectrum.

Figure 9: FPCs results for the helium production

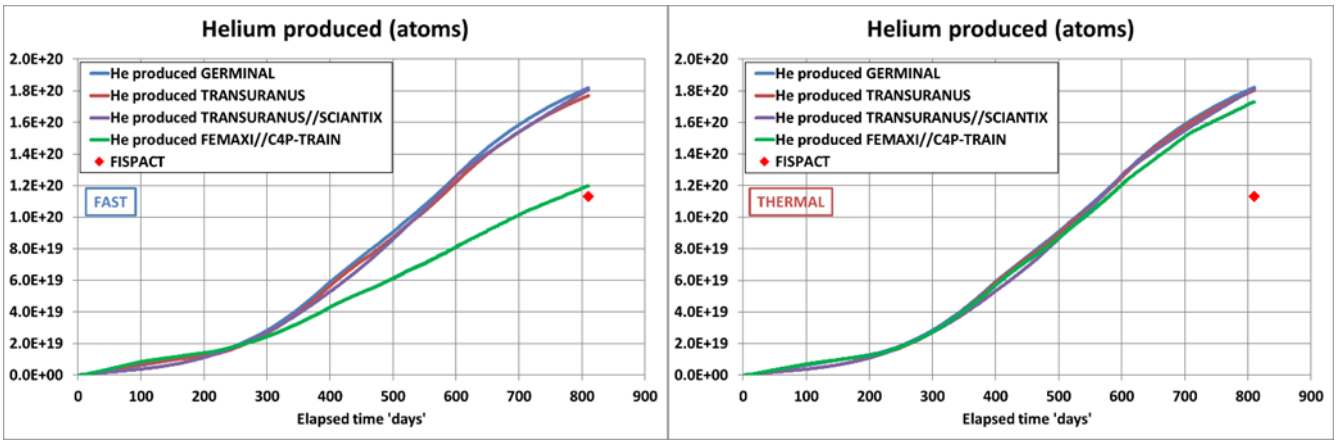

It is then interesting to analyse the predictions obtained for the helium released in the pin free volume, as shown on the Figure 10. There is an overall trend in the results obtained by the codes to underestimate the helium released quantity. This trend is observed with both assumptions of fast or thermal spectrum. The underestimation of the helium released quantity is stronger for the code aligned with FISPACT for the evaluation of the helium production, namely: FEMAXI//C^{4}P-TRAIN in fast spectrum. On the contrary, it is evident from the Figure 9 and Figure 10 that the codes accounting for a helium production greater than the FISPACT estimation are able to reduce the underestimation of the helium released quantity after irradiation and storage, when comparing to the quantity retrieved at puncturing. This indicates that probably more helium than the FISPACT estimation was produced in the SPHERE fuel. Nevertheless, the predictions of helium release by the FPCs remain lower than the measurement, even by using a tailored set of basic nuclear data. Two explanations can be proposed:

- The helium produced and released by the fuel during irradiation, at hot state, is underestimated. This would mean that the creation of the heavy nuclides contributing to the helium production by decay is underestimated during the irradiation.

- Predicting no helium release during storage, prior to puncturing, may not exactly reflect the real behaviour. The reactor temperature at null power is 40°C, and this temperature looks too low for enabling the helium release by the fuel. But a residual power in the fuel during the storage after irradiation could create a higher temperature in the fuel at that time, enabling – at least partially – the helium diffusion and release.

This firstly confirms the need for refining further the evaluation of the irradiation conditions. But there can be another need for refining the definition of the storage conditions, especially with the goal to evaluate the residual power in the fuel during the storage.

Figure 10: FPCs results for the helium in the pin free volume

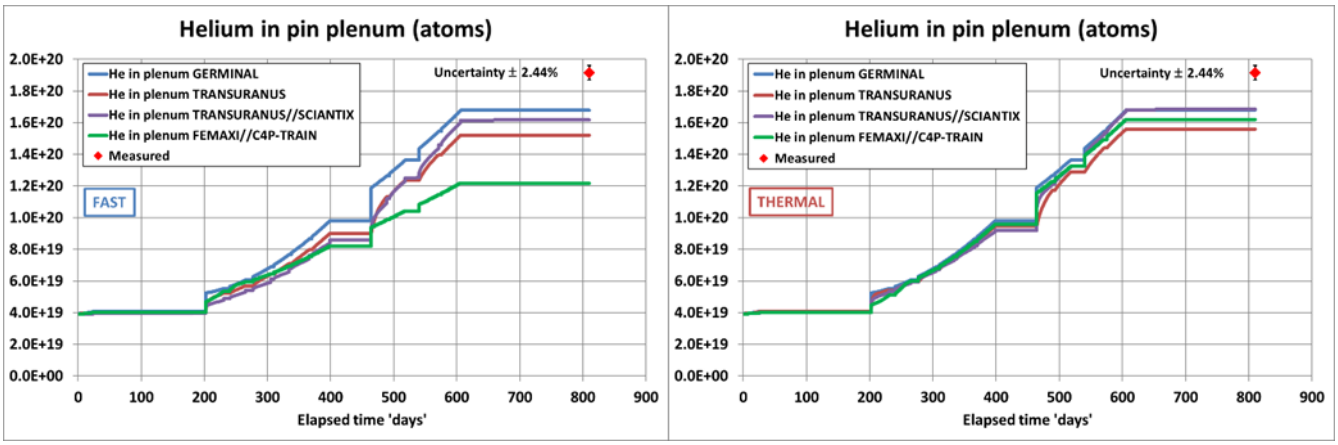

Considering both helium production and release, the assumption of thermal spectrum turns out to be more adequate, especially when considering the helium quantity retrieved in plenum at puncturing. The helium production estimated via FISPACT with the assumption of fast spectrum is much too low to predict correctly the final quantity released in plenum. This explains why the estimation of the helium release rate is greater than 100% when computed with the evaluation of the helium production by FISPACT.

Regarding the fission gases production – namely, xenon and krypton, the predictions obtained by the FPCs are presented in the Figure 11. Two different trends can be noted: for TRANSURANUS and FEMAXI//C^{4}P-TRAIN, the production of fission gases is increased when moving from fast to thermal spectrum assumption; whereas it is not really affected by the spectrum conditions, when considering the predictions by TRANSURANUS//SCIANTIX and GERMINAL. This illustrates the fact that not only the cross-sections and the fission yields affect the estimation of the fission gases production, but also the fission energies, that are not the same in fast and thermal spectrum for the TRANSURANUS and FEMAXI//C^{4}P-TRAIN computations. As TRANSURANUS//SCIANTIX and GERMINAL use a single set of values for the fission energies, their predictions for the fission gases production are logically less affected by the neutron spectrum assumption.
This indicates the need to re-evaluate the energy per fission for each nuclide, for the different spectrum conditions of interest. This can be done for example on the basis of the more recent JEFF library together with EPMA data.
The fission gas production estimated by FISPACT is surrounded by those obtained by the FPCs. A higher estimation is obtained by TRANSURANUS in thermal spectrum, indicating that more fissions are needed in these conditions to build up the heat source term, with respect to the given linear heat rating. This is the effect of lower fission energies in thermal spectrum.

Figure 11: FPCs results for the fission gases production

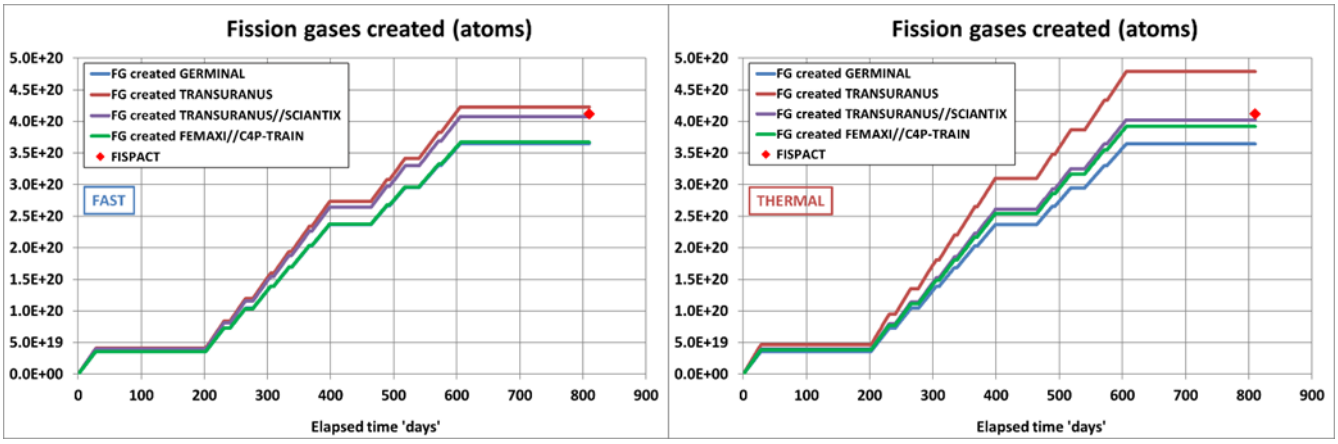

The last results related to the inert gases behaviour are the predictions of fission gas release. They are presented in the Figure 12. The predictions of fission gas release are the one showing the highest discrepancies between the codes. Again, two different trends can be noted: for TRANSURANUS and TRANSURANUS//SCIANTIX, the predicted fission gas release is significantly increased when moving from fast to thermal spectrum assumption. This is mostly visible for the TRANSURANUS result. The best agreement with the amount of fission gases retrieved at puncturing is obtained by TRANSURANUS in thermal spectrum. On the other side, the predictions by FEMAXI//C^{4}P-TRAIN and GERMINAL are very slightly changed by the spectrum conditions. There is nearly no change in the results obtained by GERMINAL. These different evolutions are linked to those of the predicted temperatures in the fuel, that are much higher for TRANSURANUS and TRANSURANUS//SCIANTIX with the assumption of thermal spectrum. This will be illustrated and discussed at the end of the Section.

Figure 12: FPCs results for the release of the fission gases

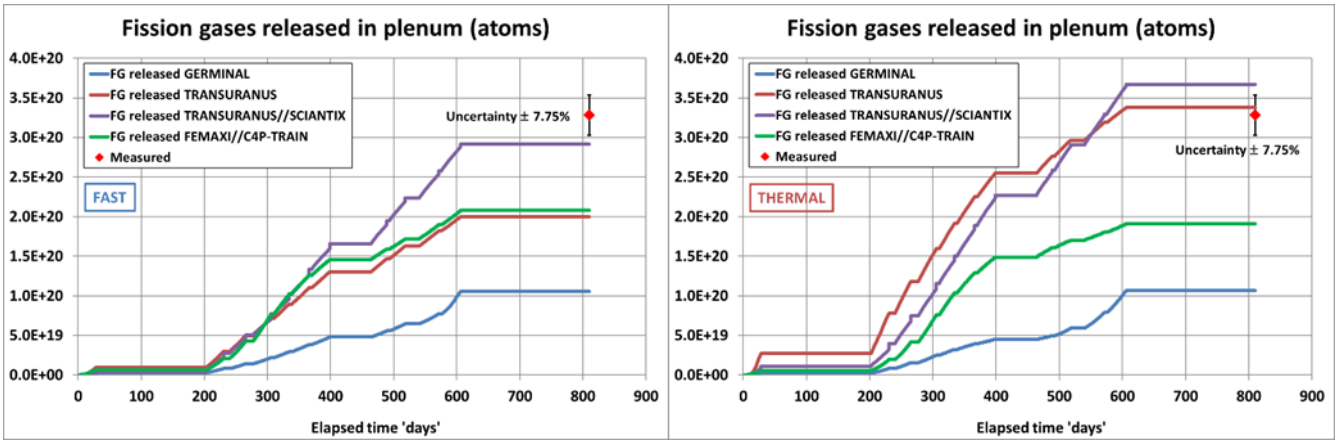

For what concerns the fuel restructuring mechanism, Figure 13 shows the central hole radius at end-of-life predicted by the different codes, along the fuel column, compared with the measurements. One can remark first the scattering of the measures, which could be the consequence of geometrical irregularities along the column, such as pellet eccentricity. The predictions by the codes do not render this effect, as they all adopt an axisymmetrical representation of the geometry. The central hole radii at end-of-life predicted by TRANSURANUS and TRANSURANUS//SCIANTIX are slightly increased in thermal spectrum, despite the radial depletion of power in fuel. The calculated temperatures in the fuel at the beginning-of-life are high enough for enabling an initial fuel restructuring. But the fuel temperatures are evaluated even higher later in irradiation (see further Figure 15 – right): the effect

of the gap size decrease along irradiation is not as strong as that of the decrease of the thermal conductivity of the gas mixture in the gap, due to the release of fission gases, the thermal conductivities of which are poor. There is consequently a delayed re-enabling of fuel restructuring, leading to a supplementary increase of the central hole radius. The results obtained by FEMAXI//C^{4}P-TRAIN are not significantly affected by the spectrum conditions. The predicted central hole is a bit wider at the bottom of the fuel column in case of fast spectrum. Regarding the GERMINAL computations, the radial depletion of power in the fuel in thermal spectrum inhibits the fuel restructuring mechanism. The trends observed for FEMAXI//C^{4}P-TRAIN and GERMINAL are also linked with the temperature evolution in the fuel. For these two codes, the peak temperature in fuel is reached at the very beginning of the irradiation, at hot state when the pellet-to-clad gap is still open. Then the maximum temperature along the rest of the irradiation is not as high as at the beginning. For GERMINAL, the threshold for fuel restructuring is exceeded only in the case of fast spectrum, i.e., with a flat radial profile of the power in fuel. The peak temperature at beginning-of-life is thus higher in fast spectrum, enabling the fuel restructuring. In the contrary, the peak temperature at beginning-of-life in thermal spectrum is decreased by the radial depletion of power and consequently not high enough to enable the restructuring mechanism.
Apart from the inhibition of fuel restructuring in thermal spectrum observed for GERMINAL, the predictions by the codes show an overall consistency.

Figure 13: FPCs results for the central hole radius at end-of-life

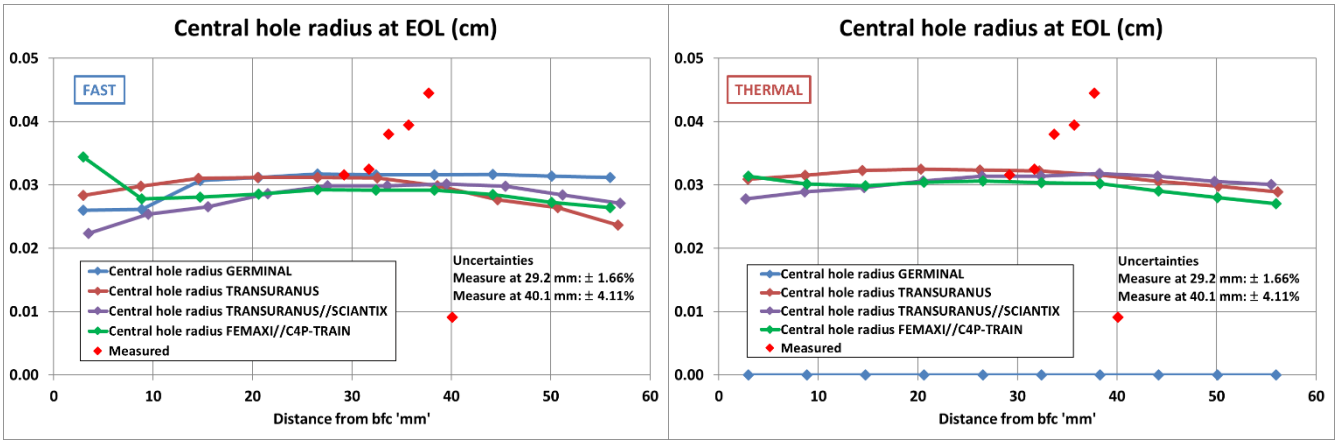

The next comparison with experimental data concerns the radial expansion of the columnar grains formation in the fuel pellets. Figure 14 shows the radius of the columnar grains region at end-of-life. With the assumption of a fast neutron spectrum (Figure 14 – left), all codes predict a columnar grains expansion wider than observed. This suggests that the calculated maximum fuel temperatures over the whole irradiation are higher than what they were in reality, with the assumption of fast spectrum. Figure 14 – right shows the results obtained when considering a thermal neutron spectrum. The values at zero for TRANSURANUS and TRANSURANUS//SCIANTIX are not significant, since they are due to the simple fact that the determination of the columnar grains formation is disabled when assuming thermal spectrum. The temperatures computed by TRANSURANUS and TRANSURANUS//SCIANTIX are practically higher with this assumption of thermal spectrum, as shown further on Figure 15. In case of FEMAXI//C^{4}P-TRAIN and GERMINAL, the determination of the columnar grains formation is still enabled and the results show a lower radial extent in thermal spectrum, in better agreement with observation. This reflects a decrease of the maximum temperature in the fuel pellets, due to the radial depletion of power in thermal spectrum.

Figure 14: FPCs results for the columnar grains region radius at end-of-life

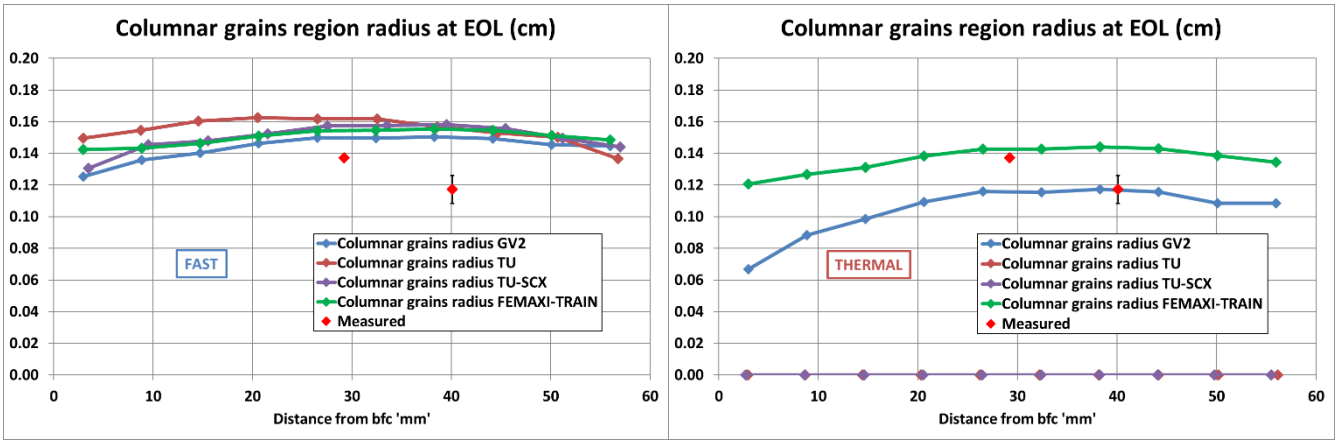

The assessments of the physical mechanisms in the fuel are strongly linked to the temperature evaluation. The evolutions with time of the maximum temperature in the fuel computed by the different codes at the Peak Power Position (namely, at the top of the column) are presented in the Figure 15. The comparison of these results helps explaining the different trends previously seen in the predictions for the gases behaviour and the fuel restructuring.

Concerning first the predictions by TRANSURANUS and TRANSURANUS//SCIANTIX, the models involved for the fuel-cladding gap thermal conductance are different for the computations in fast and thermal spectrum. This difference can be seen on the Figure 16, looking at the evolutions obtained in fast spectrum (left) and thermal spectrum (right). In fast spectrum, the model is still based on URGAP (Lassmann, Hohlefeld 1987) but takes into account a minimum value for the gap conductance based on data from (Charles, Bruet, 1984), yielding a better heat removal from the fuel, representative for a faster gap evolution towards closure in fast reactor pins. Taking into account a minimum value results in a "shifting effect" for the gap conductance evaluated in fast spectrum (Figure 16 – left), compared to that calculated in thermal spectrum (Figure 16 – right). This represents a first simple approach to take into consideration the effects due to eccentricity (Scolaro, 2021), that are assumed to be more important in FBR fuels in comparison with LWR fuels. A better, data-driven method based on multi-dimensional analysis with the OFFBEAT code, is under development. As a main consequence, the maximum temperature predicted in the fuel is significantly higher in thermal spectrum (up to 500°C higher during the cycle #7, see Figure 15 left and right). This explains why the prediction of fission gas release is strongly increased in thermal spectrum, and also why the fuel restructuring is a bit more enabled in the thermal interpretation of SPHERE, despite the radial depletion of power.

In case of GERMINAL, the same model for the gap conductance is used for both computations in fast and thermal spectrum. The pellet-to-clad gap closure is predicted to happen very early in the irradiation in case of a fast spectrum (Figure 17 – left), whereas it closes only at the end of irradiation in case of thermal spectrum (Figure 17 – right). These trends are explained by a lower magnitude of pellet relocation in thermal spectrum, as a consequence of a decreased temperature gradient in the pellets, due to the radial depletion of power in the fuel. The associated evolutions of the gap conductance in fast and thermal spectrum are thus coherent: higher gap conductance in fast spectrum with a closed gap, decreasing along irradiation with the release of fission gases (Figure 16 – left); and a lower gap conductance in thermal spectrum, increasing at the end of irradiation with the gap closure (Figure 16 – right). The radial depletion of power in the fuel in thermal spectrum compensates the lower gap conductance. Thus, the maximum temperatures reached in the fuel are quite consistent when comparing the computations in fast and thermal spectrum (Figure 15 left and right). Anyway, the temperatures calculated by GERMINAL seem to be too low in both cases, with regards to the

underestimation of the fission gas release. The highest temperatures over the whole irradiation are predicted at the very beginning of irradiation.

Finally, for the FEMAXI//C^{4}P-TRAIN computations, the same model for the gap conductance is also used for both cases of fast and thermal spectrum. When comparing the results obtained in the two cases, the evolutions obtained for the gap conductance (Figure 16) and the gap size (Figure 17) are quite consistent. As a consequence, the slightly lower maximum temperature in fuel predicted in thermal spectrum (Figure 15 – right compared to Figure 15 – left) reflects the effect of the radial depletion of power, decreasing the temperature.

Figure 15: FPCs results for the maximum temperature in fuel at Peak Power Position

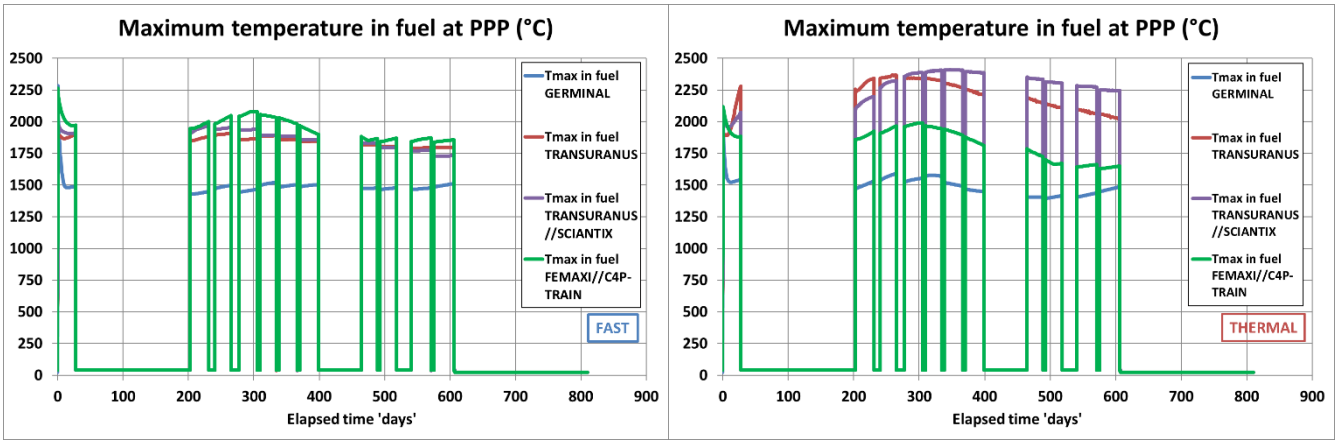

Figure 16: FPCs results for the gap thermal conductance at Peak Power Position

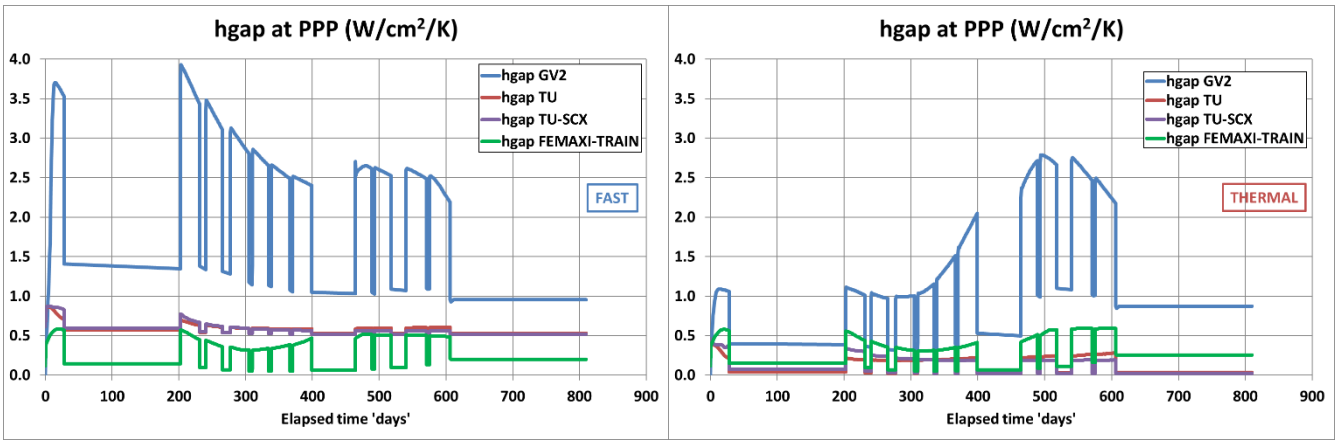

Figure 17: FPCs results for the pellet-to-clad gap size at Peak Power Position

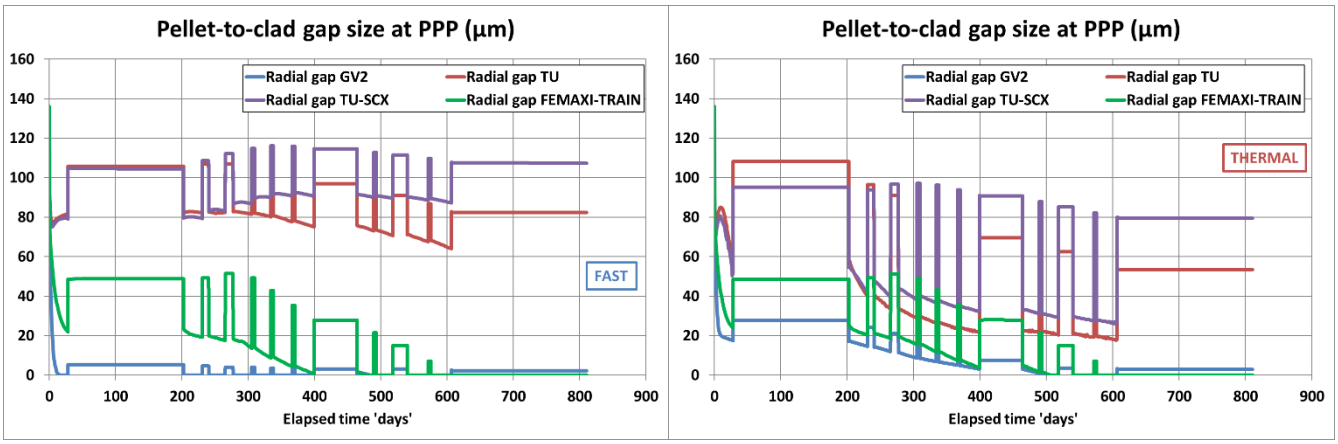

After this review of the main results obtained by the FPCs, one can underline that the predictions of the fuel behaviour in terms of fission gas release and restructuring are fully driven by the temperature calculation, and beyond that by the modelling of the heat transfer between pellet and clad and the correlated evaluation of the pellet-to-clad gap evolution. This observation is completely consistent with the outcomes of previous studies (Chauvin 2023, Lavarenne 2022). In this work, the consideration of two different options for the neutron spectrum and consequently the possibility of a radial depletion of power in the fuel introduces another cause of discrepancies between the code predictions of the fuel temperature.

3.3.3 Sensitivity studies based on the simulation of SPHERE

3.3.3.1 Sensitivity studies with TRANSURANUS & TRANSURANUS//SCIANTIX

The only difference between the two simulation sets is using SCIANTIX as a point model for generation, evolution and release of fission products, while both sets apply TRANSURANUS for the thermal and mechanical analysis. A comparison of output quantities is hence appropriate as a first sensitivity test.

Significant differences can be seen for the He content in the plenum (Figure 10) and the amount of released fission gases (Figure 12). Note that the fission product behaviour in the SCIANTIX point model (Pizzocri 2022) leads to systematically higher released fractions, even if always in reasonable agreement with other code predictions and with experimental data.

As TRANSURANUS//SCIANTIX simulates comparable or higher fuel temperatures (Figure 15) together with larger gap sizes (Figure 17), the impact of the gap conductance dominates. Here the influence of the local temperature on fuel expansion is likely compensated by lower fission-product related swelling, i.e., the physics-based model of SCIANTIX reduces local fuel expansion as soon as fission products are released. At the end of irradiation, the difference between the maximum fuel temperatures predicted by TRANSURANUS and TRANSURANUS//SCIANTIX in thermal spectrum conditions is in the order of 200°C, which indicates the need to accurately describe fission gas behaviour given its impact on both the gap size (via the gaseous swelling of the fuel) and the inner gas composition (via fission gas release), and consequently on the gap conductance.

3.3.3.2 Sensitivity studies with GERMINAL

As previously shown in the Section 3.3.2, the fuel temperatures computed by the different codes are strongly depending on the evolutions of two correlated physical quantities: the pellet-to-clad gap size, and the gap thermal conductance.
In case of GERMINAL, the pellet relocation modelling aims at describing the displacement of fuel pellet fragments towards the inner bound of the clad; the cracking of the pellets into several fragments being induced by the high radial temperature gradient in the fuel. The pellet relocation plays a key role in the evaluation of the partial or complete pellet-to-clad gap closure. As presented in the Section 3.3.2, the pellet-to-clad gap closure predicted by GERMINAL is the quickest of all codes (Figure 17), leading consequently to the lowest fuel temperatures (Figure 15).
The pellet relocation model implemented in GERMINAL is essentially empirical, thus it is of relevance to assess the sensitivity of the computation results obtained in the simulation of SPHERE experiment to the parameterization of this model. The formulation of the pellet relocation model is described in (Lainet 2019). One key parameter is the mean temperature gradient leading to the complete closure of the gap. For the sensitivity study, this key parameter was doubled, with the goal to decrease the magnitude of the pellet relocation. The intention in this study was not to get an optimized calibration for SPHERE, but to assess the effect of changing the parameter in this way on the main computation results.

The next Figure 18 shows the effect of the parameter change on the predicted pellet-to-clad gap size evolutions at Peak Power Position, for both cases of fast and thermal spectrum. The effect is clear: there is no more prediction of a complete gap closure in both cases. The minimum gap size at hot state at the end of the last irradiation cycle is about 12 µm in fast spectrum, and 17 µm in thermal spectrum. The predicted evolutions in the two cases are much more consistent, when comparing to those obtained with the reference parameterization of the relocation model. As the evolution of the gap thermal conductance is hyperbolic with respect to the gap thickness, the new estimations of this quantity at Peak Power Position are strongly decreased with regards to those in the reference computations, as shown on the Figure 19. The decrease observed in case of fast spectrum is roughly by a factor 10 all along the irradiation. There is for sure the effect of a wider gap size, but it is combined with that of an increased fission gas release – this will be discussed further. And the evolutions of the maximum fuel temperature at PPP (Figure 20) show discrepancies with the reference computations up to +600°C in case of fast spectrum.

Figure 18: Sensitivity study with GERMINAL – Effect of changing the parameterization of the pellet relocation model on the pellet-to-clad gap size at Peak Power Position

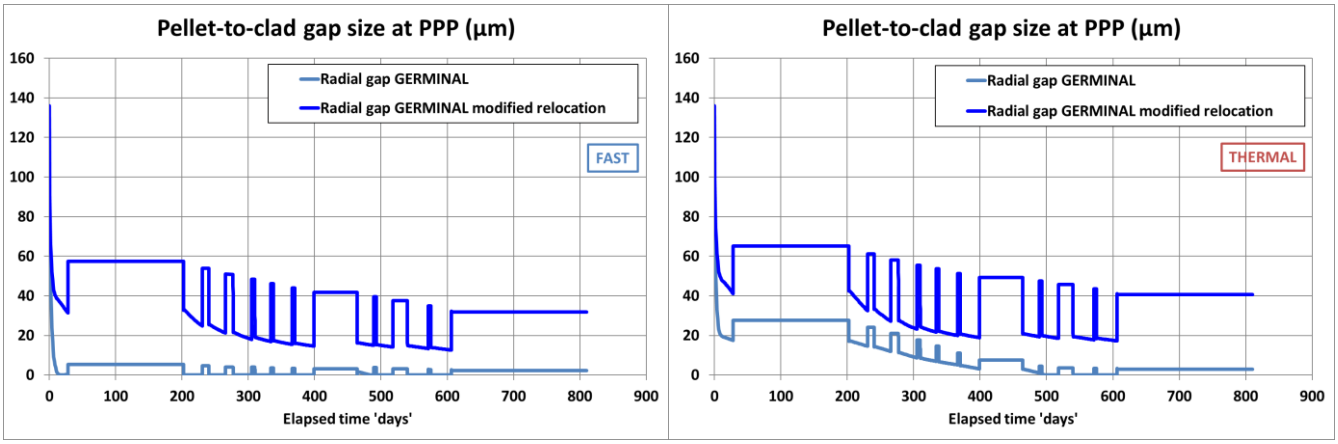

Figure 19: Sensitivity study with GERMINAL – Effect of changing the parameterization of the pellet relocation model on the gap thermal conductance at Peak Power Position

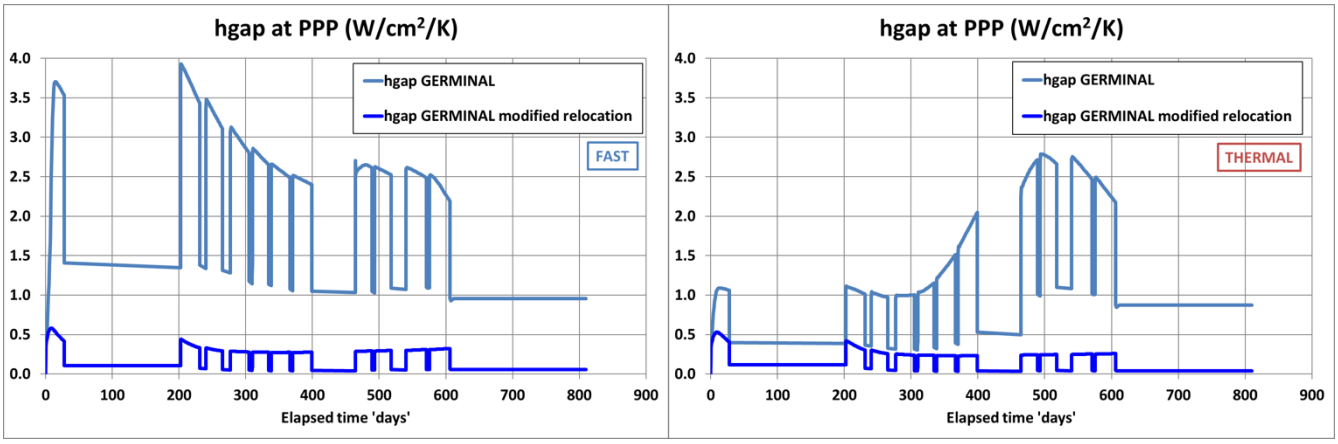

Figure 20: Sensitivity study with GERMINAL – Effect of changing the parameterization of the pellet relocation model on the maximum temperature in fuel at Peak Power Position

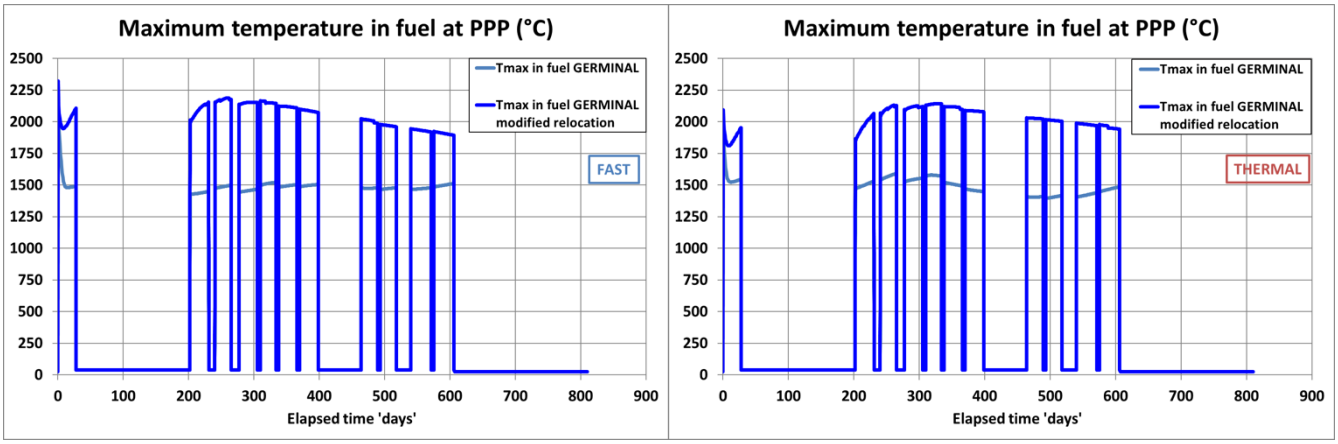

Having a look back to the comparisons with experimental data, the predictions obtained for fission gas release with the modified relocation model are much more in line with the puncturing results, as shown on the Figure 21. This is a logical consequence of evaluating higher temperatures in the fuel. But the effect on the simulated fuel restructuring (Figure 22) is not the same: as the calculated temperatures are significantly higher over the whole irradiation with the modified relocation model, the radial extent of fuel restructuring is predicted much wider than observation in the new computations. In particular, the "inhibiting" effect of the radial depletion of power in fuel in case of thermal spectrum, observed with the reference computation, completely disappears in the new calculation (Figure 22 – right), and the fuel restructuring is also overestimated in case of thermal spectrum. The modelling of the fuel restructuring in GERMINAL does not consider the presence of minor actinides in the computation of the vapor pressures, so there could be also a consequence of the approximation of using a model formulated for MOX fuel.

Figure 21: Sensitivity study with GERMINAL – Effect of changing the parameterization of the pellet relocation model on the release of the fission gases

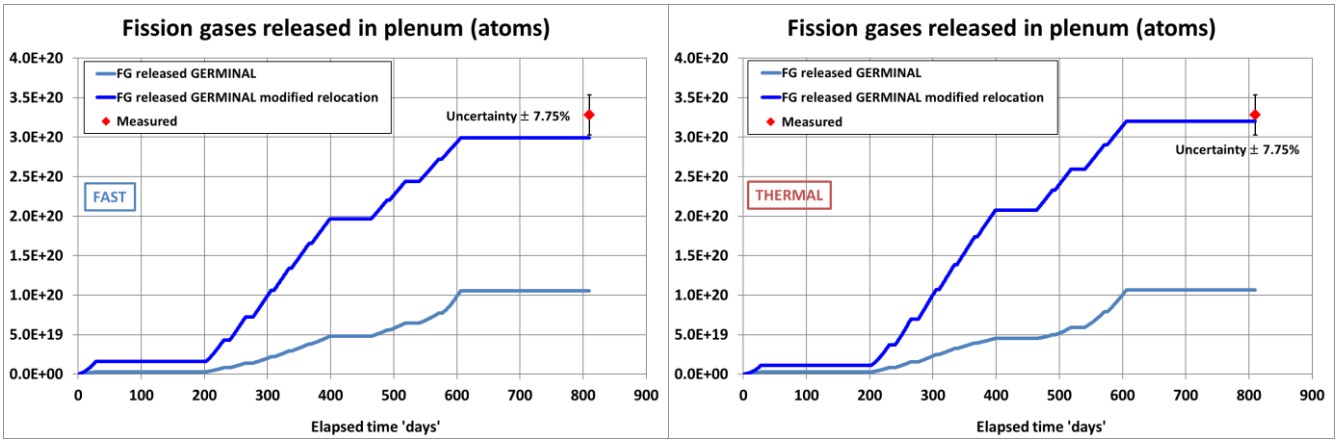

Figure 22: Sensitivity study with GERMINAL – Effect of changing the parameterization of the pellet relocation model on the central hole radius at end-of-life

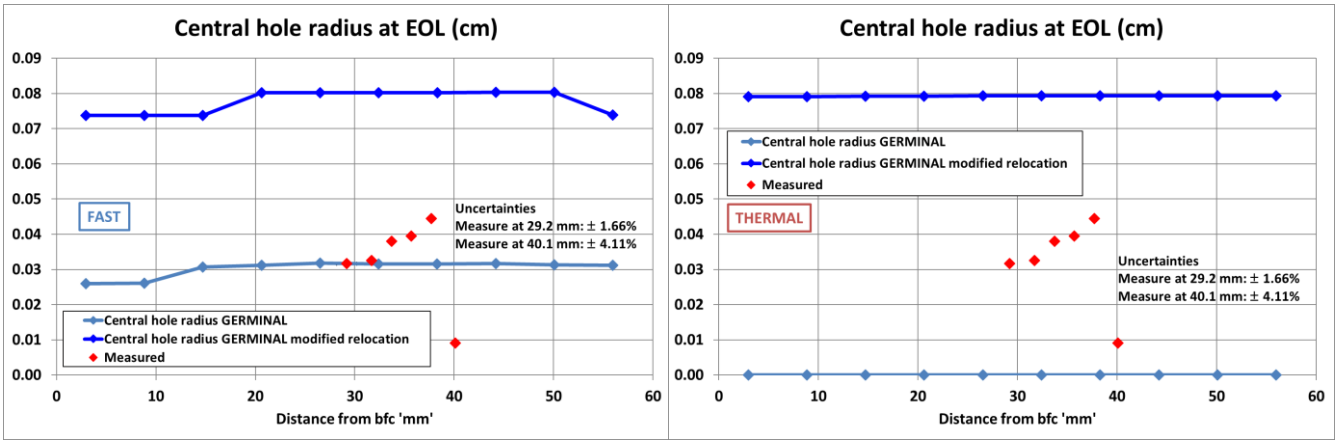

As a concluding remark, this sensitivity study essentially shows that the pellet relocation model of GERMINAL is not adapted for such an object like the SPHERE pellet pin. This fuel pin has a short height (pin height is 190 mm, fuel stack height is 58 mm, as shown on Figure 3), and it is placed inside a capsule so not in a direct contact with a coolant circulation. The pellet relocation model of GERMINAL is calibrated for longer fuel elements, directly placed inside a coolant flow. When considering that the vibrations induced by the coolant flow are one important initiator for moving the pellet fragments inside the pin, and that the natural frequencies of long fuel elements are lower than those of short elements, these are reasons for explaining that the pellet relocation model of GERMINAL may not be adapted with regards to the geometry and the environment of the SPHERE pellet pin.

3.3.3.3 Sensitivity studies with FEMAXI

The reference computation used in the following sensitivity studies with FEMAXI is the simulation of SPHERE in thermal spectrum conditions.

Sensitivity analysis on the fuel thermal conductivity

For this first sensitivity analysis, three models for the fuel thermal conductivity are considered:

- **Philipponneau** 1992, used as the reference model for the simulation of SPHERE with FEMAXI;
- **Kato** 2011;
- **Magni** 2021-2.

While the choice of the model significantly modifies the fuel centerline temperature (Figure 23), the quality of the prediction of major integral quantities (e.g. plenum gas composition, Figure 24) is not improved by changing the thermal conductivity model.

Figure 23: Sensitivity study with FEMAXI – Effect of changing the model for the fuel thermal conductivity on the fuel centerline temperature

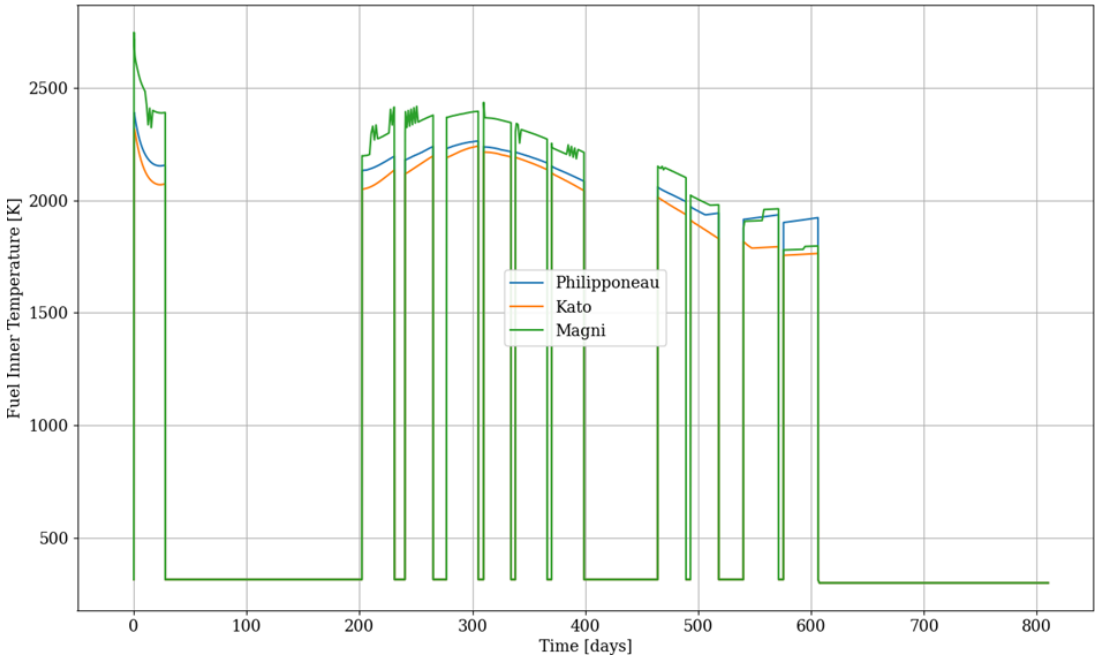

Figure 24: Sensitivity study with FEMAXI – Effect of changing the model for the fuel thermal conductivity on the plenum gas composition

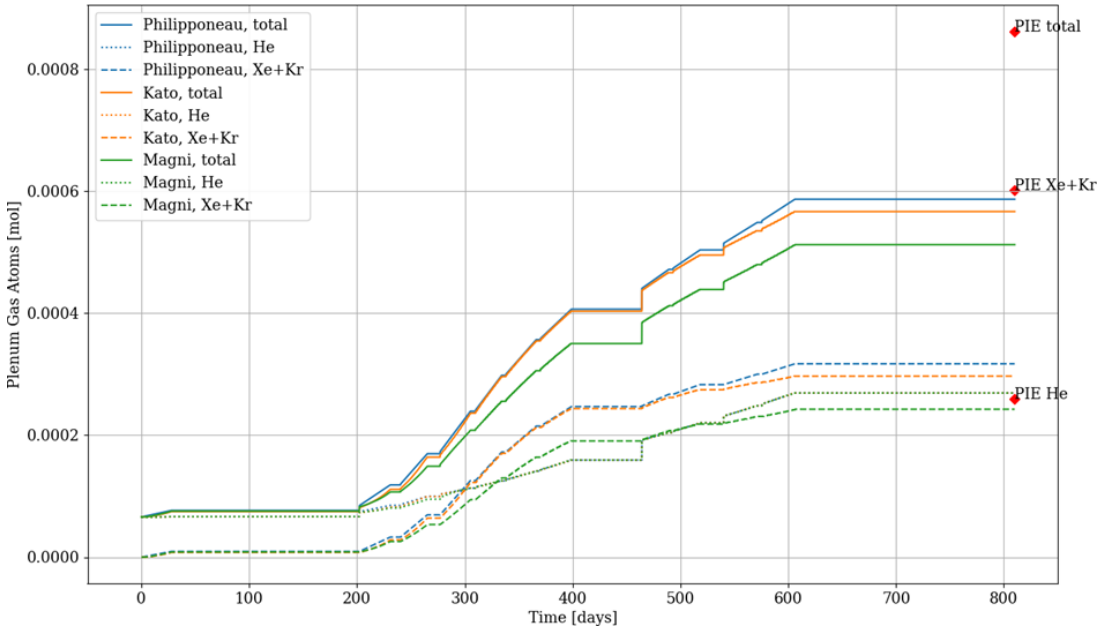

Sensitivity analysis on the fuel relocation model

Since fuel relocation can influence the fuel temperature in a major way, and therefore fission gas release and material expansion, the following available models are compared:

- **HEDL** correlation as used in the **SIEX** fuel performance code (Dutt 1975), based on EBR-II data, used as the reference model for the simulation of SPHERE with FEMAXI;
- NRA default implementation (**FMX-Default**);
- ABB Atom correlation, as implemented in **STAV**;
- **Beyer** 1975, correlation as implemented in GAPCON-THERMAL-2;
- Japanese NRA / **JNES** model.

As expected, the fuel inner temperature widely varies between the different correlations and models (Figure 25). As a consequence, the release of fission gas is impacted (Figure 26), and results seemingly get closer to PIE data with some models (e.g. STAV correlation). Yet, with increased temperature, also comes a larger central hole in the fuel pellet (Figure 27), and here the STAV correlation leads to overestimate the PIE data. These observations are consistent with those issued from the sensitivity study performed with GERMINAL, documented in the previous Section 3.3.3.2: the relocation correlations leading to the highest predicted temperatures in the fuel – namely, the FMX-Default and STAV correlations – yield a better agreement with experimental data for the fission gas release. But the discrepancies with the measured central hole radii at end-of-life are increased when using these correlations. In the contrary, the relocation correlations leading to the lowest predicted temperatures – HEDL/SIEX and Beyer – yield a good agreement with experimental data for fuel restructuring, but not for fission gas release. There is thus no relocation model yielding an overall improvement in the comparisons with the experimental data.

Figure 25: Sensitivity study with FEMAXI – Effect of changing the fuel relocation model on the fuel centerline temperature

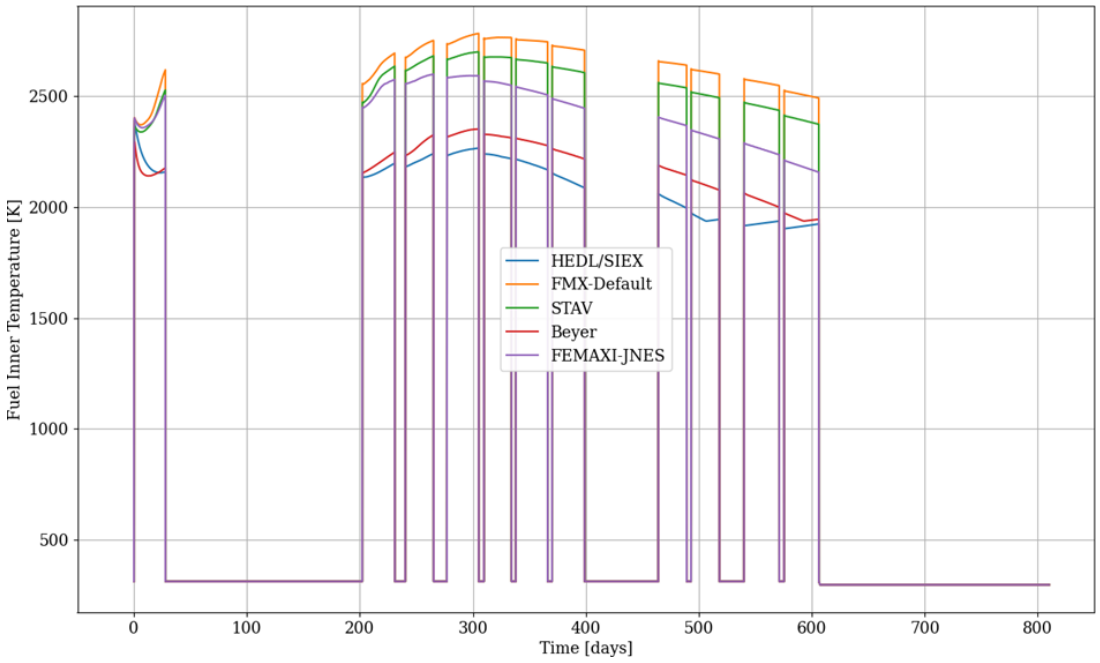

Figure 26: Sensitivity study with FEMAXI – Effect of changing the fuel relocation model on the plenum gas composition

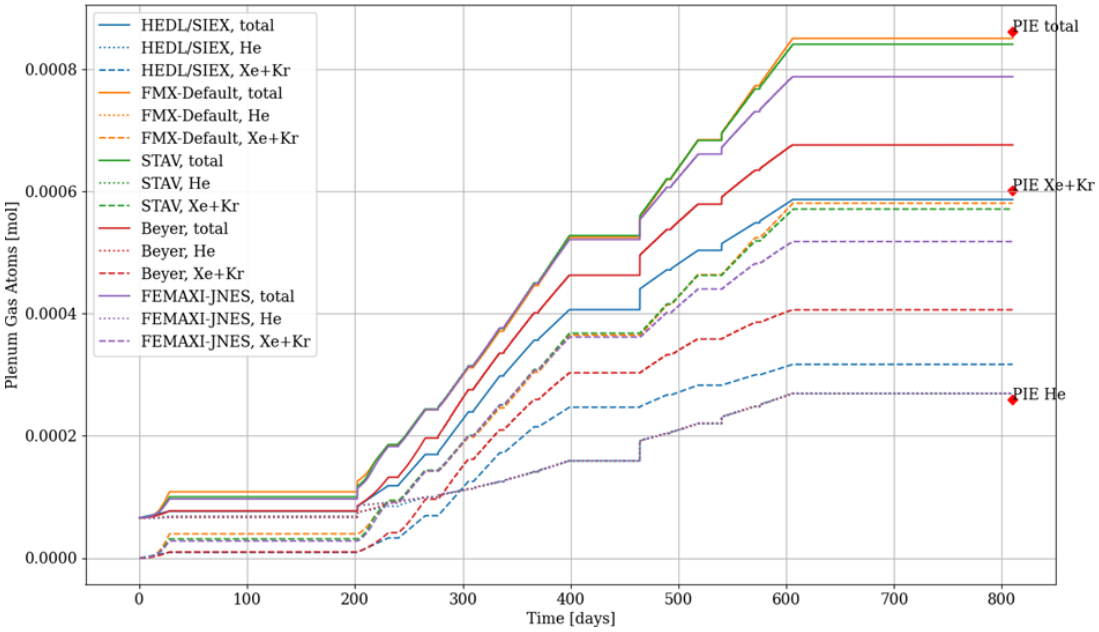

Figure 27: Sensitivity study with FEMAXI – Effect of changing the fuel relocation model on the central hole radius at end-of-life

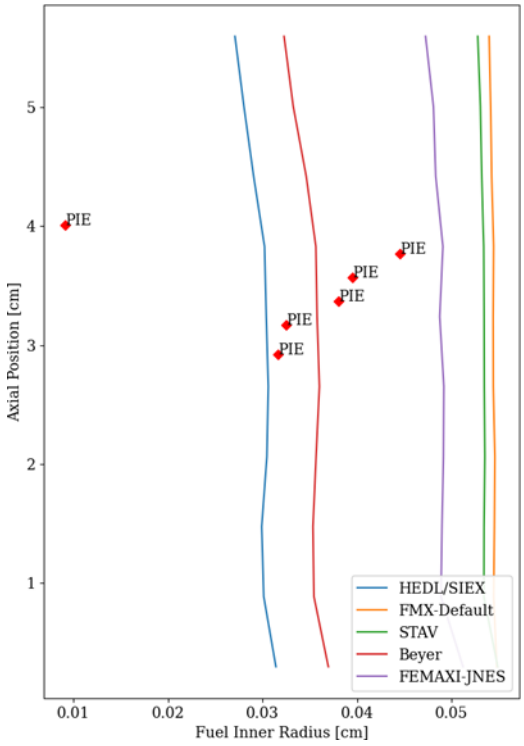

Sensitivity analysis on the initial fuel grain size

Since the initial fuel grain size in the SPHERE fuel is not reported, an assumption of 10 µm was agreed upon by the benchmark participants. However, to exclude a major impact on the quality of the computation results, a sensitivity analysis on this value is carried out with additional simulations for 9 µm and 8 µm. As for the results, there is no difference in fuel temperature or central hole radius. The fission gas release, however, is slightly impacted: smaller grains, more release, as shown on Figure 28.

Figure 28: Sensitivity study with FEMAXI – Effect of changing the initial fuel grain size on the plenum gas composition

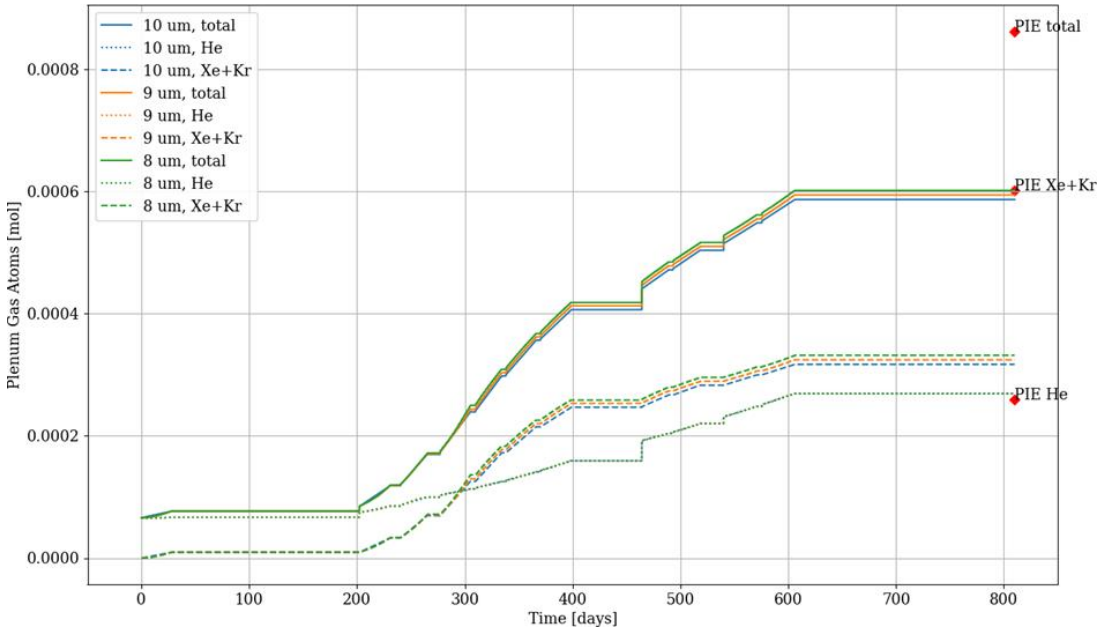

Sensitivity analysis on the gap thermal conductance model

The heat transport through the gap between fuel and clad has a major influence on fuel temperature. The different gap thermal conductance models considered for the sensitivity analysis are the following:

- The **modified Ross & Stoute** model implemented in FEMAXI (Suzuki 2005), used as the reference model for the simulation of SPHERE with FEMAXI;
- The original **Ross & Stoute** model (Ross & Stoute 1962);
- The **modified Dean** model implemented in FEMAXI (Suzuki 2005).

The effect of changing the gap thermal conductance model is shown on Figure 29 for what concerns the fuel inner temperature, on Figure 30 for the fission gas release and on Figure 31 for the central hole radius at end-of-life. The original Ross & Stoute model leads to the highest fuel temperatures, the Dean model to the lowest. The modified Ross & Stoute model – e.g. FEMAXI's default model – lies in-between. With the highest predicted temperatures, the original Ross & Stoute model decreases the discrepancy with the measured fission gas release (Figure 30); and the predicted fuel restructuring is still in line with the measured central hole radii at end-of-life (Figure 31). In this last sensitivity study, the improvement of the predictions yielded by the original Ross & Stoute model is more evident. But this conclusion is naturally only related to the simulation of SPHERE experiment.

Figure 29: Sensitivity study with FEMAXI – Effect of changing the gap thermal conductance model on the fuel centerline temperature

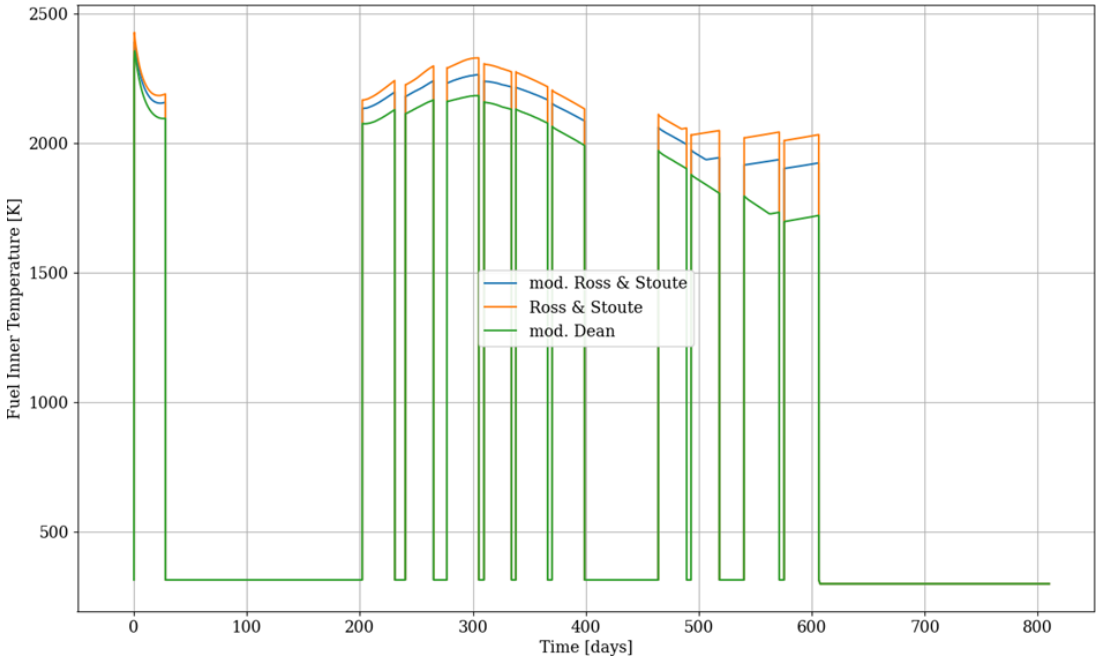

Figure 30: Sensitivity study with FEMAXI – Effect of changing the gap thermal conductance model on the plenum gas composition

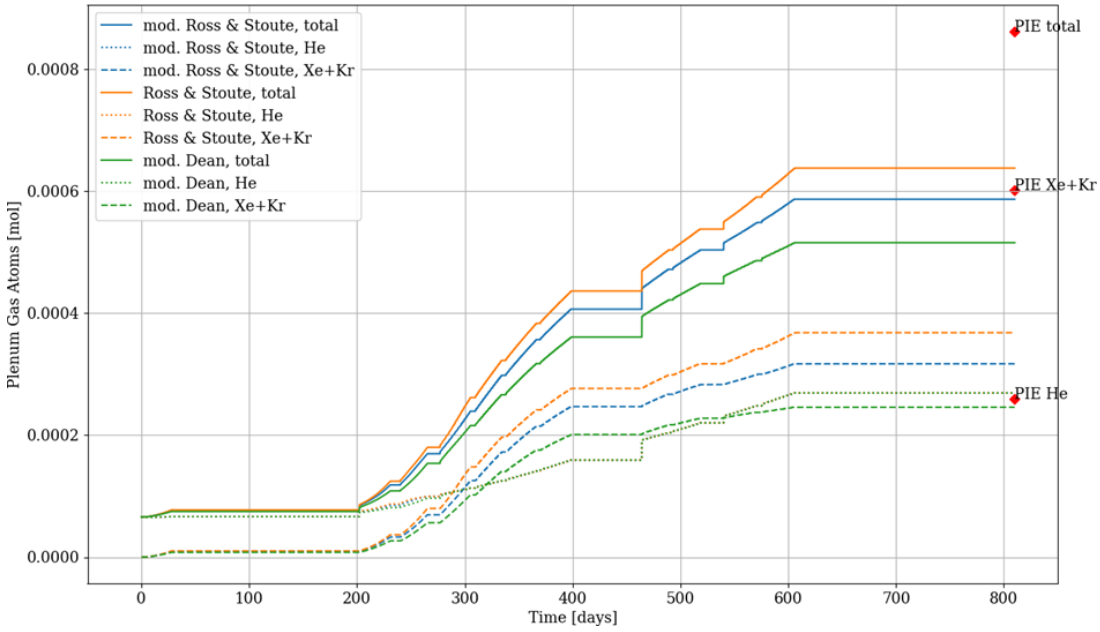

Figure 31: Sensitivity study with FEMAXI – Effect of changing the gap thermal conductance model on the central hole radius at end-of-life

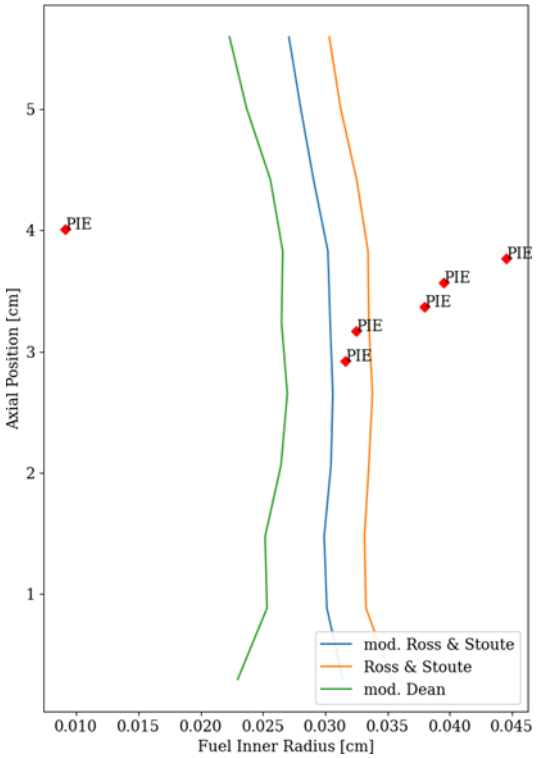

3.4 Conclusion of the interpretation of the SPHERE experiment

The interpretation of the SPHERE experiment performed in this work relies on an updated irradiation history and thermal boundary conditions, and investigates different spectrum conditions. With regards to the comparisons of the computation results with experimental data and the sensitivity studies, the main outcomes and perspectives are the following:

- Concerning the helium production and release, it turns out that the spectrum conditions for the SPHERE experiment seem closer to those in a thermal reactor, despite the hafnium neutron shield intending to harden the flux in the device. Considering the remaining discrepancies between computation results and the experimental data, the need for a complete neutronic characterization of the experiment is confirmed, with the goal to provide to the FPCs a complete set of basic nuclear data, evolving with time, due to the progressive depletion of the neutron shield. Such investigations about the performance of neutron shields have been realized (Chang 2011) for the implementation of the AFC-2C and AFC-2D transmutation experiments with oxide fuel in the Advanced Test Reactor (MacLean 2007). These investigations are absolutely necessary in case of an experiment performed in a Material Testing Reactor, with a device intending to create peculiar spectrum conditions that differ from the standard conditions of the reactor where the experiment is operated. For future experiments of this kind, one should also consider the possibility to acquire measurements quantifying the shield depletion. Other interesting data would be measurements by fission chambers, or by foil activations. Such data may help in the characterization of the neutron flux. Concerning the SPHERE experiment, the evolution of the neutronic conditions with time shall be investigated with due consideration of the successive positions of the device in the core during all the irradiation cycles. In this work, a first progression towards such neutronic characterization has been obtained, and is to be pursued.

- The systematic underestimation by the codes of the helium quantity retrieved from the plenum also suggests to investigate the fuel conditions during the storage. The possibility that a residual power in the fuel may have enabled, at least partially, the release of the helium created by alpha-decays during the storage, should be assessed.
- These investigations about the overall conditions of the experiment from the beginning of the irradiation to the end of the storage are the prerequisite for assessing the capabilities of the FPCs to simulate the SPHERE fuel behaviour in the HFR.
- As a further perspective for the simulation tools, an extended (online) coupling between neutronics tools and FPCs could be envisaged. This could enable a more precise consideration of the specific (neutronic) conditions in the material testing reactor in the fuel test.
- Another perspective for the experiment could come from advanced post-irradiation examinations of the SPHERE fuel, with one particular goal to evaluate more accurately the americium transmutation performance.

3.5 Archiving of the study related to SPHERE experiment

An archive of the data set related to the present study of the SPHERE experiment is available on the open share point ZENODO, in the working area dedicated to the PATRICIA project:
https://zenodo.org/communities/patricia

The name of the archive file is: “PATRICIA Task 5.3 SPHERE benchmark Dataset.zip”

The corresponding digital object identifier is: https://doi.org/10.5281/zenodo.13234775

When expanding the archive file, the content is structured as follows:

- “1 - Neutronics computations”: first level directory containing the input and output data related to the neutronic assessment of the SPHERE experiment.
  - ✓ “Input”: second level directory containing the input data required by the neutronic calculations. One can find in particular the definition the neutron spectrum in the HFR along the irradiation cycles of the SPHERE experiment – information provided by NRG, the operator of the HFR.
  - ✓ “Output”: second level directory containing the output data issued from the neutronic calculations. The data are distributed in two separate sub-directories, respectively related to the output from C^4P-TRAIN and SERPENT-2.
- “2 - FPCs computations”: first level directory containing the input and output data related to the simulation of the SPHERE experiment with the fuel performance codes.
  - ✓ “Input”: second level directory containing the input data required by the computations with the FPCs. One can find in particular the benchmark specifications, the nuclear data derived from the neutronic calculations and used on input by the FPCs (cross-sections and fission yields), and the adopted definition of the irradiation history.
  - ✓ “Output & Comparisons CC CM”: second level directory containing the output data issued from the computations with the FPCs. A compilation of the PIE results in one EXCEL file is provided. The data are then distributed in two separate sub-directories: “Option 1 FAST” and “Option 2 THERMAL”, corresponding to the two complementary assumptions of fast and thermal spectrum retained for the computations. In each sub-directory are provided the results files from the different codes, and a synthesis file showing the code-to-code and calculation-to-measure comparisons. The synthesis files are named “SPHERE_FAST.xlsx” and “SPHERE_THERMAL.xlsx”.

4 Interpretation of the MARINE experiment

4.1 Main characteristics of the MARINE experiment

The MARINE experiment (D'Agata 2017, Van Til 2021 & 2023) aimed at studying the behaviour of Minor Actinide Bearing Blanket material $(U,Am)O_{2-x}$ by comparing sphere-packed and pelletized fuels. It consists of two pins containing ^{241}Am (~ 13 wt.% Am) based on a natural uranium oxide matrix. The two pins were irradiated for 359 Effective Full Power Days (EFPD) in 12 cycles in the High Flux Reactor in Petten, between January 5th, 2016 and May 7th, 2017. We focus here on the pin #1 that contains 9 fuel pellets in a stack. The MARINE experiment was designed and performed in the framework of the collaborative research project PELGRIMM (European Commission 2017). The post-irradiation examinations of the MARINE fuel (Van Til 2021 & 2023) are part of the PATRICIA Project (European Union 2020). In link with the acquisition of experimental results on MARINE, an analysis of the experiment with neutronics tools and fuel performance codes is also implemented in the frame of PATRICIA, with the goal to assess the capabilities of the computational tools to simulate the behaviour of $(U,Am)O_{2-x}$ material.

A detailed description of the experiment is provided in (D'Agata 2017). The fuel irradiated was a Minor Actinide Bearing Blanket material $(U,Am)O_{2-x}$ containing about 13 wt.% of americium. The main characteristics and composition of MARINE fuel are given in the following Table 9.

Table 9: MARINE fuel characteristics

Pin Nr.	Composition	Isotopic composition	Fuel Density [g cm^{-3}]	^{241}Am contents [g]	^{238}U contents [g]	^{235}U contents [g]
#1 Pellets	$U_{0.86}Am_{0.14}O_{1.93}$	UO_2 + ^{241}Am	9.45* 10.45** ≈ 94.61 % TD	1.58	10.017	0.072
#2 Spheres	$U_{0.87}Am_{0.13}O_{1.935}$	UO_2 + ^{241}Am	6.13*	1.08	7.152	0.051

* This overall density takes into account both the density of the spheres and the overall packing density of the two size fractions in the sphere-pac column as well as the gas gap between the pellet and the cladding in the pellets column. This density, often called smear density, is given to be able to compare directly sphere-pac with pellet fuel.

** This density represents the real density of the fuel (only the pellets) as fabricated.

The fuel irradiated was in the form of:

- pellets of an average diameter of 5.37 mm stacked one on top of the other for a total length of 55.67 mm with 9 pellets, held in place with a spring. Two pellets of Hf have been placed at the top and at the bottom of the fuel stack in order to decrease the power peaking at the edge of the fuel stack. A drawing of the SPHERE pin #1 with pelletized fuel is given by the Figure 32;
- sphere-pac fuel, composed of small spherical pebbles of two sizes, 0.75 and 0.05 mm, to enhance the packing density. Also the sphere-pac fuel stack had two Hf pellets at either end to keep the sphere-pac in place and to minimize power peaking.

The two pins made of 15-15 Ti steel and containing pellets and sphere-pac fuel in an inert environment (helium) were contained into an assembly which comprises two sample holders made of stainless steel one inside the other:

- the internal sample holder was containing the two pins immersed in a bath of sodium and equipped with thermocouples, fluence detectors and pressure transducers;
- the external sample holder, containing the internal sample holder and its content. As a main difference with regards to the SPHERE experiment, the external sample holder of MARINE was **not surrounded with a liner of Hafnium**. Thus, the neutron spectrum conditions for the MARINE experiment are simply those in the HFR, namely **thermal spectrum conditions**. Finally, the external sample holder was cooled down with the water of the primary cooling system of the HFR.

The gap between the sample holders were filled with gas, either helium or neon or a mix of the two, in order to adjust the temperature of the experiment.

Figure 32: MARINE pellet pin (from D'Agata 2017)

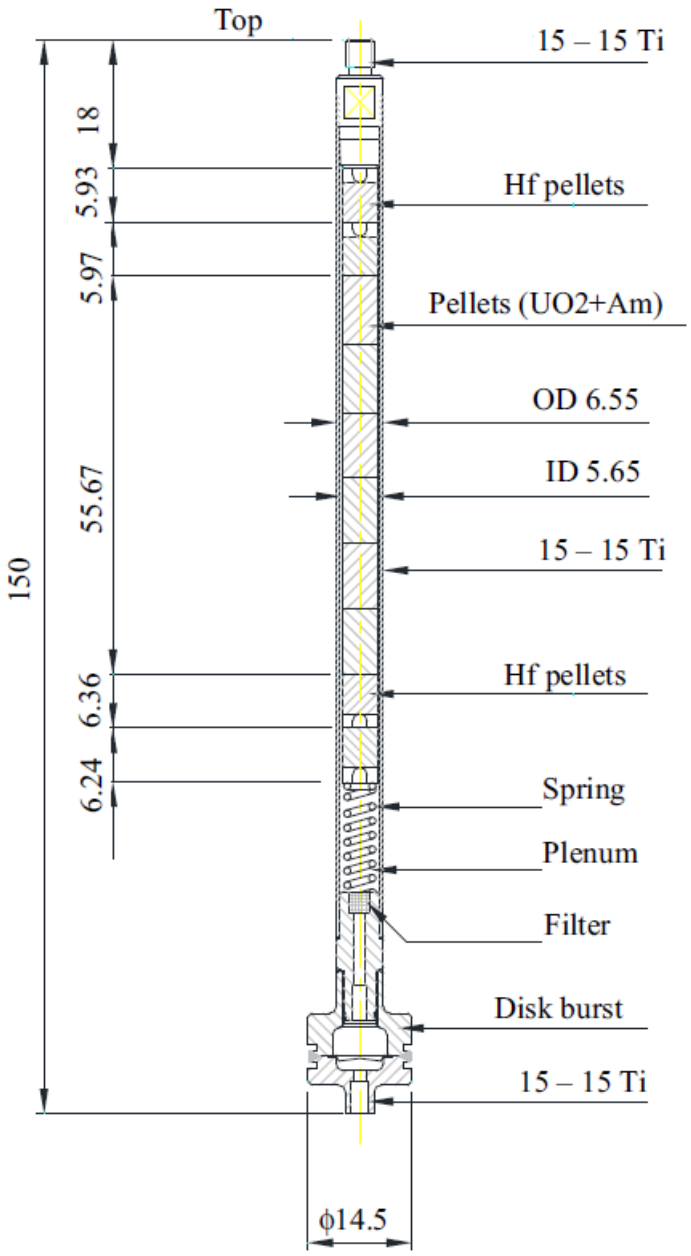

4.2 Interpretation of the MARINE experiment with the neutronics tools

4.2.1 Modelling of the MARINE experiment with the neutronics tools

The main characteristics of the MARINE pin #1 with pelletized fuel are given in the Table 10. The related fuel composition is defined in Table 11. These are the basic geometric and material data used on input for the simulations performed with the neutronics tools.

Table 10: Main characteristics of the MARINE pellet pin

Pellet diameter (mm)	5.368
Gap size (µm)	141
Cladding diameter (mm)	6.55
Cladding material	15-15 Ti
Cladding thickness (mm)	0.45
Fuel weight (g)	13.182
Fuel stack length (mm)	55.67
Free plenum (cm^3)	3.28

Table 11: Composition of the MARINE pellet fuel

Type	$(U,Am)O_{2-x}$
Am/metal (mol %)	13.38
U/metal (mol %)	86.62
^{234}U (mol %)	0.00
^{235}U (mol %)	0.72
^{236}U (mol %)	0.00
^{238}U (mol %)	99.27
^{241}Am (mol %)	93.40
^{237}Np (mol %) *	6.60
O/M	1.93

* Impurity in Am-batch

In addition, the neutron energy spectrum of the high-flux reactor (HFR) was provided by the PATRICIA partner NRG – NRG being the operator of the HFR.

The SERPENT-2 simulation of the MARINE irradiation was carried out through 12 simulations with the restart option, i.e., reading the composition from the previous simulation and starting a new one with the new boundary neutron flux conditions, since each irradiation cycle adopted a different spectrum as boundary condition according to the data provided by NRG (Figure 33). The geometry adopted is the same as in Figure 4 (in particular, 10 radial points subdivision), but obviously with dimensions and materials indicated in Table 10 and Table 11, respectively; the power history implemented is shown in Figure 34. Also in this case, the adopted neutron library was JEFF-3.1.1 and the simulation was run in subcritical mode with 10^7 neutrons per generation; the simulation was set to achieve maximum performance (at the expense of memory usage). Helium gas was included in the inventory of actinides and fission products. One-group averaged cross-sections were obtained using the same procedure described in Section 3.2.1.

Figure 33: Neutron spectra calculated in the voided pellet position for the first 12 irradiation cycles (different colors)

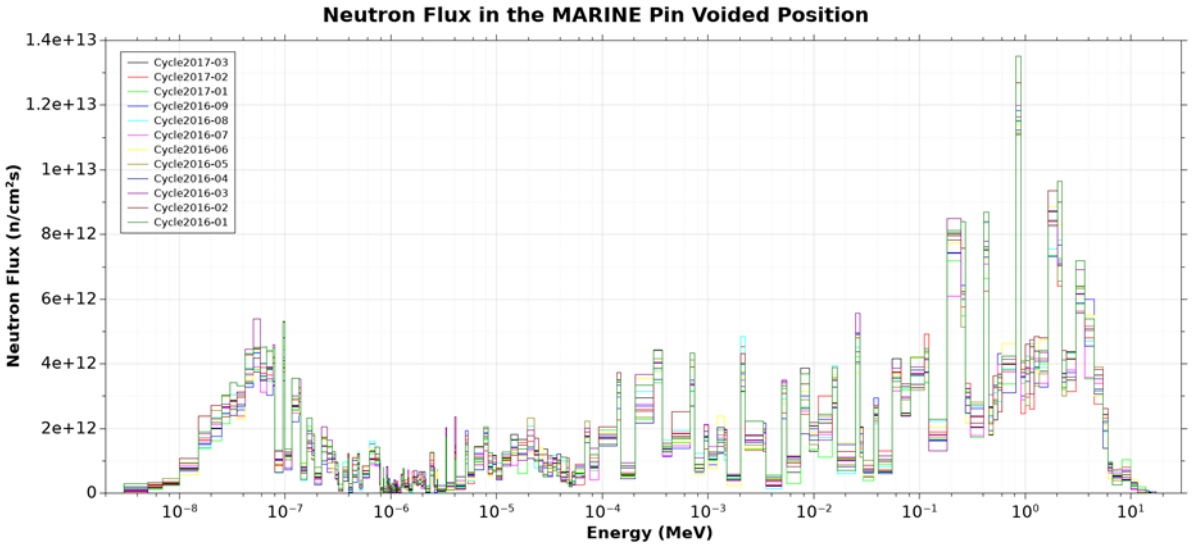

Figure 34: LHR history vs. irradiation for the MARINE irradiation experiment

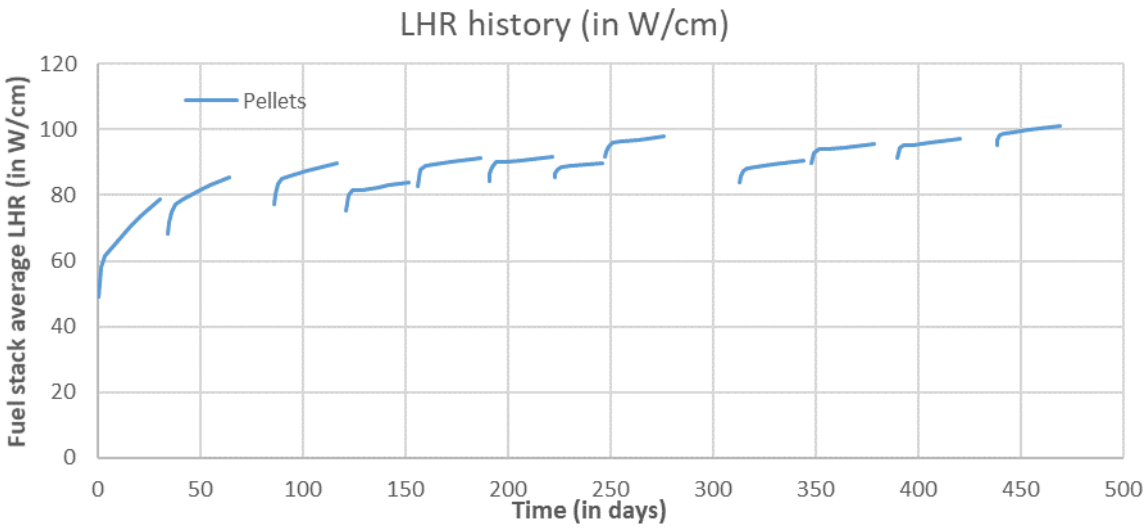

Based on the basic geometric and composition data defined in the previous Table 10 and Table 11, and using the neutron energy spectrum of the HFR provided by NRG, a 1D neutronic model of MARINE was also created for C^{4}P-TRAIN, as shown on the Figure 35. This model includes the fuel pin in the very center, the sample holder and an equivalent 1D radially symmetric representation of the surrounding driver fuel of the HFR. The methodology for simulating MARINE experiment was similar to that previously implemented for SPHERE, as described earlier in the Sections 2.1 and 3.2.1.

Running and tuning this model in C^{4}P-TRAIN for an empty sample holder at MARINE's irradiation position in the HFR, the resulting neutron energy spectrum, as shown in Figure 36, is in agreement with the provided spectrum by NRG. This verifies the consistency of the 1D pin-cell neutronic model used by C^{4}P-TRAIN.

Figure 35: MARINE 1D pin-cell neutronic model for C^{4}P-TRAIN

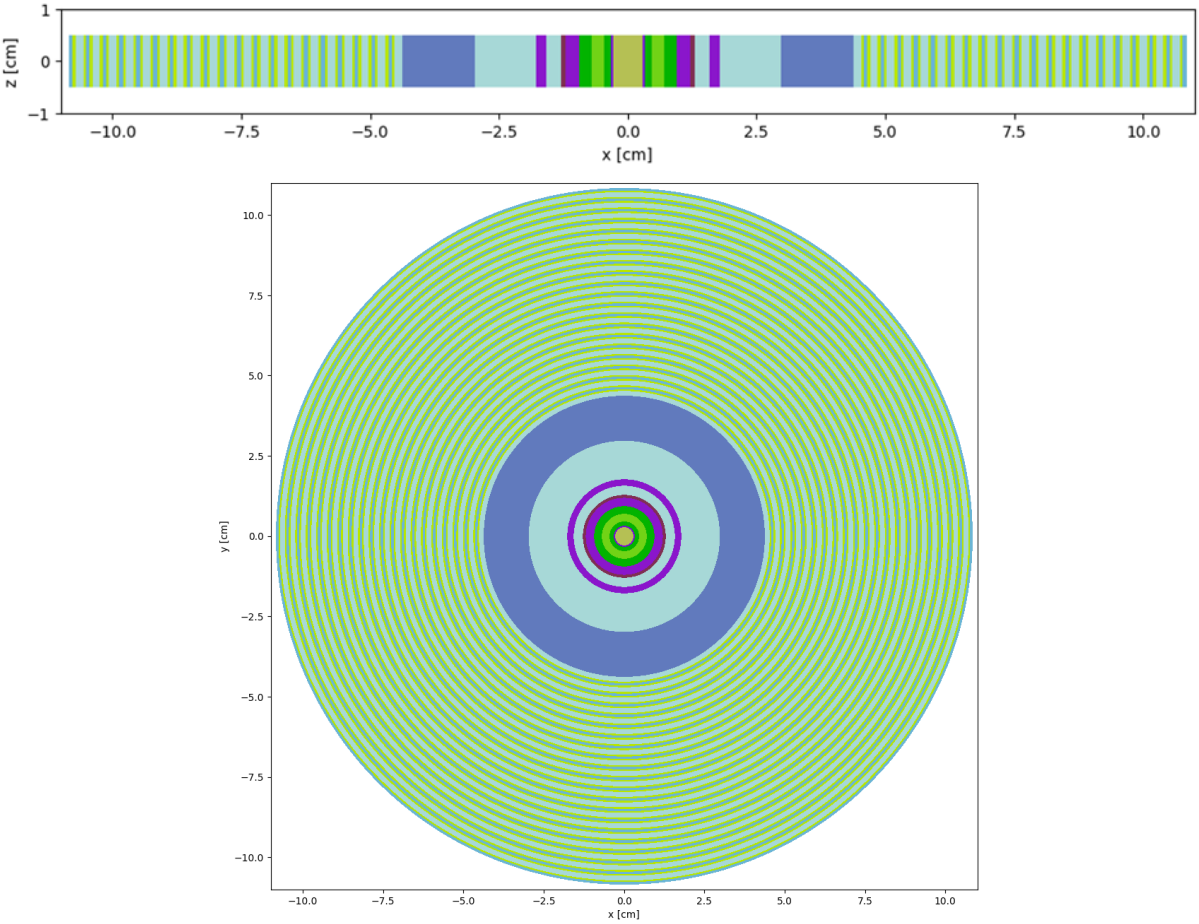

Figure 36: Neutron energy spectrum for empty irradiation position in HFR. NRG monte-carlo results (green) vs. KIT 1D pin-cell model (red).

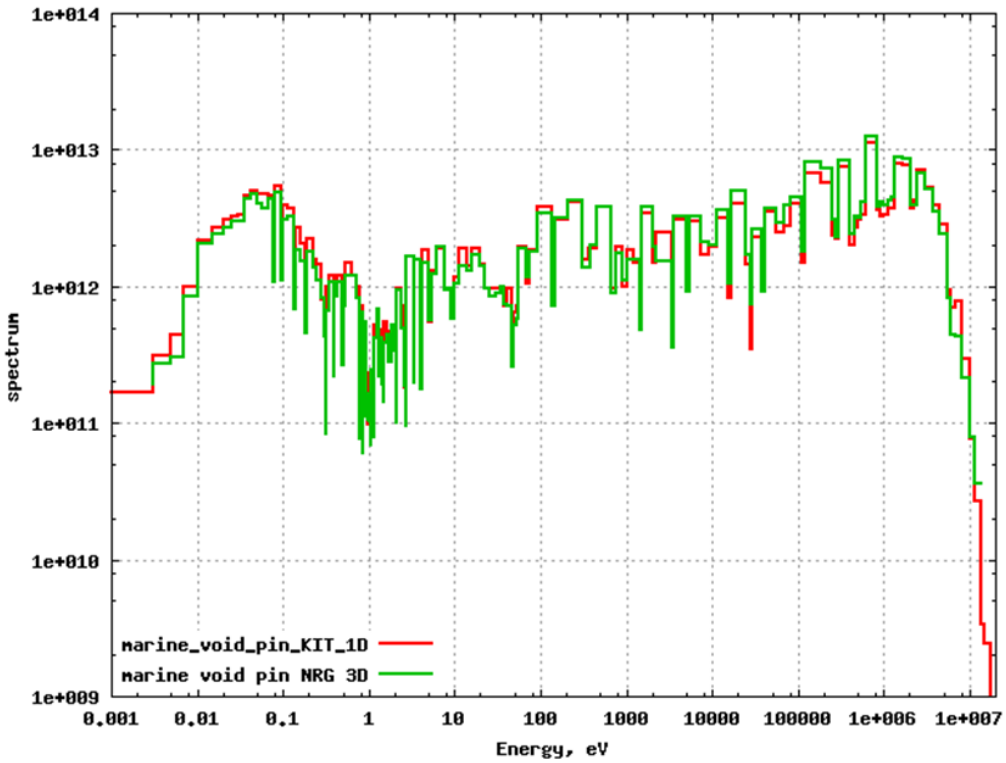

4.2.2 Results from the neutronics simulations of MARINE

The results issued from the SERPENT-2 computation and further used on input by TRANSURANUS and GERMINAL are the same than those already used for the simulation of SPHERE: the chaining process between SERPENT-2 and the different FPCs is identical. These data are the following:

- the one-group averaged cross-sections of the heavy nuclides considered in the point-kinetic neutronics models embedded in the FPCs. These data are provided in the Table 12. The cross-sections are evaluated as an average between the first, middle and last irradiation cycles (i.e., cycles 1, 6 and 12), in order to be representative of the global irradiation conditions;
- the fission yields of Xe, Kr, Nd, Cs isotopes and He-4, associated to the previously considered heavy nuclides. These data are provided in the Table 13. The fission yields are calculated with the OVERPROTECT tool, according to the methodology already described in the Section 3.2.2, based on Equation 1. As in the case of cross-sections, also for yields values an average between the first, middle and last irradiation cycles was estimated.

Table 12: Fission and capture cross-sections computed with SERPENT-2

Nuclide	***Fiss. XS***	***Rad.Capt. XS***
U-234	0.670	11.505
U-235	31.215	6.233
U-236	0.266	2.104
U-238	0.054	0.545
U-239	1.738	3.594
Np-237	0.772	22.009
Np-238	108.485	10.905
Np-239	0.915	10.729
Pu-238	2.447	23.237
Pu-239	56.647	26.591
Pu-240	0.829	130.612
Pu-241	66.752	22.422
Pu-242	0.727	12.583
Pu-243	16.261	7.759
Am-241	1.012	56.172
Am-242	134.383	14.933
Am-242m	415.404	79.754
Am-243	0.500	22.080
Cm-242	1.603	5.380
Cm-243	51.681	8.295
Cm-244	1.236	10.200
Cm-245	99.173	15.519

Table 13: Fractional fission yields calculated with the OVERPROTECT tool, further used on input by the TRANSURANUS and GERMINAL FPCs

	U-234	*U-235*	*U-236*	*U-238*	*Np-237*	*Np-238*	*Pu-238*	*Pu-239*	*Pu-240*	*Pu-241*	*Pu-242*	*Am-241*	*Am-242m*	*Am-243*	*Cm-243*	*Cm-244*	*Cm-245*
Kr-83	0.007765	0.005717	0.005952	0.003364	0.004877	0.003538	0.002950	0.002911	0.002308	0.002045	0.001806	0.002514	0.002229	0.001244	0.001192	0.001363	0.001383
Kr-84	0.012600	0.010469	0.010234	0.006719	0.007964	0.006831	0.004538	0.004872	0.004130	0.003766	0.003604	0.003822	0.002755	0.002005	0.001868	0.002058	0.002149
Kr-85	0.003874	0.002876	0.002954	0.001857	0.002042	0.001876	0.001475	0.001362	0.000957	0.000928	0.000682	0.001181	0.000842	0.000624	0.000641	0.000651	0.000855
Kr-86	0.025528	0.020149	0.019456	0.012071	0.013385	0.011170	0.009577	0.007912	0.006532	0.006358	0.005457	0.007108	0.005588	0.004383	0.003993	0.004267	0.007083
Nd-143	0.051152	0.058250	0.051152	0.046195	0.047129	0.042353	0.044644	0.044401	0.045236	0.044158	0.045815	0.038482	0.043290	0.041432	0.040868	0.043510	0.044293
Nd-144	0.042862	0.053538	0.047204	0.045882	0.041226	0.036122	0.038495	0.037058	0.039798	0.041334	0.042890	0.034015	0.042124	0.039284	0.033755	0.040246	0.041224
Nd-145	0.035247	0.038945	0.042478	0.038171	0.032162	0.038224	0.033339	0.030359	0.031377	0.031625	0.033914	0.034799	0.038424	0.035909	0.033298	0.035212	0.031540
Nd-146	0.027342	0.029641	0.034917	0.035034	0.028111	0.034009	0.026506	0.025024	0.025769	0.026709	0.029195	0.028184	0.031049	0.030061	0.025372	0.031193	0.026608
Nd-148	0.014112	0.016729	0.019527	0.022283	0.017419	0.018346	0.016173	0.016659	0.017979	0.018917	0.020242	0.018463	0.022057	0.020604	0.017567	0.023427	0.026714
Nd-150	0.006160	0.006618	0.010079	0.012867	0.009859	0.009419	0.008365	0.009807	0.010654	0.011619	0.013169	0.011975	0.001979	0.012650	0.004301	0.014478	0.003812
Cs-133	0.073178	0.065891	0.066532	0.066416	0.066912	0.066236	0.070109	0.070010	0.069835	0.066232	0.068301	0.057925	0.053241	0.055082	0.053300	0.050784	0.054348
Cs-134	0.000004	0.000002	0.000000	0.000000	0.000003	0.000000	0.000051	0.000008	0.000002	0.000000	0.000000	0.000020	0.000003	0.000001	0.000066	0.000027	0.000003
Cs-135	0.077665	0.065477	0.061551	0.063635	0.076160	0.074730	0.077684	0.074150	0.075614	0.070602	0.068896	0.072530	0.069787	0.070290	0.063887	0.064038	0.061755
Cs-137	0.061652	0.061304	0.057881	0.059924	0.062663	0.068680	0.064228	0.065412	0.065276	0.062982	0.061486	0.067173	0.061266	0.064284	0.074483	0.065880	0.067731
Cs-139	0.061154	0.062924	0.063322	0.057793	0.055667	0.052085	0.049978	0.056116	0.056628	0.059509	0.059020	0.063219	0.055800	0.055386	0.054379	0.051879	0.065483
Xe-131	0.029039	0.030139	0.029857	0.033428	0.037341	0.034826	0.036076	0.037959	0.035716	0.030902	0.030971	0.038370	0.034873	0.035237	0.032579	0.030020	0.030320
Xe-132	0.053211	0.043994	0.040527	0.047524	0.046879	0.052550	0.055160	0.052552	0.046522	0.045396	0.044860	0.046572	0.043089	0.044786	0.044911	0.039847	0.043389
Xe-134	0.080692	0.077590	0.077107	0.067928	0.073510	0.062660	0.078405	0.070009	0.071879	0.075596	0.073452	0.062248	0.062769	0.063829	0.063663	0.059880	0.058485
Xe-136	0.070440	0.065084	0.068313	0.072347	0.070554	0.080860	0.067453	0.069470	0.067076	0.070038	0.072106	0.067509	0.067001	0.071130	0.066666	0.062187	0.047656
He-4	0.002309	0.001700	0.001899	0.001439	0.002060	0.001860	0.002420	0.002192	0.002781	0.001860	0.002370	0.002370	0.002100	0.001820	0.002580	0.002420	0.002280

For what concerns the neutronics simulation of MARINE with C^{4}P-TRAIN, the variations of the isotopic composition and the radial power profile computed by C^{4}P-TRAIN at several times during irradiation are further used on input in the FEMAXI simulations. The chaining process between C^{4}P-TRAIN and FEMAXI is the same than that previously implemented for simulating the SPHERE experiment. The radial power profiles issued from the C^{4}P-TRAIN computation at different burn-up steps along the irradiation are shown in Figure 37.

Figure 37: Radial power profile evolution of MARINE issued from the C^{4}P-TRAIN computation

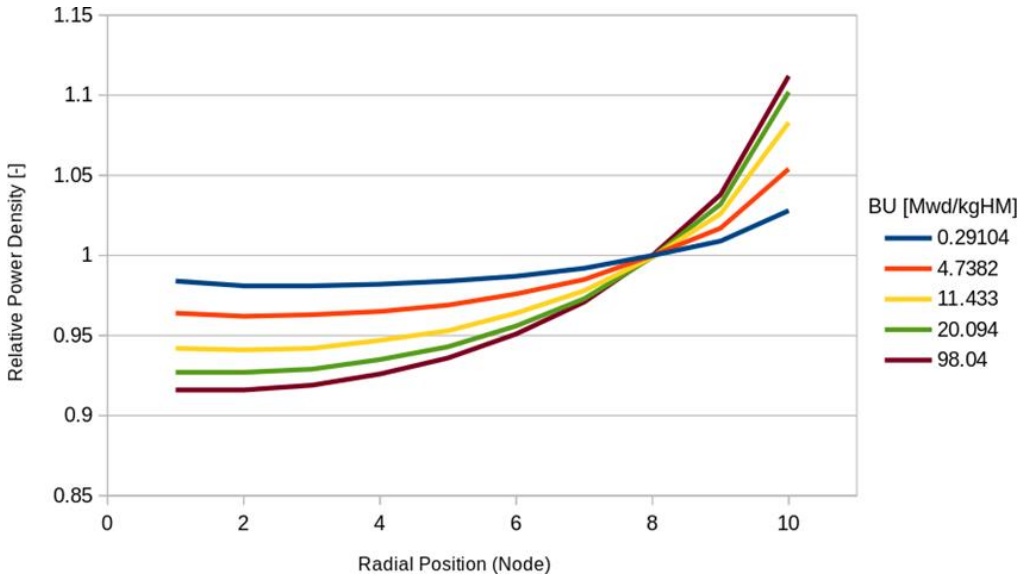

The burn-up calculation with C^{4}P-TRAIN yields to the final average composition, at time of PIE, defined below in Table 14.

Table 14: Final average composition issued from the C^{4}P-TRAIN computation (weight-%)

U	Pu	Am	Np	Cm
86.45 %	6.74 %	5.99 %	0.71 %	0.11 %

Due to the high amount of americium and natural uranium in the pin, especially when comparing to driver fuels, there is only a relatively small amount of fissile material present at the beginning of irradiation. **Consequently, the energy fraction produced by the (n,gamma) reactions is relatively large as compared to fuels with contents of fissile isotopes well above 1% HM.** Therefore, the fission energy fraction is relatively low, leading to the total burn-up of 0.95% FIMA.

This estimation of the final burn-up for the MARINE experiment is significantly lower than that provided in the PATRICIA D4.1 (Van Til 2021): 1.57% FIMA, issued from the post irradiation nuclear analysis performed by the operator of the HFR, accounting for the activities measured on the fluence monitor sets after the dismantling of the device. The other estimations yielded by TRANSURANUS, by the neutronic module of SCIANTIX and by GERMINAL, based on the tailored data for MARINE presented in the previous Table 12 and Table 13, are also closer to 1.57% FIMA. But these estimations from the FPCs are obtained with the assumption that the heat generation only comes from the fission reactions. As a main consequence, the calculated fission gas productions will be increased when considering that only the fission reactions contribute to the heat generation.

It is thus very important to highlight here the **necessity to include a comprehensive neutronic assessment of MARINE as a requirement for the interpretation of the experiment with FPCs**. As the contribution of the (n,gamma) reactions to the heat generation is not accessible to the FPCs, this introduces an **approximation in the simulated behaviour**, and it is necessary to keep this in mind for the interpretation of all the computation results.

N.B. To a lower extent, the heat creation coming from the curium decay is currently neglected in all computations, whereas it can be not negligible in case of Am-bearing fuels. In such fuels, more Cm will be produced along the irradiation, when comparing to standard MOX. The Cm decay contribution to the power production can thus be more than 1 % of total power, depending on the Am content.

4.3 Interpretation of the MARINE experiment with the upgraded fuel performance codes

4.3.1 Modelling of the MARINE experiment with the fuel performance codes

The main characteristics related to the geometry of MARINE pin #1 with pellet fuel, to the geometry of the pellets and the blanket material $(U,Am)O_{2-x}$ have been already provided in the Table 9, Table 10 and Table 11. The clad material is the austenitic stainless steel 15-15Ti.

The evolution with time of the pin average Linear Heat Rating for the MARINE experiment was made available by NRG for this study. The complete definition is given in Table 15. This corresponds to the revised LHR history, issued from the post irradiation nuclear analysis by NRG. The time evolution of the pin average LHR is shown on the Figure 38, for both pins with pellet and sphere-pac fuel.
In addition, an estimate of the **maximum dose in clad** at the end of the irradiation was evaluated at 0.91 dpa. This represents a very low final dose in the clad, simply consistent with the spectrum conditions encountered in the HFR. As a first approximation, and in absence of any detailed history, the evolution with time of the dose in clad was assumed to be homothetic with that of the energy released by the fuel. The corresponding evolution is given in the last column of Table 15. With regards to the very low final dose, one should expect a negligible impact of this assumption on the predicted behaviour, especially with a 15-15Ti austenitic steel clad material with an enhanced resistance to the irradiation-induced swelling.
The storage period prior to puncturing was also simulated with the FPCs, at null power, with the goal to evaluate the helium production by decay during that period. The storage lasted for 1282 days from the end of irradiation to the puncturing.

Table 15: Pin average Linear Heat Rating history of MARINE experiment – Dose evolution in clad

	Cumulated days Since beginning of Irradiation	**Pin #1 Pellets** **W/cm**	Pin #2 Sphere-Pac W/cm	**Dose in clad** **dpa**
Cycle 16-01	0	49.0	35.9	0.000
	0.5	53.4	40.0	0.001
	1.5	58.0	44.1	0.002
	3.5	61.4	47.2	0.006
	7.5	64.8	50.3	0.013
	15.5	70.8	55.2	0.028
	20.5	73.8	57.9	0.039
	30	78.7	61.8	0.059
Cooling	30			
Cycle 16-02	34	68.3	52.9	0.059
	34.5	71.7	56.2	0.060
	35.5	75.1	59.3	0.063
	37.5	77.2	61.3	0.067
	41.5	78.9	62.6	0.076
	49.5	81.6	64.7	0.094
	54.5	83.0	66.1	0.106

	Cumulated days Since beginning of Irradiation	**Pin #1 Pellets** **W/cm**	Pin #2 Sphere-Pac W/cm	**Dose in clad** **dpa**
	64	85.5	67.9	0.129
Cooling	64			
Cycle 16-03	85.9	77.2	61.0	0.129
	86.4	80.3	63.9	0.130
	87.4	83.3	66.7	0.132
	89.4	85.0	68.2	0.137
	93.4	85.9	68.7	0.147
	101.4	87.3	69.7	0.166
	106.4	88.2	70.3	0.179
	116.6	89.6	71.3	0.205
Cooling	116.6			
Cycle 16-04	120.6	75.4	61.1	0.205
	121.1	77.8	63.6	0.206
	122.1	80.1	65.9	0.208
	124.1	81.4	67.0	0.213
	128.1	81.7	67.4	0.222
	136.1	82.5	67.9	0.241
	141.1	83.0	68.2	0.253
	151.6	83.9	68.8	0.277
Cooling	151.6			
Cycle 16-05	155.7	82.8	64.9	0.278
	156.2	85.3	67.2	0.279
	157.2	87.8	69.5	0.281
	159.2	89.1	70.5	0.286
	163.2	89.5	70.8	0.296
	171.2	90.2	71.3	0.317
	176.2	90.7	71.6	0.330
	186.6	91.4	72.1	0.357
Cooling	186.6			
Cycle 16-06	190.5	84.2	68.7	0.357
	191	86.6	71.0	0.358
	192	88.7	73.1	0.361
	194	90.0	74.1	0.366
	198	90.4	74.3	0.376
	206	90.7	74.7	0.397
	211	91.1	74.9	0.410
	221.5	91.8	75.6	0.437
Cooling	221.5			
Cycle 16-07	222.4	85.5	72.1	0.437
	222.9	86.8	73.4	0.438
	223.9	88.0	74.6	0.441
	225.9	88.7	75.2	0.446
	229.9	88.9	75.6	0.456
	237.9	89.5	76.1	0.476
	245.8	89.8	76.5	0.496

	Cumulated days Since beginning of Irradiation	**Pin #1 Pellets** **W/cm**	Pin #2 Sphere-Pac W/cm	**Dose in clad** **dpa**
Cooling	245.8			
Cycle 16-08	247.1	91.6	71.5	0.496
	247.6	93.4	72.9	0.498
	248.6	95.0	74.3	0.500
	250.6	95.9	75.1	0.506
	254.6	96.3	75.4	0.517
	262.6	97.0	76.1	0.539
	267.6	97.4	76.4	0.553
	275.8	98.1	77.0	0.576
Cooling	275.8			
Cycle 16-09	312.8	84.1	67.0	0.576
	313.3	85.9	68.5	0.577
	314.3	87.5	70.0	0.579
	316.3	88.4	70.6	0.584
	320.3	88.7	71.0	0.594
	328.3	89.3	71.5	0.615
	333.3	89.8	72.0	0.627
	343.7	90.5	72.6	0.654
Cooling	343.7			
Cycle 17-01	347.6	89.6	69.3	0.654
	348.1	91.4	70.6	0.656
	349.1	93.0	72.0	0.658
	351.1	93.9	72.6	0.664
	355.1	94.1	72.9	0.674
	363.1	94.7	73.6	0.696
	368.1	95.0	73.9	0.709
	378.5	95.7	74.6	0.738
Cooling	378.5			
Cycle 17-02	389.4	91.3	74.1	0.738
	389.9	92.9	75.4	0.739
	390.9	94.3	76.7	0.742
	392.9	95.2	77.4	0.747
	396.9	95.4	77.7	0.758
	404.9	96.1	78.2	0.780
	409.9	96.5	78.7	0.793
	420.1	97.4	79.5	0.822
Cooling	420.1			
Cycle 17-03	438.1	95.2	73.6	0.822
	438.6	96.8	74.7	0.823
	439.6	98.3	75.9	0.826
	441.6	99.0	76.4	0.831
	445.6	99.3	76.7	0.843
	453.6	100.1	77.4	0.865
	458.6	100.4	77.7	0.880
	469.1	101.3	78.5	0.910

Figure 38: Evolution with time of the pin average Linear Heat Rating for MARINE experiment

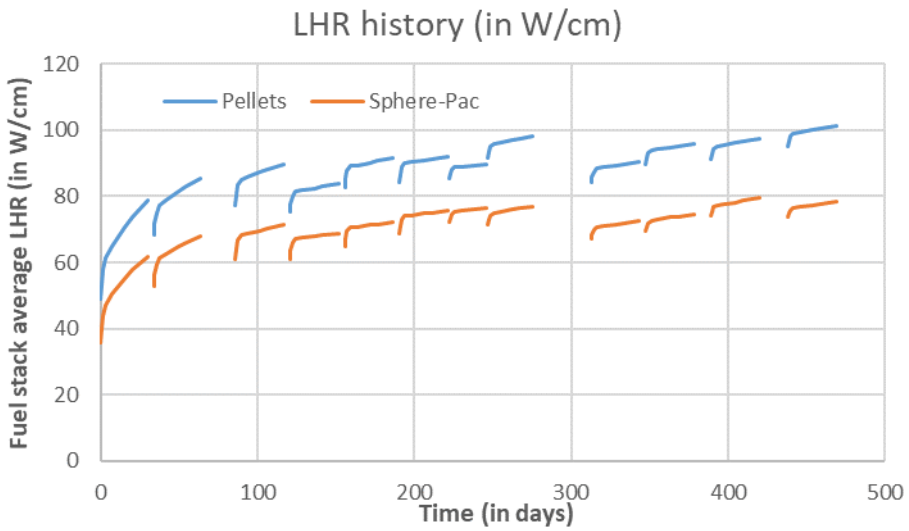

In addition, the **relative axial heating profile** along the fuel stack was digitalized from the plots shown in the PATRICIA D4.1 (Van Til 2021). The resulting axial weighting of the LHR along the fuel stack is given in the Table 16. Even if the variation of the weighting from the bottom to the top of the fuel stack is quite limited, this variation is not negligible and it will consequently impact the burn-up and the fission gas production computations. This is why it was decided to take into account this relative axial heating profile.

Table 16: Relative axial heating profile for MARINE pin #1 with pellet fuel

z from bfc (mm)	φ(z) (-)
3.09277778	0.83823917
9.27833333	0.84751750
15.4638889	0.85679583
21.6494444	0.86607417
27.835	0.87535250
34.0205556	0.88463083
40.2061111	0.89390917
46.3916667	0.90318750
52.5772222	0.91246583

As already pointed out, the spectrum conditions for the MARINE experiment are thermal spectrum conditions – namely those in the HFR. It is thus necessary to consider a **radial depletion of power in the fuel pellets**.

A preliminary simulation of MARINE experiment with TRANSURANUS in LWR spectrum conditions yielded a time dependent radial depletion shape of the power created in the fuel pellets. The dimensionless radial shapes obtained at different times along the irradiation are plotted on the Figure 39. The plots show a sharp increase of the peaking in the pellet periphery 493 hours after the beginning of the irradiation. Then the peaking progressively decreases up to the end of the irradiation, ending with a final ratio $\varphi_{max}/\varphi_{min}$ close to 2.05/0.83. This time dependent radial depletion of power in the fuel

pellets was used in the computations by TRANSURANUS and TRANSURANUS//SCIANTIX, and also in the GERMINAL simulation, being introduced as an additional loading in the irradiation history.
For the FEMAXI computation, the radial power profiles issued from the C^{4}P-TRAIN neutronic modelling of MARINE are taken into account. These profiles are shown on the previous Figure 37.
When comparing the depletion shapes issued from the C^{4}P-TRAIN and TRANSURANUS computations (Figure 37 and Figure 39, respectively), the discrepancy between the calculated shapes is noticeable. This underlines again the necessity of a comprehensive neutronic assessment of MARINE.

Figure 39: Time dependent radial depletion shape for MARINE experiment issued from a TRANSURANUS computation in LWR spectrum conditions

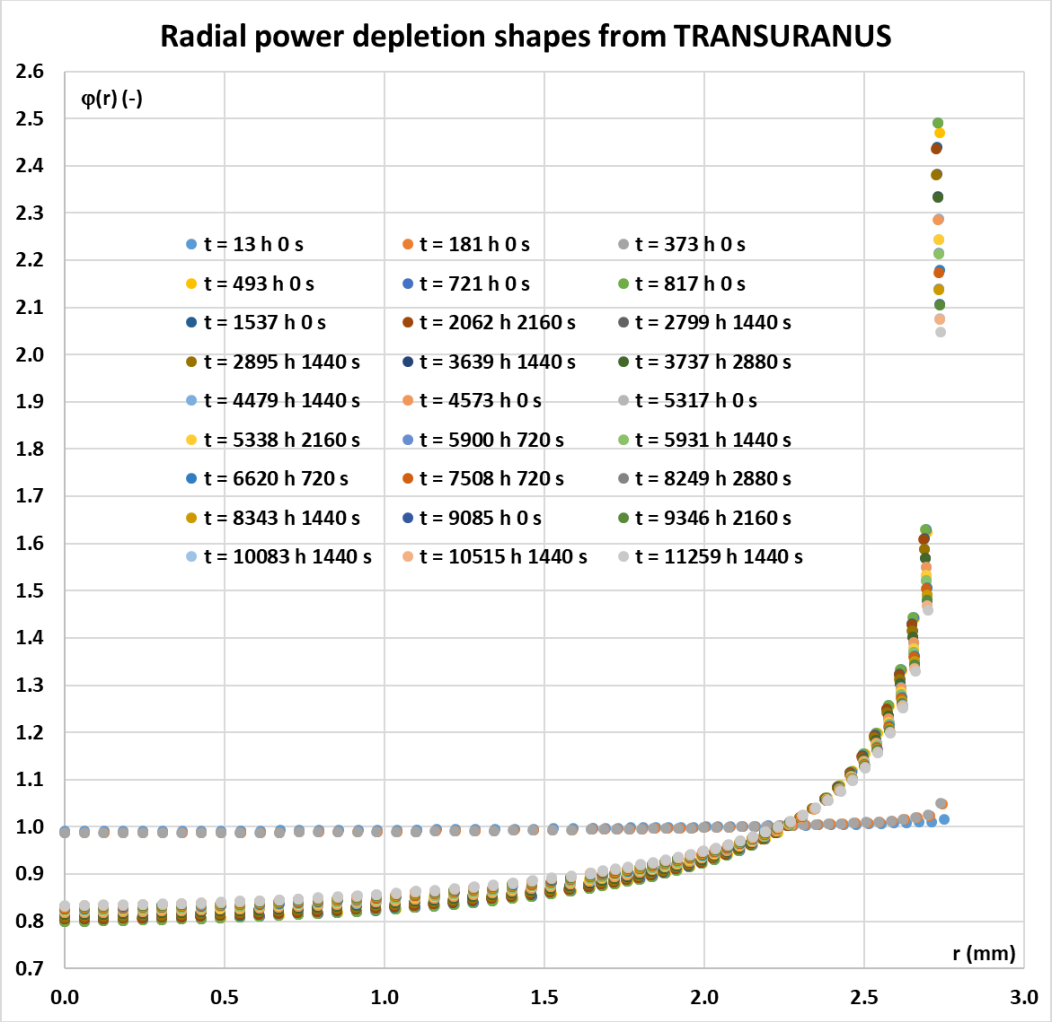

For what concerns the **thermal boundary condition**, the clad outer temperature was considered as axially constant along the height of the fuel pin. It was defined at 40°C during the inter-cycles and the storage period, and at 410°C when being on power.

The **modelling options involved for the computations** are summarized in the Table 17. With regards to those adopted for the simulation of SPHERE in thermal spectrum conditions (option 2 in Table 7), the main adaptations are related first to the fuel material, which is not the same for MARINE. In case of the GERMINAL and FEMAXI computations, the choice of the law for the fuel thermal conductivity is changed in order to evaluate more specifically the property of the (U,Am)O_{2-x} material. And all the computations are now using basic nuclear data tailored for MARINE.

Table 17: Details about the main modelling options adopted by the fuel performance codes for the simulations of the MARINE irradiation experiment

Thermal spectrum ("LWR simulation")	TRANSURANUS	TRANSURANUS //SCIANTIX	GERMINAL[1]	FEMAXI[2]
Gap conductance	URGAP model (Lassmann, Hohlefeld 1987)	URGAP model (Lassmann, Hohlefeld 1987)	Arnaud-Roche model	Modified Ross & Stoute model (Suzuki 2005)
Fuel relocation	Modified FRAPCON-3 model	Modified FRAPCON-3 model	Empirical correlation to the temperature gradient	Beyer 1975
Fuel densification	Empirical model for LWR conditions	Empirical model for LWR conditions	Empirical correlation to the temperature	Schlemmer & Ichikawa model
Fuel thermal conductivity	Magni 2021-2	Magni 2021-2	λ of $(U,Am)O_{2-x}$ Recommendation issued from CP-ESFR Project	Kato 2011
Fission gas production	Fission yields for Xe and Kr from MARINE neutronic modelling (Section 4.2.2) **Radial depletion of power in fuel**	Fission yields for Xe and Kr from (Motta, Olander 2017) **Radial depletion of power in fuel**	Point kinetic neutronics model with cross-sections and fission yields tailored for MARINE (Section 4.2.2) **Radial depletion of power in fuel**	Neutronics by C^4P-TRAIN in **thermal spectrum**
Helium production	From TUBRNP (TRANSURANUS burn-up module), including fission yields for He from MARINE neutronic modelling (Section 4.2.2)	Surrogate model tailored for MARINE	Point kinetic neutronics model with fission yields tailored for MARINE (Section 4.2.2)	Neutronics by C^4P-TRAIN
Helium release	Based on He diffusion according to Fédérici, 2007	Treated by SCIANTIX physics-based module	Temperature threshold for helium release	Power threshold for helium release
Inert gas behaviour	Mechanistic TRANSURANUS model for LWR conditions	Treated by SCIANTIX physics-based module	Fission gas release model	Mechanistic fission gas release model
Cladding properties/behaviour	TRANSURANUS models for 15-15Ti stainless steel	TRANSURANUS models for 15-15Ti stainless steel	AIM1	Stainless steel 15-15Ti

[1] The models implemented in GERMINAL and used for this study are mainly described in (Lainet 2019).

[2] The models implemented in FEMAXI and used for this study are mainly described in (Suzuki 2005). The neutronics analysis is performed by C^4P-TRAIN (Rineiski 2018) prior to the FEMAXI computation, providing the fission gas and helium productions on input.

4.3.2 Results from the simulations of MARINE with the fuel performance codes

The first analysed results focus on the production and release of inert gases: namely, fission gases (Xe, Kr) and helium, which is a major concern for fuels bearing minor actinides, and more particularly in case of a blanket material $(U,Am)O_{2-x}$ with a high americium content of about 13 wt.%. The calculation results are summarized in Table 18, along with the corresponding puncturing examination results on the MARINE pelletized fuel pin. The analysis of the results is developed further, based on the discussion of the computed evolutions shown on different plots.

Table 18: FPCs results for inert gas production and release and puncturing examination results

FPCs results Thermal spectrum	Xe + Kr produced (atoms)	Xe + Kr released (atoms)	Xe + Kr release rate (%)	He produced (atoms)	He released (atoms)	He release rate (%)
TRANSURANUS	1.46E+20	1.24E+17	0.085%	1.96E+21	1.96E+20	10%
TRANSURANUS //SCIANTIX	1.17E+20	3.25E+18	2.8%	1.65E+21	1.25E+20	7.6%
GERMINAL	1.06E+20	9.17E+16	0.087%	1.97E+21	1.34E+21	68%
FEMAXI //C[4]P-TRAIN	8.3E+19	4.15E+17	0.5%	1.69E+21	8.97E+20	53%
Experimental data from puncturing [1] N.B. Xe, Kr and He productions issued from computations [2]	Xe + Kr produced (atoms)	Xe + Kr released (atoms)	Xe + Kr release rate (%)	He produced (atoms) [3]	He released (atoms) [4]	He release rate (%) [5]
	1.38E+20	3.33E+18	2.41%	1.64E+21	9.37E+20	57.1%

[1] The data are issued from the PATRICIA D4.1 (Van Til 2021).

[2] The productions of xenon, krypton and helium used for estimating the release rates with the puncturing results are issued from a FISPACT (Sublet 2017) computation performed by the reactor operator. The produced quantities extracted from the PATRICIA D4.1 are taken at EOI + 3 years, corresponding to the date of puncturing.

[3] The produced quantity of helium is determined with the total amount of helium at EOI + 3 years, as provided in the PATRICIA D4.1, decreased by the helium quantity in the filling gas.

[4] The released quantity of helium is determined with the total helium quantity retrieved in the pin plenum at puncturing, decreased by the helium quantity in the filling gas.

[5] The helium release rate is determined by the ratio of the two previous released and produced quantities. It is estimated in this way at the date of puncturing, and not at the end of irradiation.

The helium production predicted by the different codes is shown on the Figure 40.

Figure 40: FPCs results for the helium production

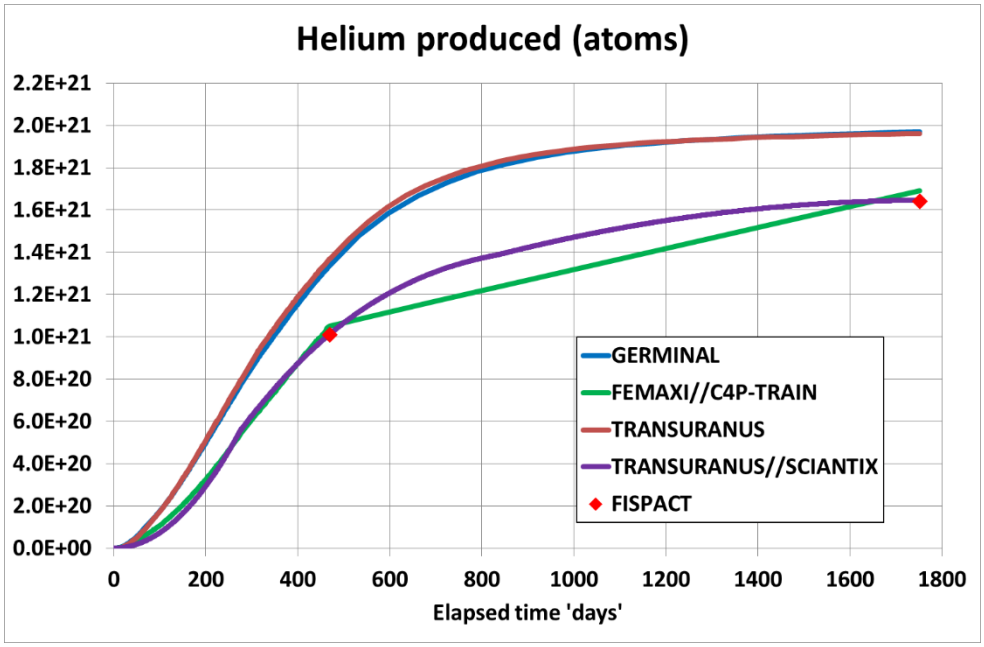

In case of the TRANSURANUS//SCIANTIX and FEMAXI//C[4]P-TRAIN computations, the calculation of the helium production was adjusted with the goal to match the estimation by FISPACT. The consistency with FISPACT is thus logically observed.

The predictions by TRANSURANUS standalone and GERMINAL are very close, as a consequence of using the same set of basic nuclear data on input – cross-sections and fission yields – issued from the neutronic assessment of MARINE by SERPENT-2 (cf. Section 4.2.2). The final helium production obtained by the two codes exceeds the estimation by FISPACT. It is here interesting to consider separately the helium production during the irradiation, and the one during the storage period, resulting only from the decay of heavy nuclides. The helium creation by decay during the storage, estimated by FISPACT, is about 6.3×10^{20} atoms (corresponding to the difference between the two red points on the Figure 40). The estimations issued from the TRANSURANUS and GERMINAL computations are 5.94×10^{20} and 6.32×10^{20} atoms, respectively. These values are thus consistent with that predicted by FISPACT, and this means that the discrepancy observed for the final amount of helium production essentially comes from different estimations of the quantity produced during the irradiation; the difference at EOI being further kept during the storage. This observation is mainly questioning the fission yields related to helium used in the different computations.

The next Figure 41 shows the predicted evolutions of the helium quantity in the pin free volume. The final values are compared with the helium quantity retrieved at puncturing. In case of the FEMAXI//C^{4}P-TRAIN computation, the release of helium was adjusted to match the PIE result, with the goal to assess the prediction of other internal pin quantities (especially the fuel temperature) in a reverse-modelling approach.

For what concerns the results obtained by TRANSURANUS and TRANSURANUS//SCIANTIX, the underestimation of the helium released quantity is essentially questioning the thermal activation of the diffusional mechanisms that are solved for determining the helium release. The consideration of a supplementary contribution by an athermal release mechanism may also improve the computation results. This represents a perspective of future work on the modelling.

In case of GERMINAL, the contrary trend is observed, namely an overestimation of the final helium quantity in the pin plenum. Two possible explanations can be proposed. First, overestimating the helium released quantity may be the consequence of overestimating first the production during the irradiation, as previously discussed. But another possibility is that the helium created in fuel during the irradiation may have not been completely released, due to the low temperatures in the fuel in case of the MARINE experiment. This assumption is also suggested by the results yielded by TRANSURANUS and TRANSURANUS//SCIANTIX. In the GERMINAL computation, a temperature criterion is considered for the helium release (300°C), inhibiting temporarily the release during the inter-cycles, and further during the storage period – the temperature during the inter-cycles and the storage is taken at 40°C, as the temperature in the HFR core at null power. When considering that higher temperatures would be needed to enable helium release (namely, higher than 300°C), the overestimation by GERMINAL of the final helium quantity in the pin plenum may also come from overestimating the release itself, due to an inadequately low temperature criterion. A sensitivity analysis to this temperature criterion for helium release is presented further in Section 4.3.3.2.

Figure 41: FPCs results for the helium in the pin free volume

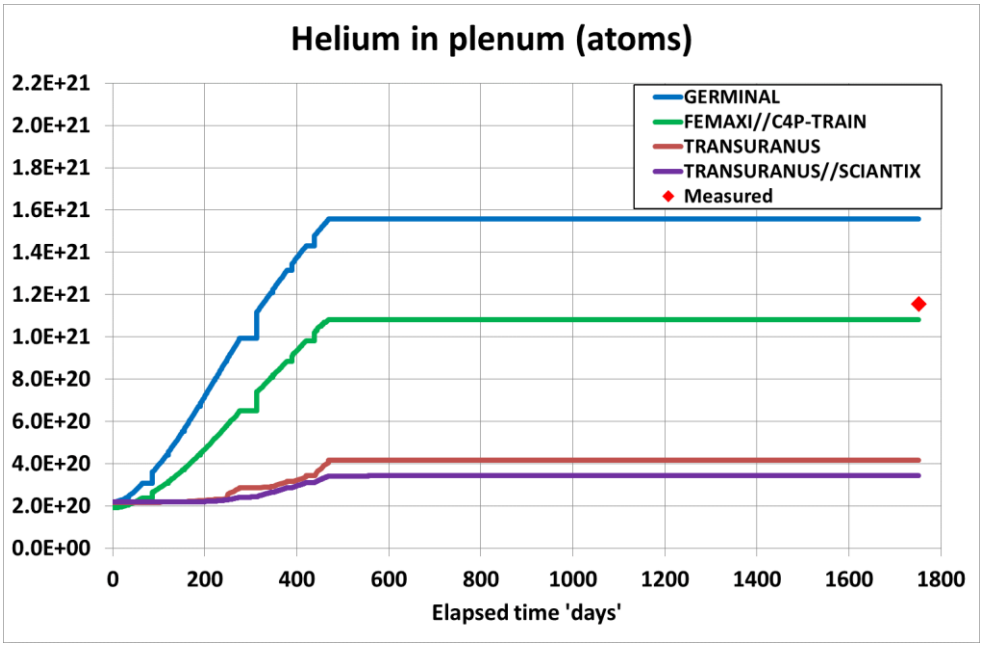

For what concerns the production and release of the fission gases – xenon and krypton, the results obtained by the different codes are respectively shown on the Figure 42 and Figure 43.

Important discrepancies are found for the fission gas production. In case of the FEMAXI//C^{4}P-TRAIN computation, as already pointed out, the preliminary neutronic assessment by C^{4}P-TRAIN takes into account the contribution of the (n,gamma) reactions to the heat generation; whereas the other codes determine the heat creation only from the fission reactions. As a consequence, less fissions are needed in the C^{4}P-TRAIN computation for building the same heat source term defined by the LHR given on input; less fissions leading logically to a lower prediction of the fission gas production. As a complementary indication, the Table 19 presents the estimations of the pin average burn-up issued from the different computations. The value yielded by C^{4}P-TRAIN is thus significantly lower when being compared to the others: about –41% when taking the FISPACT estimation as the reference. This quantifies the relative contribution of the (n,gamma) reactions to the heat generation in the C^{4}P-TRAIN computation. The discrepancy for the fission gas production between TRANSURANUS standalone and TRANSURANUS//SCIANTIX, as visible on the Figure 42, can be ascribed to the use of different basic nuclear data – see details in the Table 17. And the discrepancy between TRANSURANUS standalone and GERMINAL comes from the use of different fission energies in the computations: this was already pointed out in the simulation of SPHERE with the assumption of thermal spectrum, in the discussion of the results in Section 3.3.2.

On the Figure 43 for the fission gas release, one can remark the excellent agreement between the prediction by TRANSURANUS//SCIANTIX and the puncturing result. The other codes predict a negligible fission gas release. The value obtained by FEMAXI corresponds to a minimum release rate of 0.5% considered by the code.

Figure 42: FPCs results for the fission gases production

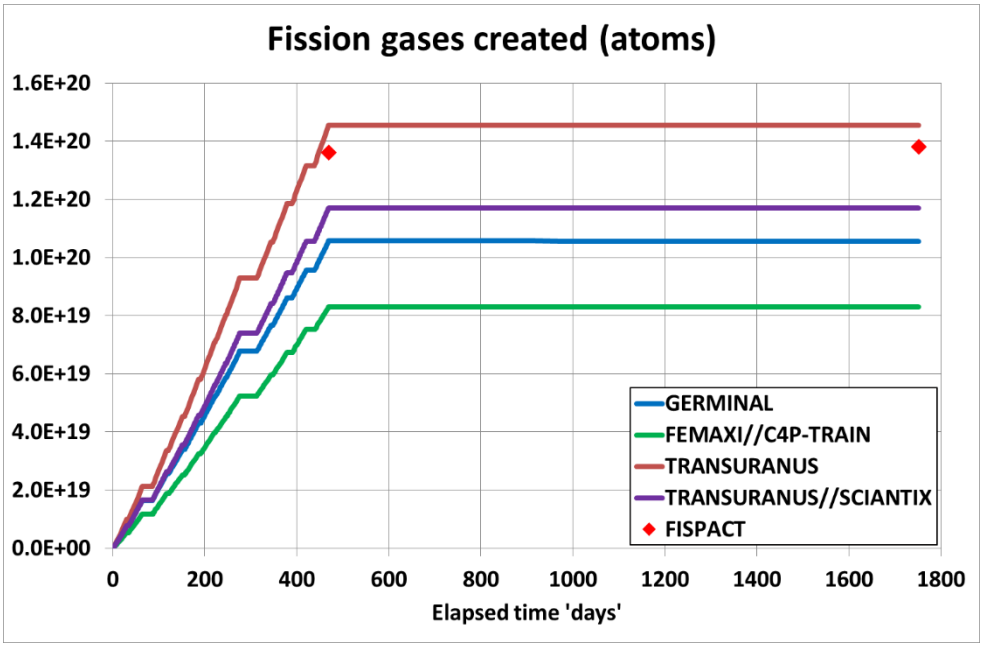

Table 19: Pin average burn-up (% FIMA) issued from the different computations

MCNP-FISPACT [1]	TRANSURANUS	TRANSURANUS //SCIANTIX	FEMAXI //C^{4}P-TRAIN	GERMINAL
1.57	1.470	1.478	0.928	1.540

[1] This estimation by MCNP-FISPACT issued from the post-irradiation nuclear analysis by NRG, as mentioned in the PATRICIA D4.1 (Van Til 2021).

Figure 43: FPCs results for the release of the fission gases

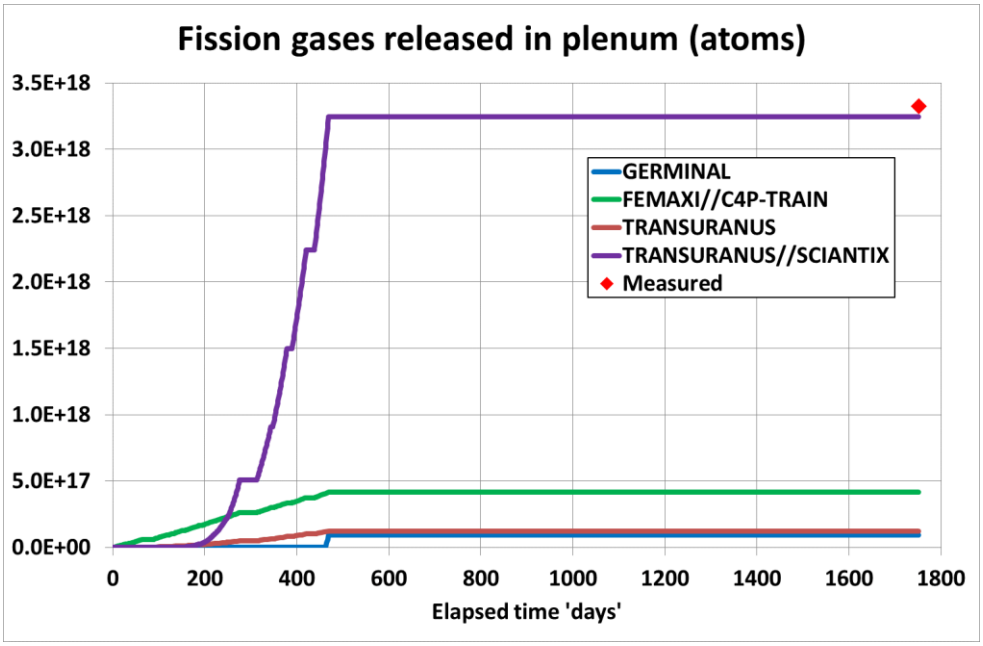

Even if the computation results show important discrepancies for the fission gas production and release, it is legitimate to consider that this will have no real impact on the predicted behaviour of the MARINE fuel. Practically, the puncturing results show that the final helium fraction in the pin plenum gas is 99.72%. There is thus nearly no release of fission gas during the MARINE experiment, and this is essentially the result yielded by all the codes. With the best estimate of the fission gas released quantity obtained by TRANSURANUS//SCIANTIX, the corresponding fractional composition of the plenum gas at end-of-life is 99.07% of helium, and 0.93% of fission gases – xenon representing 0.83%. So, as the plenum gas composition essentially remains constant along the whole irradiation (about 100% helium), the calculated temperatures in the fuel will mainly depend on the predicted evolutions of the pellet-to-clad gap size. This will be discussed further in this Section.

It is important to underline here that the destructive examination results of the MARINE fuel could provide very valuable information for checking the computation results, especially the final elemental composition of the fuel: quantities of major and minor actinides – also with the goal to evaluate the transmutation performance of Am, neodymium as a burn-up marker, and the quantities of the retained fission gases, as being representative of the gas production in absence of a significant release.

The calculated evolutions with time of the fuel inner temperature at the Peak Power Node (namely, at the top of the fuel stack) are presented on the Figure 44. These evolutions are analysed in link with those of the pellet-to-clad gap size (Figure 45) and of the gap thermal conductance (Figure 46).

Figure 44: FPCs results for the fuel inner temperature at Peak Power Position

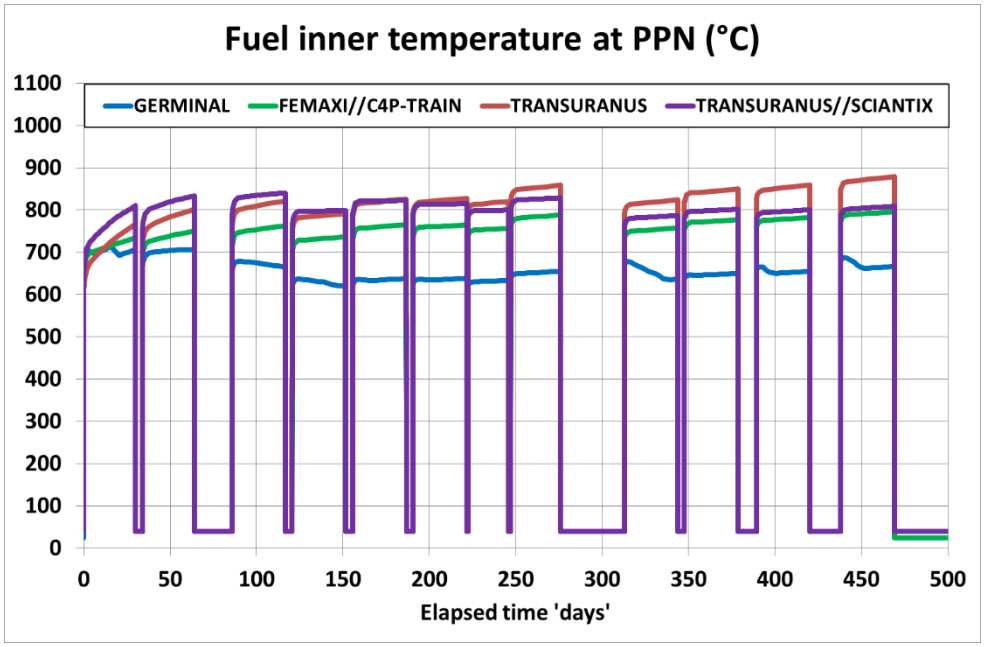

For what concerns the TRANSURANUS standalone results, one can firstly remark on the Figure 44 an increase of the fuel inner temperature at the beginning of irradiation, mainly during the two first cycles. The trend is the same for the TRANSURANUS//SCIANTIX computation. This initial increase of the fuel temperature can be correlated to that of the pellet-to-clad gap, in the same time (Figure 45): one can see here an effect induced by the pellet densification, decreasing the pellet diameter, and widening consequently the gap with the clad. When going further in the irradiation, the pellet-to-clad gap size stabilizes in the TRANSURANUS standalone computation, around 120 µm, and slightly decreases up to 115 µm at the end the last cycle. The temperature evolution then follows that of the power created in the fuel, which is progressively increasing up to the end of the irradiation, in link with the creation of fissile isotopes in the fuel – this behaviour predicted here with an $(U,Am)O_{2-x}$ material with a low initial

fissile content is consistent with that of a fertile material. In case of the TRANSURANUS//SCIANTIX computation, the trend for the pellet-to-clad gap size evolution is not exactly the same: after the initial increase during the two first cycles, the gap thickness progressively decreases up to 75 µm at the end of irradiation. We can see here an effect of the fuel swelling, induced by the retentions of both the fission gases and helium. The evolutions of the gap thermal conductance (Figure 46) predicted by TRANSURANUS standalone and TRANSURANUS//SCIANTIX are fully linked to those of the pellet-to-clad gap size, since there is no real change in the plenum gas composition (~100% helium). The evolution is quite flat in case of TRANSURANUS standalone, with a stabilized gap size, and slightly increasing with the progressive gap decrease in case of TRANSURANUS//SCIANTIX. As the gap remains open along the whole irradiation, its thermal conductance is quite poor: the minimum value is about 0.25 W/cm^2/K when the gap is the widest, namely at the end of the second cycle after the densification of the pellets, then the TRANSURANUS//SCIANTIX computation describes a slight increase up to 0.35 W/cm^2/K at the end of irradiation. The maximum temperature in the fuel predicted by TRANSURANUS standalone is obtained at the end of the last cycle, when the power released by the fuel is the highest. It does not exceed 880°C. In case of TRANSURANUS//SCIANTIX, the maximum is reached earlier in irradiation – at the end of the 8th cycle, and does not exceed 830°C. These very low temperatures in the fuel explain a preponderant retention of gases.

Figure 45: FPCs results for the pellet-to-clad gap size at Peak Power Position

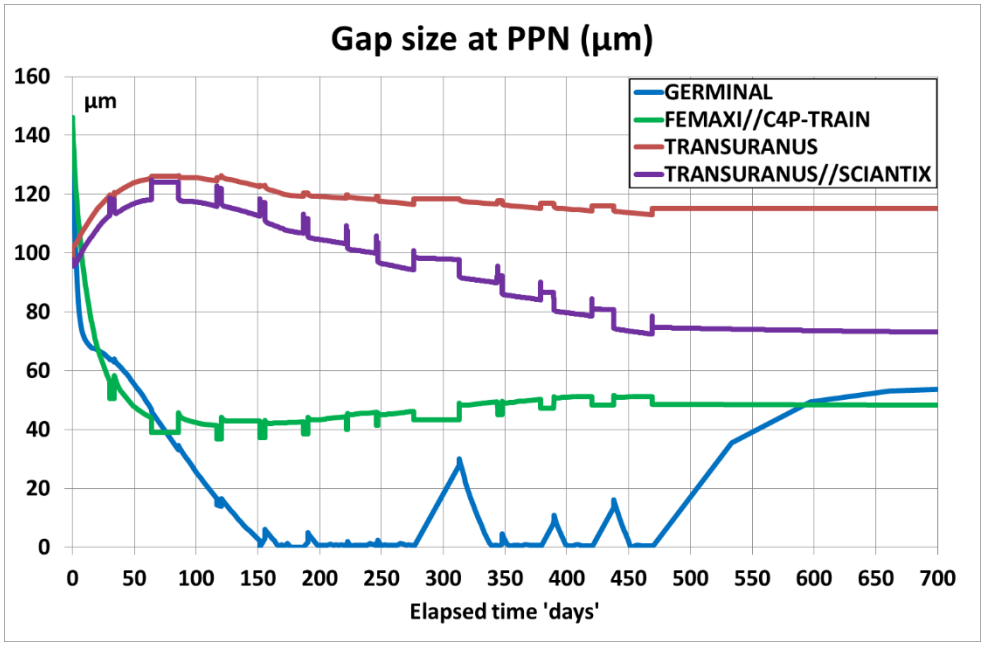

In case of the FEMAXI//C^{4}P-TRAIN computation, one can observe on the Figure 45 a quick decrease of the gap size during the two first cycles of the irradiation – this evolution being very different from those calculated by TRANSURANUS standalone and TRANSURANUS//SCIANTIX, previously commented. The gap size decreases from its initial value (141 µm) up to 40 µm at the end of the second cycle, then there is a very slow increase up to 50 µm at the end of the irradiation. The gap thermal conductance evolves consistently, with a significant increase during the two first cycles – from 0.15 to 0.83 W/cm^2/K, then the evolution becomes very smooth, with a slight decrease ending at 0.75 W/cm^2/K at the end of the last cycle. With a gap size predicted smaller, when compared to those computed by TRANSURANUS and TRANSURANUS//SCIANTIX, the temperatures obtained by FEMAXI//C^{4}P-TRAIN are logically lower, ranging between 700°C and 800°C along the irradiation, and slightly increasing at the end with the power in the fuel.

Figure 46: FPCs results for the gap thermal conductance at Peak Power Position

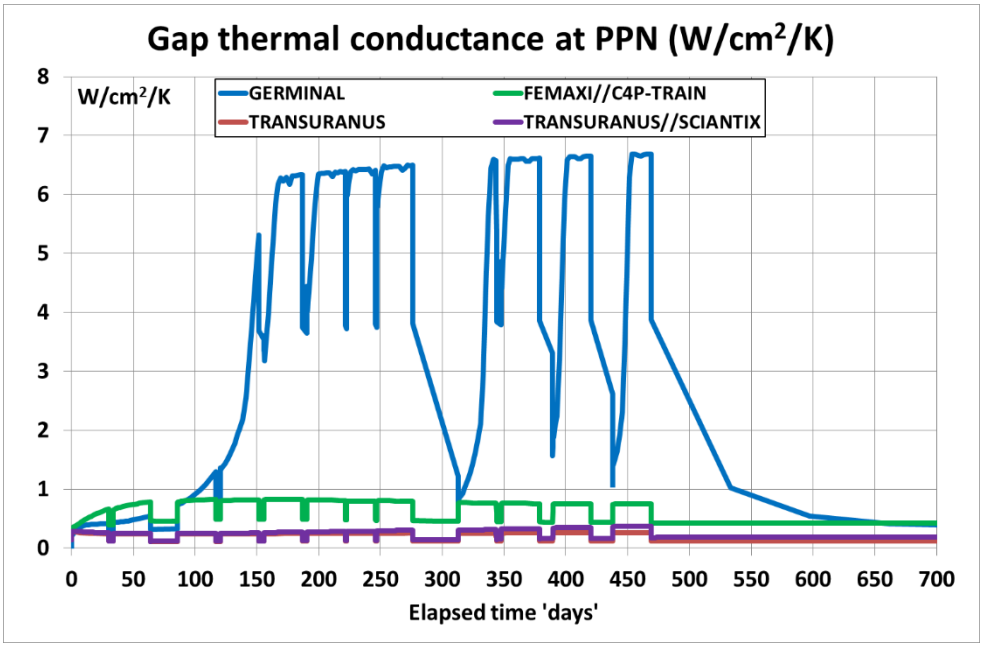

Finally, for what concerns the GERMINAL computation, the predicted evolution of the gap is the single one leading to a complete closure at the end of the 4th cycle (Figure 45). When comparing to the other computations, this evolution of the gap consistently leads to the lowest predicted temperatures in the fuel (Figure 44) and the highest values for the gap thermal conductance (Figure 46), ranging between 6 and 7 W/cm^2/K when the gap is closed. The temperatures calculated by GERMINAL never exceed 700°C after the two first cycles of the irradiation. As already observed with other codes, there is a trend for a slight temperature increase in the last cycles of the irradiation, in link with the power increase in the fuel. The complete gap closure, which is singularly predicted by GERMINAL, mainly results from the deformation of the fuel induced by gaseous swelling. In case of an (U,Am)O_{2-x} material, GERMINAL involves an empirical correlation essentially driven by the gas production and the temperature. The swelling kinetics is driven by a time constant that was calibrated with a few experimental data – thus the goal of this empirical swelling correlation is to provide a physically representative evaluation of the volume swelling of the fuel at hot state, rather than a "best-estimate". Involving this correlation in the simulation of the MARINE experiment yields a radially averaged gaseous swelling of about 7.5% at the end of the last cycle. This estimate is to be compared to that issued from the first PIE results performed with MARINE fuel: about 16% of volume swelling, according to the PATRICIA D4.1 (Van Til 2021). Thus, the gaseous swelling evaluated by GERMINAL at the end of the irradiation even looks low, when compared to the first estimation issued from the PIEs. The increase of the gap size predicted by GERMINAL after the end of the irradiation, visible on the Figure 45, results from the kinetics of the swelling correlation: as the maximum local swelling in the conditions of the storage (40°C) is lower than the swelling reached at the end of the irradiation, the kinetics determines a decrease of the swelling at cold state, leading to a progressive gap reopening, up to an asymptotic value of 54 µm. This explains the predicted behaviour at cold state after the end of irradiation, such evolution remaining debatable.

The last physical quantity analyzed in this Section is the temperature jump in the fuel at the Peak Power Node, presented on the Figure 47. Two main reasons can explain the discrepancies observed between the results yielded by the different codes:

- the law used to evaluate the fuel thermal conductivity is not the same in the different computations. The choice for each code is defined in the Table 17, in the Section 4.3.1. The laws used by TRANSURANUS standalone, TRANSURANUS//SCIANTIX and FEMAXI//C^{4}P-TRAIN are related to MOX fuel loaded with minor actinides, whereas the one used by GERMINAL is related to hypostoichiometric $(U,Am)O_{2-x}$;
- the radial depletion shapes of power in the fuel considered in the FEMAXI//C^{4}P-TRAIN are not the same than those taken into account in the other computations.

One can firstly remark that the temperature jump in the fuel computed by FEMAXI//C^{4}P-TRAIN is systematically higher, when compared to the other results. The discrepancy with GERMINAL at the end of the 8th cycle is about 76°C. Having a look back on the radial depletion shapes of power used in the different computations, it turns out to be clear that the shapes issued from the preliminary computation by TRANSURANUS in LWR conditions (Figure 39, these shapes being used further by TRANSURANUS, TRANSURANUS//SCIANTIX and GERMINAL) show a sharper peaking in the pellet periphery, when compared to those issued from the C^{4}P-TRAIN assessment (Figure 37). Thus, in case of the FEMAXI//C^{4}P-TRAIN computation, creating more power in the central region of the pellet results in a higher temperature jump in the fuel. This highlights the influence of the radial depletion of power on the temperature calculation. With the goal to quantify the effect induced by the power depletion on the temperature assessment, sensitivity analyses have been performed with TRANSURANUS and GERMINAL and are presented further in the Sections 4.3.3.1 and 4.3.3.2, respectively.
It is also interesting to observe that the discrepancies between GERMINAL, TRANSURANUS standalone and TRANSURANUS//SCIANTIX tend to decrease when irradiation progresses. But we can also see on the Figure 44 that the discrepancies for the maximum temperature in the fuel are increasing in the same time, while the calculated ΔT in fuel become consistent. We can see here a kind of compensating effect: with shifted temperature fields and different laws for the fuel thermal conductivity, the computations by GERMINAL, TRANSURANUS standalone and TRANSURANUS//SCIANTIX yield consistent estimations of the ΔT in fuel at the end of irradiation.

Figure 47: FPCs results for the temperature jump in fuel at Peak Power Position

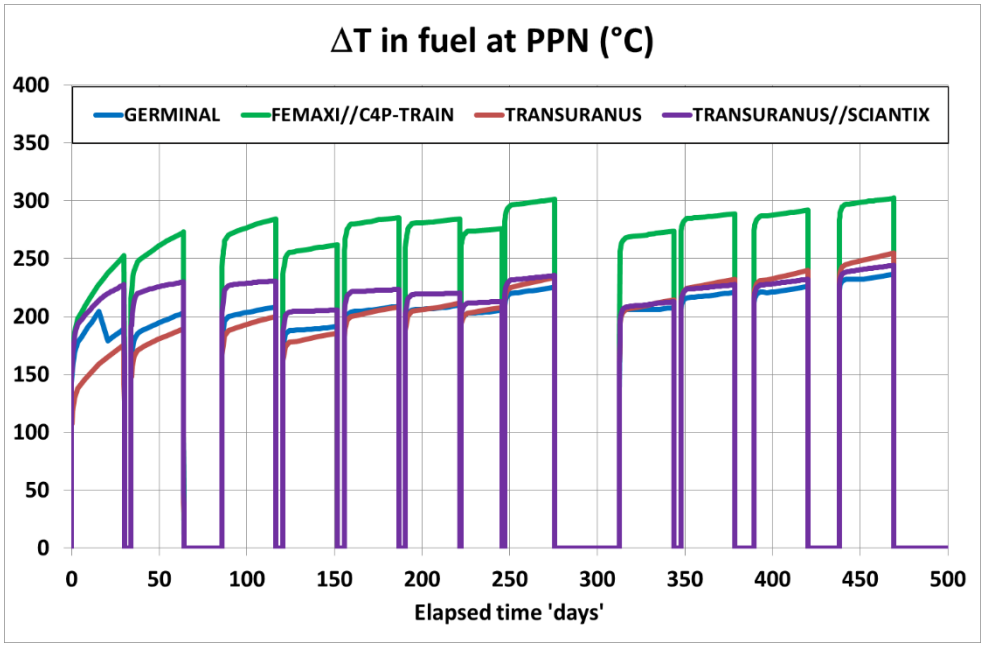

After this review of the main results obtained by the FPCs for the simulation of MARINE experiment, the major identified needs for improving the computations are clearly concerning the modelling of the helium behaviour in the fuel, especially the assessment of the helium release in a low temperature range, such as the one along the MARINE experiment. The prediction of a representative amount of helium in the pin plenum at end-of-life clearly depends on the reliability of the release assessment. The accurate evaluation of the helium creation rates in the fuel is needed beforehand, especially during the irradiation. The representativeness of the calculated temperature is also required, with the goal to capture the thermal activation of the helium release. Again, the necessity of a comprehensive neutronic characterization of the experiment is highlighted: for the evaluation of the above-mentioned creation rates of helium in the fuel, and for the determination of the radial depletion of the power in the pellets, which modifies the temperature field. A first step towards such a neutronic characterization was obtained in this work. Other important needs are related to the assessment of the fuel swelling induced by the retained gases – the fission gases xenon and krypton, but helium as well – with regards to the influence of the gaseous swelling on the evolution of the pellet-to-clad gap size, and consequently on the temperature in the fuel.

4.3.3 Sensitivity studies based on the simulation of MARINE

4.3.3.1 Sensitivity studies with TRANSURANUS & TRANSURANUS//SCIANTIX

As for the SPHERE experiment, the only difference between these two simulation sets is using SCIANTIX as a point model for generation, evolution and release of fission products, while both sets apply TRANSURANUS for the thermal and mechanical analysis.

We see a consistent relative difference between the calculations of the released fission gas (Figure 43). Nevertheless, unlike for SPHERE, the total amounts are low, hence there is no or limited actual impact on the predicted thermo-mechanical fuel behaviour. Despite the somewhat lower temperatures, TRANSURANUS//SCIANTIX predicts a gap size systematically smaller than TRANSURANUS standalone, i.e., revealing a larger fuel expansion that to a large extent is due to retention of fission products in the fuel pellets.

Using TRANSURANUS standalone, a complementary sensitivity study was made estimating the maximum impact of fuel thermal conductivity, densification as well as of the radial power depletion on the predicted fuel center temperatures. Assuming an early irradiation phase (burn-up between 0 and 10 MWd/kgHM) for the MARINE fuel pellets (characterized in Table 10 and Table 11), Figure 48 outlines different correlations for the fuel thermal conductivity available in TRANSURANUS:

- the correlation derived for MA-MOX fuels in the INSPYRE project (Magni 2020, 2021-2), cf. Table 17;
- the correlation recommended for irradiated LWR-MOX fuels with low Pu content, based on experimental data obtained at JRC (Staicu 2011, 2013);
- the earlier reference correlation for hypo-stoichiometric MOX fuel (Philipponneau 1992).

Note the significant differences between these three correlations in particular in the low temperature region, mainly due to the large coefficients for the O/M term in the earlier hypo-stoichiometric MOX correlation (Philipponneau 1992) and the Am-content term in the MA-MOX correlation of INSPYRE. In addition, the impact of densification and radial power profiles was tested by applying extreme settings, combining option (a) with (i) zero densification and (ii) flat radial power profiles (i.e., no radial power depletion).

Figure 48: Sensitivity study with TRANSURANUS: Thermal conductivity of the MARINE fuel pellets - tested correlations for sub-stoichiometric MOX with O/M=1.93, a moderate porosity of 5.39 %, in the low burnup range up to 10 MWd/kgHM

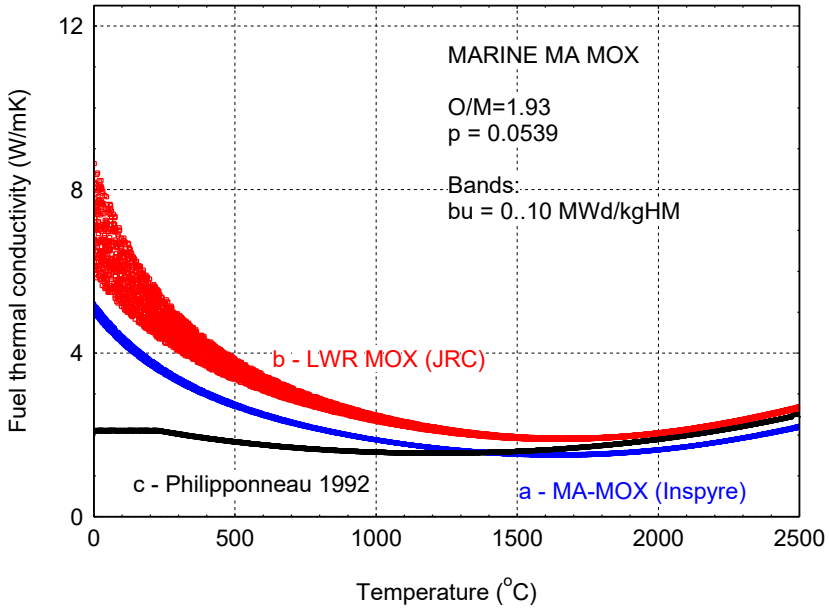

Figure 49 summarizes the main results: making extreme assumptions in the simulation of the given MARINE fuel pellets by TRANSURANUS, the fuel centre temperature at PPN and EOL is approximately 120°C higher when completely neglecting the radial power profile, or approximately 50°C lower when completely neglecting densification. The largest impact (temperature increase of 170°C) arises from applying an alternative thermal conductivity correlation (Philipponneau 1992) that seems to be inapplicable for the degree of hypo-stoichiometry of the MARINE fuel (O/M=1.93). For the specific case of MARINE, our study reveals that the fuel thermal conductivity, densification as well as the shape of the radial power profile have a comparable influence on the calculated fuel temperatures.

Figure 49: Sensitivity study with TRANSURANUS: Simulated fuel centre temperature and radial gap size at PPN

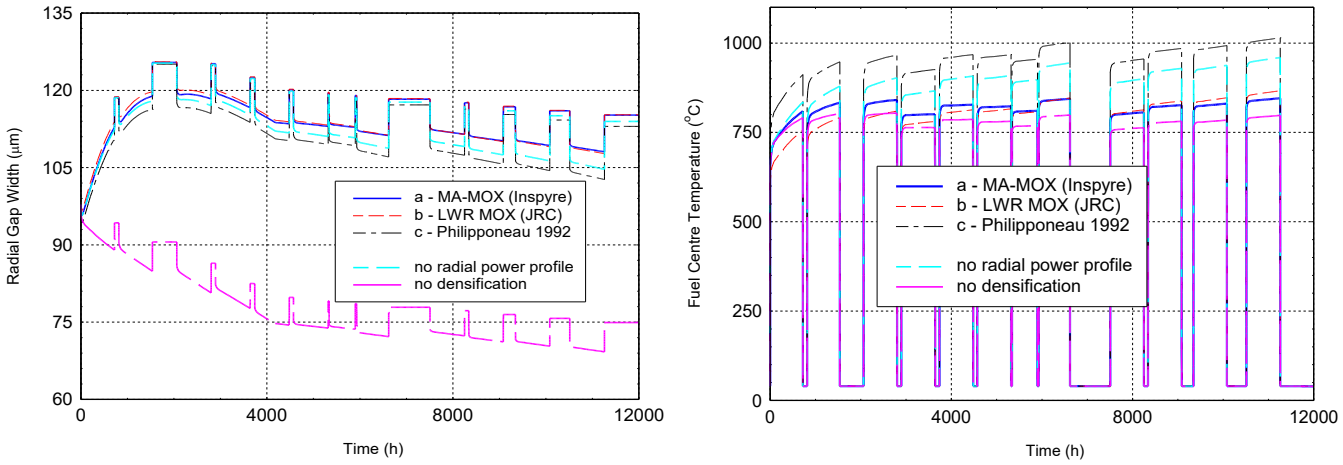

4.3.3.2 Sensitivity studies with GERMINAL

Sensitivity analysis to the temperature criterion for helium release

As previously pointed out in the Section 4.3.2, the discrepancies observed between the different codes in the prediction of the helium quantity in the pin plenum (Figure 41) is questioning the thermal activation of the helium release mechanism. This is suggested by both the results obtained by:

- TRANSURANUS or TRANSURANUS//SCIANTIX: the helium quantity in plenum at end-of-life is underestimated with regards to the puncturing result, possibly showing that the diffusional properties are not adequately calibrated in the temperature range of MARINE experiment;
- GERMINAL: conversely, the helium quantity in the plenum at EOL is overestimated when a low temperature threshold for helium release (300°C) is considered. This threshold effectively prevents helium release only during the storage phase, as the helium produced during one inter-cycle is not released immediately but instead during the subsequent power cycle.

Thus, the possibility of a partial helium retention during the irradiation is to be considered.

With the goal to figure out what could be a temperature range for the thermal activation of the helium release mechanism, a sensitivity study was performed with GERMINAL, by increasing the temperature threshold up to an optimal value yielding the best agreement with the puncturing results. The optimal threshold was found at 530°C, all other modelling options being kept identical – especially the radial depletion of power in the fuel, as issued from the preliminary TRANSURANUS computation (Figure 39). The evolution of the computation results for the helium quantity in the pin plenum and the gas pressure are shown on the Figure 50.

Figure 50: Sensitivity study with GERMINAL – Effects of the temperature threshold for helium release on the helium quantity in the pin plenum and the gas pressure

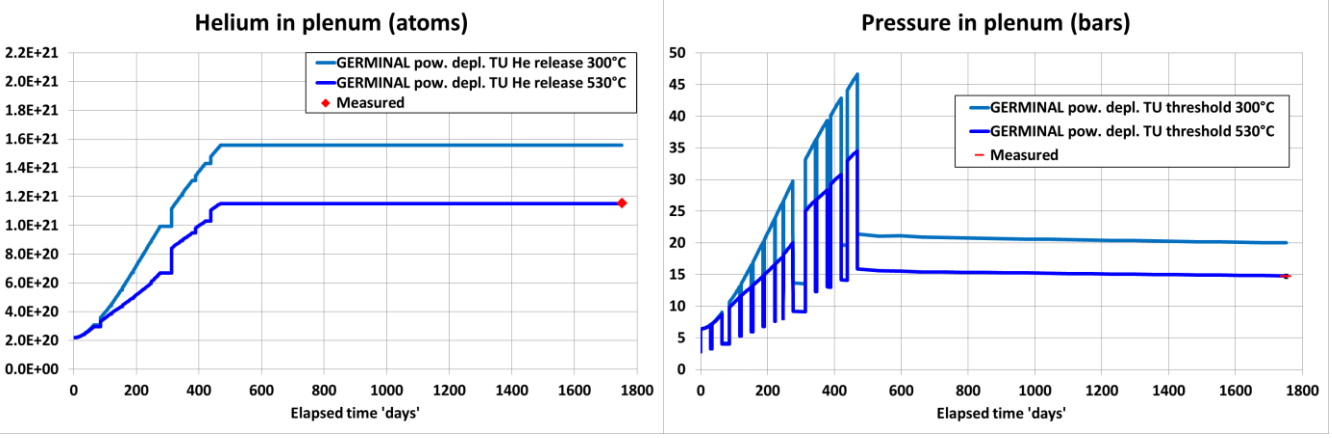

Obviously, these results do not prove that the temperature threshold for helium release is 530°C, since this optimal value is fully depending on the temperature calculation by GERMINAL.

Having a look back on the results obtained by the different codes for the fuel inner temperature (Figure 44), one can note at the end of the last irradiation cycle a discrepancy between the calculations, ranging from 666°C (GERMINAL) to 879°C (TRANSURANUS); with quite consistent ΔT in fuel predicted at the same time (Figure 47). So, the temperature field computed by TRANSURANUS is shifted about 210°C higher than that issued from GERMINAL. This may represent an uncertainty on the temperature computation, yielded by the comparison between different results. And GERMINAL may represent the lower bound for the temperature computation.

Then, coming back to the optimal value of 530°C for the temperature threshold for helium release, issued from the sensitivity study with GERMINAL, and accounting for an uncertainty of about 210°C on the temperature computation, with GERMINAL representing the lower bound, one may consider a possible range of [530°C - 740°C] for the temperature threshold for helium release. This still represents

a rough estimation, but supported by the results obtained by the different simulations of MARINE performed in this work. Such information could be useful for investigating further the thermal activation of the diffusional properties involved in mechanistic models for the evaluation of the helium release.

Sensitivity analysis to the radial depletion of power in the fuel

It was also pointed out in the Section 4.3.2 that different radial depletion shapes of power in the fuel can naturally induce discrepancies in the temperature calculation, especially with regards to the ΔT in fuel (Figure 47). In order to quantify the effect induced by the power depletion on the temperature assessment, a second sensitivity study was performed with GERMINAL, by adopting the radial shapes issued from the C^{4}P-TRAIN computation (Figure 37) instead of those from TRANSURANUS (Figure 39). It was noted that the shapes from TRANSURANUS show a sharper peaking in the pellet periphery, leading to concentrate more power in the periphery than in the central region of the pellet. This implies a decrease of the maximum temperature reached at the center. Thus, the temperatures computed by using the depletion shapes from C^{4}P-TRAIN are expected to be higher.

It is also important to consider that the radial depletion of power in a fuel pellet depends on both the spectrum conditions in the reactor where the irradiation is performed, and on the fuel material itself. As an example, when considering the standard LWR conditions, the shapes related to UO_2 and MOX are not the same, and the magnitude of the peaking in the periphery depends on the ^{235}U enrichment in case of UO_2, and on the Pu content in case of MOX. This underlines the approximation done in the computations when adopting the standard depletion shapes in LWR conditions for an $(U,Am)O_{2-x}$ material irradiated in the HFR, as for the MARINE experiment. Nevertheless, this approximation was necessary in order to take into account the radial depletion of power in thermal spectrum conditions, but the motivations for a sensitivity study are clear.

The evolution of the computation results obtained by GERMINAL when adopting the depletion shapes issued from C^{4}P-TRAIN are shown on the Figure 51, in terms of fuel inner temperature and ΔT in fuel at Peak Power Node.

Figure 51: Sensitivity study with GERMINAL – Effects of the radial depletion shapes of power on the fuel inner temperature and the ΔT in fuel

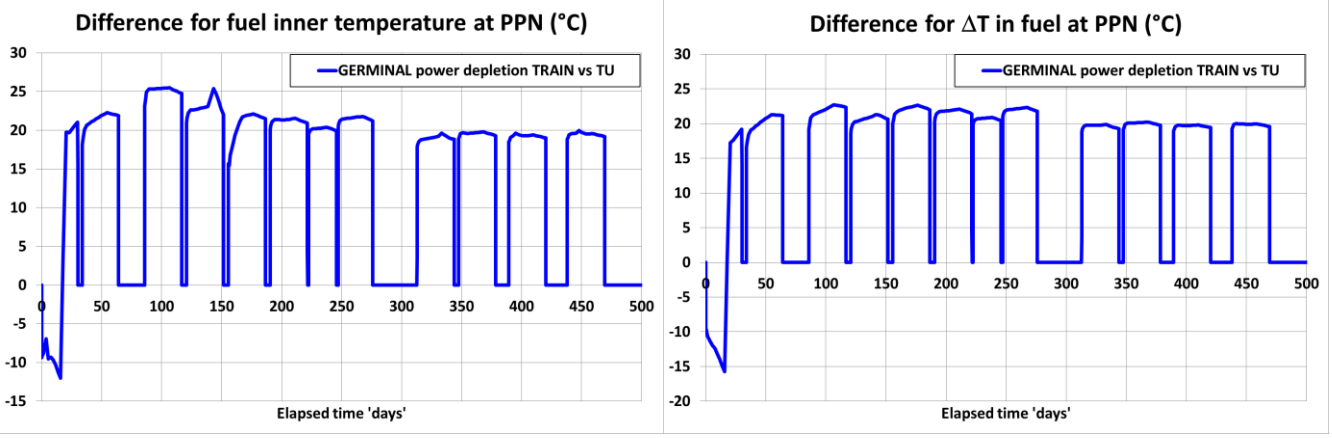

The first irradiation cycle being excepted, the maximum temperature in fuel is about 20 to 25°C higher when using the depletion shapes from C^{4}P-TRAIN. The difference observed for the computed fuel inner temperature is fully consistent with that for the ΔT in fuel. The fuel outer temperature is thus predicted very consistently in the two computations, as well as the pellet-to-clad gap evolution. From a general point of view, the overall calculation results remain very close. The predicted helium release does not

change significantly, as the results summarized in Table 20 tend to show. This trend is logical since the definition of the temperature threshold is the same in both computations (300°C).

Table 20: Sensitivity study with GERMINAL – Effects of the radial depletion shapes of power on the helium quantity in the pin plenum and the inner gas pressure at EOL

	GERMINAL – Radial depletion shapes from TRANSURANUS	GERMINAL – Radial depletion shapes from C^{4}P-TRAIN
Helium quantity in pin plenum at end-of-life	1.556×10^{21} atoms	1.580×10^{21} atoms +1.54%
Plenum gas pressure at end-of-life	19.98 bars	20.30 bars +1.60%

Practically, the most visible effect is the slight increase of the maximum temperature in the fuel, of about 20 to 25°C. This effect remains low because the power itself is low in case of the MARINE experiment – the maximum Linear Heat Rating at end-of life being close to 100 W/cm. More significant effects would be observed while changing the depletion shapes in case of a higher power.

Finally, the effect of changing the depletion shapes was also checked with regards to the optimal value of the temperature threshold for helium release –namely, the optimum targeted in the previous sensitivity study. As a logical consequence, the optimal threshold is found a bit higher when using the depletion shapes issued from C^{4}P-TRAIN, in link with a slightly higher maximum temperature in the fuel. The new optimum yielding the best agreement with the puncturing results is 541°C, remaining close to the previous value (530°C). The consideration of a possible range of [530°C - 740°C] for the temperature threshold for helium release, being the conclusion of the previous sensitivity study, is thus not challenged.

4.4 Conclusion of the interpretation of the MARINE experiment

The interpretation of the MARINE experiment realized in this work is based on the post irradiation nuclear analysis performed by NRG (Van Til 2021). Additional dedicated neutronic assessments have been carried out with the goal to refine the definition of the irradiation conditions, in terms of adequate nuclear data (cross-sections, fission yields) for an (U,Am)O_{2-x} blanket material irradiated in the HFR, as well as for investigating the radial depletion of the power created in the fuel – this depletion influencing the temperature in the pellets, and potentially the overall behaviour. On the basis of the comparisons of the computation results with experimental data and the sensitivity studies, the main conclusions and recommendations are the following:

- The fuel temperature during the MARINE experiment is predicted to be very low: this is not surprising with a (U,Am)O_{2-x} material having a low initial fissile content. The highest temperature calculated at the end of the last irradiation cycle, when the power reaches its maximum, does not exceed 900°C.
- As a first consequence, the modelling of the behaviour of the fission gases (xenon and krypton) is not as critical for MARINE experiment as it was for SPHERE. Even if the computation results show important discrepancies for the fission gas production (cf. discussion below), all the codes essentially predict no fission gas release in the temperature conditions of MARINE experiment, and this result is in line with the puncturing data. In these conditions, the main effect induced by the production and the retention of the fission gases is the swelling of the fuel created by the retained gases.
- In contrast, the modelling of the helium behaviour is more critical in the MARINE experiment. The temperatures reached during the irradiation fall within the range of the thermal activation of helium release. The capability to capture the release mechanism at low temperatures is thus the key point. By means of a sensitivity analysis, a range for a temperature threshold for helium

release was roughly estimated between 530°C and 740°C. Again, the results obtained by the codes show important discrepancies for the helium production and the subsequent evolution of the helium quantity in the pin plenum. This highlights the necessity to improve the neutronic assessment of the MARINE experiment.

- In the first place, a comprehensive nuclear analysis could provide refined information about the respective contributions of the different nuclear reactions (fission and (n,gamma) reactions) to the heat generation in the fuel. At this stage, the point kinetic neutronics models embedded in the FPCs do not have the capability to consider the contribution from the (n,gamma) reactions. The main consequences have been observed by reviewing the computation results: if more fissions are needed to build up the power corresponding to the given LHR, then the production of fission gases and helium are overestimated during irradiation. Secondly a comprehensive nuclear analysis would help characterize the radial depletion of power in the fuel, in order to improve the representativeness of the calculated temperature, and as a corollary better capture the helium release. As a remark, in the fuel temperature and burnup range of this experiment, it should be clarified that inert gas behaviour models may require further developments to better describe specific physical phenomena that are relevant in these conditions whereas typically negligible in standard irradiation conditions, e.g., athermal release, recoil of fission gases. Equipping fuel performance codes and meso-scale tools with these capabilities is a currently ongoing activity.
- The last recommendation concerns the experimental work. As already pointed out, the destructive examination results of the MARINE fuel could provide very useful data for the validation of the codes, especially the final elemental composition of the fuel. Estimating the americium quantity at end-of-life will allow for the evaluation of transmutation performance during the MARINE experiment. Additionally, determining the final neodymium quantity will enable the calculation of burn-up. The quantities of retained fission gases can provide an estimate of their production, assuming minimal release occurred during the experiment.

4.5 Archiving of the study related to MARINE experiment

An archive of the data set related to the present study of the MARINE experiment is available on the open share point ZENODO, in the working area dedicated to the PATRICIA project:
https://zenodo.org/communities/patricia

The name of the archive file is: “PATRICIA Task 5.3 MARINE benchmark Dataset.zip”

The corresponding digital object identifier is: https://doi.org/10.5281/zenodo.13806646

When expanding the archive file, the content is structured as follows:

- “1 - Neutronics computations”: first level directory containing the input and output data related to the neutronic assessment of the MARINE experiment.
  - ✓ “Input”: second level directory containing specific input data required by the neutronic calculations, namely the definition the neutron spectra in the HFR along the irradiation cycles of the MARINE experiment – information provided by NRG, the operator of the HFR.
  - ✓ “Output”: second level directory containing the output data issued from the neutronic calculations. The data are distributed in two separate sub-directories, respectively related to the output from C^4P-TRAIN (radial power profiles) and SERPENT-2 (cross-sections and fission yields).
- “2 - FPCs computations”: first level directory containing the input and output data related to the simulation of the MARINE experiment with the fuel performance codes.
  - ✓ “Input”: second level directory containing the input data required by the computations with the FPCs. One can find in particular the benchmark specifications, the nuclear

data derived from the neutronic calculations and used on input by the FPCs (cross-sections and fission yields), and the adopted definition of the irradiation history. The relative axial heating profile along the fuel stack and the time-evolving radial power profiles in the fuel, issued from the preliminary computation by TRANSURANUS, are also provided.

- ✓ "Output & Comparisons CC CM": second level directory containing the output data issued from the computations with the FPCs. A compilation of the PIE results in one EXCEL file is provided. The computation results are put in a dedicated sub-directory: "THERMAL spectrum", in reference to the single assumption retained for the simulation of MARINE. In this sub-directory are provided the results files from the different codes, and a synthesis file showing the code-to-code and calculation-to-measure comparisons. The synthesis files is named "MARINE.xlsx".

5 Conclusion and perspectives

The main objective of Task 5.3 of the PATRICIA project is to assess the capability of different Fuel Performance Codes (FPCs) to simulate Am-bearing fuel behaviour under irradiation. Two complementary irradiation experiments are considered for benchmarking the computation results against experimental data: the SPHERE experiment with Minor Actinide Bearing Driver Fuel $(U,Pu,Am)O_{2-x}$, and the MARINE experiment with Minor Actinide Bearing Blanket material $(U,Am)O_{2-x}$. Both experiments have been performed in the past years in the High Flux Reactor (HFR) at Petten.

The main outcome from this work is the recommendation to better characterize the experimental conditions of both SPHERE and MARINE irradiations, by the means of comprehensive neutronic analyses. This should help reduce the uncertainties on the experimental conditions for a better interpretation, and eventually enable use in a validation process of the codes. A first step was made in this work, with that goal, by implementing a chaining of neutronic tools with Fuel Performance Codes for the simulation of both experiments. For this purpose, it would be required in the future to include in the irradiation reports the necessary information to reproduce the detailed irradiation conditions from the neutronic point of view, so that specific information (such as cross-sections, yields or power radial depletion vs. irradiation) can be easily obtained and used for more accurate FPC simulations.

The requirement to refine the definition of the experimental conditions is more critical in case of the SPHERE experiment, from the beginning of the irradiation until the end of the storage. This need arises from the neutron shield that surrounded the device in order to harden the neutron flux and make it representative to that in a fast spectrum reactor. This device created peculiar conditions for the experiment different from the standard ones in the HFR. The depletion of the neutron shield along the irradiation may have induced an evolution of the spectrum conditions, progressively changing from those with a hardened flux at beginning-of-life to more thermalized conditions at end-of-life, i.e., closer to the "native" conditions in the HFR. This would lead to a progressive increase of the radial power depletion in the fuel pellets. Investigations about the performance of neutron shields have already been realized (Chang 2011) for the AFC-2C and AFC-2D transmutation experiments with oxide fuel in the Advanced Test Reactor (MacLean 2007). It is recommended to implement in the future a similar process for improving the interpretation of SPHERE. The predictions of inert gas production and their release by the codes are clearly depending on the representativeness of the experimental conditions defined on input. As far as helium release in the pin plenum is concerned, the conditions during the storage are to be refined since the residual power created in the fuel in combination with particular cooling may enable – at least partially – the release of the helium produced by alpha-decay during the storage. Considering that the quantities produced during the irradiation may have been completely released during a hot state, a supplementary helium release during the storage is to be investigated with the goal to explain the high quantity retrieved at puncturing.

This benchmark exercise based on the SPHERE experiment also brought some lessons about the modelling. The key roles played by the pellet relocation and gap thermal conductance models are confirmed, as pointed out in previous studies (Chauvin 2023, Lavarenne 2022). The pellet relocation correlations are essentially empirical and can show some limitations when being applied to such an object like the SPHERE pellet pin, having a short height and being placed inside a capsule, so not in a direct interaction with a coolant flow. Other lessons concern the fuel restructuring modelling, the limitations being here linked to the consideration of the fuel composition, especially the presence of americium for the calculation of the vapour pressures, in combination with the effect of the radial power profile mentioned above.

In case of the MARINE experiment, there is also a need to refine the definition of the experimental conditions with a comprehensive neutronic analysis. The focus here will be to reduce the uncertainties on the creation rates of the fission gases and helium during the irradiation, and to evaluate properly the respective contributions of fission and (n,gamma) reactions to the heat generation in the fuel. Another expectation is a dedicated evaluation of the radial power depletion in the fuel for $(U,Am)O_{2-x}$ blanket material irradiated in the HFR, in order to improve the temperature assessment. The reduction of the uncertainties on the experimental conditions seems more achievable in the case of MARINE, when comparing to SPHERE, since there was no neutron shield aiming at modifying the local neutron spectrum. This is a major difference when comparing the two experiments. Nevertheless, it is recommended to implement in the future a comprehensive nuclear analysis both of MARINE and SPHERE. The experiment with $(U,Am)O_{2-x}$ blanket material is of major interest since the temperature conditions of the experiment fall within the range of the thermal activation of helium release. This makes the link with the main lesson learned in this benchmark exercise with the simulation of MARINE: there is a need to improve the modelling of the helium behaviour at low temperatures, especially for capturing the threshold of helium release.

Finally, as main outcome from this work, the simulations lead us to recommend in general detailed neutronic analyses of the experiments for the simulation of the behaviour of Gen IV fuel materials during irradiation experiments performed in Material Testing Reactors. For this purpose, even the coupling of the neutronic analysis with the fuel behaviour assessment is to be envisaged, especially in case of experiments intending to modify the neutron spectrum conditions with regards to those in the reactor where they are to be operated.

References

Alcouffe R. E. et al. (1995), "DANTSYS: A Diffusion Accelerated Neutral Particle Transport Code System", LA-12969- M, Los-Alamos.

Beyer C.E. et al. (1975), "GAPCON-THERMAL-2: A COMPUTER PROGRAM FOR CALCULATING THE THERMAL BEHAVIOR OF AN OXIDE FUEL ROD", BNWL-1898, https://inis.iaea.org/collection/NCLCollectionStore/_Public/07/244/7244987.pdf

Botazzoli P. et al. (2011), "Extension and validation of the TRANSURANUS burn-up model for helium production in high burn-up LWR fuels", Journal of Nuclear Materials, vol. 419, pp. 329–338, https://doi.org/10.1016/j.jnucmat.2011.05.040

Chang G.S. (2011), "Cadmium Depletion Impacts on Hardening Neutron Spectrum for Advanced Fuel Testing in ATR", International Conference on Mathematics and Computational Methods Applied to Nuclear Science and Engineering, Rio de Janeiro, Brazil, ISBN 978-85-63688-00-2, https://inis.iaea.org/collection/NCLCollectionStore/_Public/48/031/48031790.pdf?r=1

Charles M., Bruet M. (1984), "Gap conductance in a fuel rod: modelling of the FURET and CONTACT results", in: IAEA, International Working Group on water reactor Fuel Performance and Technology, IWGFPT/19, "Water reactor fuel element performance computer modelling", Meeting proceedings, https://inis.iaea.org/collection/NCLCollectionStore/_Public/16/057/16057359.pdf

Chauvin N. et al. (2023), "Benchmark Study on Innovative Fuels for Fast Reactors with Fuel Performance Codes", NEA/NSC/R(2022)5, https://www.oecd-nea.org/jcms/pl_79983/benchmark-study-on-innovative-fuels-for-fast-reactors-with-fuel-performance-codes

D'Agata E. et al. (2014), "SPHERE: Irradiation of sphere-pac fuel of $UPuO_{2-x}$ containing 3% Americium", Nuclear Engineering and Design, vol. 275, pp. 300-311, https://doi.org/10.1016/j.nucengdes.2014.05.021

D'Agata E. et al. (2017), "The MARINE experiment: Irradiation of sphere-pac fuel and pellets of UO_{2-x} for americium breading blanket concept", Nuclear Engineering and Design, vol. 311, pp. 131-141, http://dx.doi.org/10.1016/j.nucengdes.2016.11.023

Dutt D. S., Baker R. B. (1975), "SIEX – A correlated code for the prediction of Liquid Metal Fast Breeder Reactor (LMFBR) Fuel Thermal Performance", HEDL-TME 74-55 UC-79b, https://doi.org/10.2172/4181413

Eaton J. W. et al. (2016), "GNU Octave – A high-level interactive language for numerical computations", Edition 4 for Octave version 4.2.1.

European Commission (2015), "FAIRFUELS Euratom Project", https://cordis.europa.eu/project/id/232624

European Commission (2017), "PELGRIMM Euratom Project", https://cordis.europa.eu/project/id/295664

European Union's Horizon 2020 Research and Innovation programme (2020), "PATRICIA - Partitioning And Transmuter Research Initiative in a Collaborative Innovation Action", https://patricia-h2020.eu/

Fédérici É. et al. (2007), "Helium production and behaviour in nuclear fuels during irradiation in LWR", Proceedings of the International LWR Fuel Performance Meeting, San Francisco, USA, 30 Sep. – 3 Oct. 2007, pp. 664-673 (paper 1057)

Gallais-During A. et al. (2018), "Outcomes of the PELGRIMM project on Am-bearing fuel in pelletized and spherepac forms", Journal of Nuclear Materials, vol. 512, pp. 214–226, https://doi.org/10.1016/j.jnucmat.2018.10.016

Kato, M. et al. (2011), "Physical Properties and Irradiation Behavior Analysis of Np- and Am-Bearing MOX Fuels", Journal of Nuclear Science and Technology, vol. 48, No. 4, pp. 646–653, https://doi.org/10.1080/18811248.2011.9711745

Kulesza, J.A. et al. (2022), "MCNP Code Version 6.3.0 - Theory & User Manual", LA-UR-22-30006, Rev. 1, https://mcnp.lanl.gov/pdf_files/TechReport_2022_LANL_LA-UR-22-30006Rev.1_KuleszaAdamsEtAl.pdf

Labonne B. et al. (2023), "Development of an interatomic potential for mixed uranium-americium oxides and application to the determination of the structural and thermodynamic properties of

(U,Am)O_2 with americium contents below 50%", Journal of Nuclear Materials, vol. 579, https://doi.org/10.1016/j.jnucmat.2023.154390
Lainet M. et al. (2019), "GERMINAL, a fuel performance code of the PLEIADES platform to simulate the in-pile behaviour of mixed oxide fuel pins for sodium-cooled fast reactors", Journal of Nuclear Materials, vol. 516, pp. 30-53, https://doi.org/10.1016/j.jnucmat.2018.12.030
Lassmann K., Hohlefeld F. (1987), "The revised URGAP model to describe the gap conductance between fuel and cladding", Nuclear Engineering and Design, vol. 103, pp. 215–221, https://doi.org/10.1016/0029-5493(87)90275-5
Lavarenne J. et al. (2022), "Burn-Up Dependent Modeling of Fuel-to-Clad Gap Conductance and Temperature Predictions for Mixed-Oxide Fuel in the ESFR-SMART Core", Journal of Nuclear Engineering and Radiation Science, vol. 8, https://doi.org/10.1115/1.4050479
Leppänen J. (2015), "Serpent – A Continuous-energy Monte Carlo Reactor Physics Burnup Calculation Code", User's Manual, http://montecarlo.vtt.fi/download/Serpent_manual.pdf
MacLean H.J., Hayes S.L. (2007), "Irradiation of Metallic and Oxide Fuels for Actinide Transmutation in the ATR", Global 2007, Boise, Idaho, USA, https://citeseerx.ist.psu.edu/document?repid=rep1&type=pdf&doi=31c494e9cd15a8b950f4fd4d98a74ab962a3c7be
Magni A. et al. (2020), "Modelling and assessment of thermal conductivity and melting behaviour of MOX fuel for fast reactor applications", Journal of Nuclear Materials, vol. 541, https://doi.org/10.1016/j.jnucmat.2020.152410
Magni A. et al. (2021-1), "The TRANSURANUS fuel performance code", in: Nuclear Power Plant Design and Analysis Codes - Development, Validation and Application, pp. 161–205, https://doi.org/10.1016/B978-0-12-818190-4.00008-5
Magni A. et al. (2021-2), "Modelling of thermal conductivity and melting behaviour of minor actinide-MOX fuels and assessment against experimental and molecular dynamics data", Journal of Nuclear Materials, vol. 557, https://doi.org/10.1016/j.jnucmat.2021.153312
Motta T., Olander D. R. (2017), "Light Water Reactor Materials, Volume I: Fundamentals", American Nuclear Society Scientific Publications.
Okawa T. et al. (2015), "Fuel behavior analysis code FEMAXI-FBR development and validation for core disruptive accident," Progress in Nuclear Energy, vol. 82, pp. 80–85, https://doi.org/10.1016/j.pnucene.2014.11.002
Philipponneau Y. (1992), "Thermal conductivity of (U,Pu)O_{2-x} mixed oxide fuel", Journal of Nuclear Materials, vol. 188, pp194–197, https://doi.org/10.1016/0022-3115(92)90470-6
Pizzocri D. et al. (2022), "SCIANTIX open-source code for fission gas behaviour: objectives and foreseen developments", in: IAEA Technical Meeting on the Development and Application of Open-Source Modelling and Simulation Tools for Nuclear Reactors, Milano, Italy.
Rineiski A., Sinitsa V. (2018), "C4P-TRAIN Neutronics Tool For Supporting Safety Studies Of Innovative Fast Reactors", PHYTRA4 – The Fourth International Conference on Physics and Technology of Reactors and Applications, on CD-ROM, Marrakech, Morocco.
Romano P.K. et al. (2015), "OpenMC: A state-of-the-art Monte Carlo code for research and development", Annals of Nuclear Energy, vol. 82, pp. 90-97, https://doi.org/10.1016/j.anucene.2014.07.048
Ross A.M. and Stoute R.L. (1962), "Heat transfer coefficient between UO_2 and Zircaloy-2", CRFD-1075, AECL report 1552
Santamarina A. et al. (2009), "The JEFF-3.1.1 Nuclear Data Library", ISBN 978-92-64-99074-6, NEA No. 6807, https://www.oecd-nea.org/jcms/pl_14470/the-jeff-3-1-1-nuclear-data-library?details=true
Scolaro A. et al. (2021), "Investigation on the effect of eccentricity for fuel disc irradiation tests", Nuclear Engineering and Technology, vol. 53, pp. 1602-1611, https://doi.org/10.1016/j.net.2020.11.003
Staicu, D. et al. (2011), "Thermal conductivity of homogeneous and heterogeneous MOX fuel with up to 44 MWd/kgHM burn-up", Journal of Nuclear Materials, vol. 412, pp. 129-137, https://doi.org/10.1016/j.jnucmat.2011.02.042

Staicu, D. and Barker M. (2013), “Thermal conductivity of heterogeneous LWR MOX fuels”, Journal of Nuclear Materials, vol. 442, pp. 46-52, https://doi.org/10.1016/j.jnucmat.2013.08.024

Sublet J.-Ch. et al. (2017), “FISPACT-II: An Advanced Simulation System for Activation, Transmutation and Material Modelling”, Nuclear Data Sheets, vol. 139, pp77–137, https://doi.org/10.1016/j.nds.2017.01.002

Suzuki M., Saitou H. (2005), “Light Water Reactor Fuel Analysis Code FEMAXI-6 (Ver.1) – Detailed Structure and User’s Manual”, JAEA/Data/Code 2005-003, https://jopss.jaea.go.jp/pdfdata/JAEA-Data-Code-2005-003.pdf

Van Til S. (2021), “MARINE gas puncturing and swelling behaviour of (U,Am)0_2”, PATRICIA deliverable D4.1

Van Til S. et al. (2023), “Irradiation performance and first examinations of Americium bearing blanket fuel from the MARINE irradiation experiment”, Journal of Nuclear Materials, vol. 587, https://doi.org/10.1016/j.jnucmat.2023.154699

Zullo G. et al. (2023), “The SCIANTIX code for fission gas behaviour: Status, upgrades, separate-effect validation, and future developments”, Journal of Nuclear Materials, vol. 587, https://doi.org/10.1016/j.jnucmat.2023.154744

List of Tables

List of Figures